2016

The Owl Sensor: A Smart Nanostructure for Single Nucleotide Variation Analysis

Rebekah Karadeema
University of Central Florida

THE OWL SENSOR: A SMART NANOSTRUCTURE FOR SINGLE NUCLEOTIDE VARIATION ANALYSIS

by

REBEKAH J. KARADEEMA
B.S. University Central Florida, 2015

A thesis submitted in partial fulfillment of the requirements
for the degree of Master of Science
in the Department of Chemistry
in the College of Science
at the University of Central Florida
Orlando, Florida

Summer Term
2016

Major Professor: Dmitry M. Kolpashchikov

ABSTRACT

Analysis of single nucleotide variations (SNVs) in DNA and RNA sequences is extensively used in healthcare for detection of genetic mutations and analysis of drug resistant pathogens. Here we developed a nucleic acid sensor able to differentiate between a fully matched analyte and one with a SNV in a wide temperature range of 5°C-32°C. The sensor, dubbed here the ‘Owl Sensor’ due to the complex’s resemblance to owl eyes, utilizes recent developments in DNA nanotechnology and synthetic biology to self-assemble a fluorescent DNA nanostructure called a Double Crossover, or DX Tile, capable of differentiating SNVs in a large temperature range, including ambient temperature. In the presence of fully matched nucleic acid analytes, a stable complex is formed with high fluorescent signal; however in the presence of a single base variation in the analyte, unfavourable helicity results in little-to-no observed complex formation. The novelty of the approach is that selectivity of analyte recognition is, at least in part, determined by the structural rigidity of the entire nanostructure rather than by the stability of analyte-probe hybrid, as is the case for conventional hybridization probes. The rigid nanostructure collapses if a minor imperfection, e.g. if a single-base mispairing, is present. Owl Sensor differentiates fully matched analyte from mismatched in a wide temperature range, with mismatched analyte producing only the background fluorescence, selectivity that is hard to achieve by conventional hybridization probes. Owl Sensor therefore promises to add to the toolbox for diagnosis of genetic disorders and infectious diseases at ambient temperatures.

ACKNOWLEDGMENTS

I would like to thank my advisor Dr. Dmitry Kolpashchikov for his support, advice, and guidance over the past 2.5 years. He invited me to begin research in his lab as an undergraduate student back in 2014, sparking my love for scientific research, and it was his encouragement and guidance that has helped me to mature into a better student, scientist, and researcher. He has been vital to my success, and I will always be grateful to him as my first research advisor. I would also like to thank my committee other committee members: Dr. James Harper and Dr. Karin Chumbimuni-Torres.

I would like to especially thank two undergraduate students, Tyler Steidl and Sophia Bertot, for their help on this project. Advising you has been a pleasure, and I hope you will continue the work after I graduate. I would like to thank the other members of the Kolpashchikov Lab who provided moral support and scientific advice, and for which I had the pleasure of sharing the lab. They are: Dr. Yulia Gerasimova, Dr. Maria Stancescu, Martin O'Steen, Hillary Bengsten, Nanami Kikuchi, Alex Smith, Carlos Ledezma, Tatiana Fedotova Molden, Amanda Cox, Brooke Bayless, Derick Miller, and Elliot Williams.

Financial support from the NSF CCF 1423219 is appreciated.

Finally, I would like to thank my friends and family for their love and encouragement throughout the years. I would especially like to thank my mother who has been my biggest cheerleader from day one.

TABLE OF CONTENTS

LIST OF FIGURES

LIST OF TABLES

LIST OF ABBREVIATIONS

A	Adenine
bp	Base pairs
C	Cytosine
DNA	Deoxyribonucleic acid
dF	The derivative of fluorescence
F	Fluorophore
F_d	Fluorescence of the deletion analyte
F_i	Fluorescence of the insertion analyte
F_M	Fluorescence of the matched analyte
F_{mm}	Fluorescence of the mismatched analyte
G	Guanine
HPLC	High Performance Liquid Chromatography
hr	Hour(s)
4WJ	Four-way junction
LOD	Limit of detection
MB	Molecular beacon
min	minutes
Mtb	*Mycobacterium tuberculosis*
peg	Polyethylene glycol
Q	Quencher
rcf	Relative centrifuge force
RNA	Ribonucleic acid
s	seconds
SD	Standard Desalting
SNP	Single nucleotide polymorphism
SNV	Single nucleotide variation
T	Thymine
UMB	Universal molecular beacon

CHAPTER 1: GENERAL INTRODUCTION

On May 23, 2013, the I-5 Skagit River Bridge collapsed in Washington State when a semi-truck with an oversized load struck the bridge's support beams. The 1955 through-truss bridge had previously been rated "functionally obsolete" due to the outdated engineering and lack of proper support to the bridge's structure. In addition, its rating of "fracture critical" meant that a collapse was imminent if a single, vital component was compromised.[1,2] This bridge had imperfections in its structure, making it susceptible to collapse when a strong enough stress was introduced. If the semi-truck had not rammed into a critical support structure, the bridge would likely still be standing today, allowing normal traffic of 71,000 cars/day to continue. It was the added stress into the system that caused the whole structure to collapse (Figure 1).

In this study, a nanostructure 30 billion times smaller than the Skagit River Bridge is introduced that has its own designed imperfection. The nanostructure takes advantage of recent developments in DNA Nanotechnology and Synthetic Biology to form a small nucleic acid complex with the ability to differentiate a DNA or RNA analytes from similar sequences with only one nucleotide difference.

Single nucleotide variations (SNVs) are abundant in genomes, providing genetic diversity between members of the same species. While some of these variations are harmless, pathogens can also accumulate genetic variations that allow them to evade the mechanism of action of common drugs, leading to antibiotic resistance and making

treatment of disease more difficult. One type of SNV occurs when the correct nucleotide is mutated into a different nucleotide, which is referred to as a mismatch, or a single nucleotide polymorphism (SNP), which have been analyzed to determine drug resistance in bacteria and parasites, for cancer prognosis, and predicting the prevalence of mental illnesses such as schizophrenia.[3-7] For diagnostic purposes, accurate detection of SNPs enables health care professionals to properly diagnose and treat patients suffering from diseases and infections. In an age when effective treatment for many diseases is known and available, a hurdle for a worldwide cure is proper diagnosis of disease.[8] Waiting weeks for lab results is inconvenient and delays treatment for patients, especially in developing countries where infections like *Mycobacterium tuberculosis* (*Mtb*) cause the most deaths. In rural areas where patients may walk hours to a clinic for treatment, point of care (PoC) diagnostic tools allow for proper treatment to be given at the same time as diagnosis. An ideal PoC test is cost-efficient, non-invasive, portable, utilizes stable reagents, and can be performed by someone without extensive training preferably under ambient temperature without the need for a precise temperature control.

Molecular diagnostics analyze biomarkers including proteins and nucleic acids to determine patients' conditions and is a promising avenue for the PoC setting. While many current molecular diagnostic tests are effective, they are often unsuitable for a PoC setting as they can be expensive, require complicated equipment, highly-trained personnel, and reagents that are unstable at room temperature.

Nucleic acid tests are a promising choice for the molecular diagnostics field, because nucleic acid targets can be amplified by either a polymerase chain reaction or isothermal amplification methods. After amplification, nucleic acid sensors typically do not require protein enzymes, which is a big advantage because proteins are easily denatured at room temperatures. Common methods for nucleic acid sequence analysis include the use of hybridization probes including the linear probe (LP) or a molecular beacon (MB) probe (Figure 2).[9,10] While these probes can differentiate between similar nucleic acid sequences, they do so in a narrow temperature range of about 1-15°C (Figure 4Figure 5,Figure 6). In addition, the high temperatures required for differentiation does not include ambient temperature, which is a requirement for ease of reading and especially for PoC diagnostics.

The linear probe consists of a fluorescently labeled DNA or RNA oligonucleotide that binds directly to the analyte of interest, which can be conjugated to a quencher (Figure 4). As temperature increases, the linear probe melts from the analyte of interest, producing a fluorescent response.

MB probes developed in 1996 by Tyagi and Kramer and consist of a single-stranded nucleic acid sequence with a fluorophore (F) on the 5’ end and a quencher (Q) on the 3’ end. A region specific to the target is flanked by nucleotides that form a small stem at low temperatures. In this closed state, the fluorophore is in close proximity to the quencher, allowing for quenching and a low fluorescent response. When a MB probe is bound either

directly to an analyte or to a complex of the analyte bound to adapter strands (Figure 2, 3, and 11), the stem loop is opened, allowing for the fluorophore to be separated from the quencher and high fluorescence to be observed, indicating that the target is present.

MB probes that directly hybridize to their target can be expensive due to optimization costs for each new analyte. The cost of conjugating the F and Q to the MB sequence is expensive ($300/probe), and multiple versions may need to be tested for optimization.[12] As MB probes are sequence specific, each new analyte requires a new MB probe, adding cost for transitioning between different analyte sequences. In addition, due to the long length of the MB probe, nonspecific binding to strands other than the target analyte may occur, leading to opening of the hairpin and a false positive signal. The Kolpashchikov lab has previously developed a number of MB based sensors that allow for the use of a Universal MB (UMB) probe that can be used with many different analytes. This is accomplished by changing the sequences of adapter strands, a much cheaper alternative to changing the ordering an entirely new MB.[13-15]

One of these sensors is the X Sensor, which showed excellent differentiation ability for highly structured analytes in a wide temperature range from 5-40°C (Figure 4, 5, and 6).[16] When the X Sensor was designed to target an analyte with little secondary structure (*inhA* analyte shown in Figure 7), differentiation in a wide range of temperatures from 5-40°C was only achieved by introducing more conformational constraint through the addition of hairpin loops to the adapter strands (Figure 8, 9, and 10). Kinetic studies of the X Sensor

showed that long equilibration times were required for complete complex formation when the system had conformational constraints (either the analyte or the sensor had stable secondary structure). It was concluded that the large temperature range for differentiation was achieved by utilizing non-equilibrium conditions, meaning that if analysis was conducted at a time before the mismatched analyte could bind to the sensor, then high differentiation could be achieved. While the X Sensor provides a means for differentiating matched and mismatched analytes, it requires the use of unnatural polyethylene glycol linkers, optimization of adapter strand lengths, and the addition of stem loops on adapter strands for linear analytes.[16]

Here, we report a new method of analysis for detection of SNVs using a nucleic acid sensor termed the ‘Owl Sensor’ due to its resemblance of owl eyes (when drawn in complex with an analyte). The Owl Sensor utilizes a rigid nanostructure to allow for increased selectivity over commercial probes when binding to nucleic acid analytes (Figure 11). The Owl Sensor uses inexpensive, unmodified DNA adapter strands to bind to a UMB probe (UMB5) and a target of interest, allowing selective target recognition with a fluorescent output.

The adapter strands serve two purposes: provide target recognition and aid in signal transduction. The central portion of each adapter strand is an analyte binding domain which allows for target recognition. The 4-5 nucleotide-long overhangs serve as MB binding domains for signal transduction (Figure 11). Due to the short length of the UMB5

adapter strands, opening of the MB probe is only highly favored when the correct analyte is present, as is evidenced by low signal of the ‘Control’, which contains the adapter strands and UMB with no analyte present (seen in Figure 22 and 23).

Besides the benefit of producing a broader differentiation range than commercial probes, the Owl Sensor is able to differentiate at ambient temperature in a more cost effective manner. Because the Owl Sensor utilizes a UMB probe, any analyte of interest can be analyzed with the same UMB probe by simply altering the sequence of the unmodified nucleic acid adapter strands P and R that hybridize with the analyte.

The Owl Sensor was compared to the X sensor, which also uses adapter strands, here f and m, where f is analogous to R and m is analogous to P. Although the adapter strands for the X Sensor also uses UMB5, they have the disadvantage of being modified oligonucleotides, as triethylene glycol (peg) linkers separate the UMB5 and analyte binding arms (Figure 6C). In contrast, the Owl sensor uses unmodified DNA adapter strands, R and P, to modulate hybridization of UMB5 to the analyte. The model analyte chosen is a short synthetic DNA mimic of the known *inhA* SNP site in rRNA from *Mtb*, whose mismatch indicates antibiotic resistance to the commonly used drug isoniazid.[17-20] With 25% of avoidable adult deaths coming from *Mtb* patients, proper diagnosis of the disease and its virulent state is essential.[21] This study used a probe specific to the inhC analyte, which contains a cytosine in the 26th position, with the mutated analyte, inhT,

having a thymine in this position. However, an Owl sensor specific to inhT was also tested and showed a similar response to the Owl sensor specific to inhC.

Figures and tables

Figure 1: Collapsed I-5 Skagit River Bridge.[2]

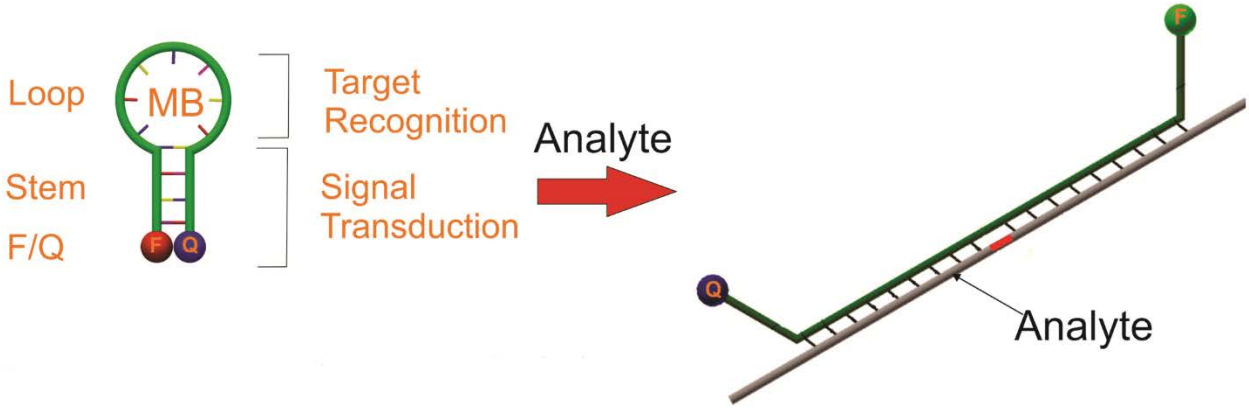

Figure 2. Working mechanism of a molecular beacon.[16]
When no analyte is present, the MB stays in the closed conformation (on the left) where quenching results in a low fluorescent output. The loop portion acts as a target recognition domain where, in the presence of a sequence complementary to the loop, hybridization between the MB probe and the analyte allows for separation of the fluorophore and the quencher, allowing for a high fluorescent output.
This figure was adopted with permission from the PhD thesis of Maria Stancescu.

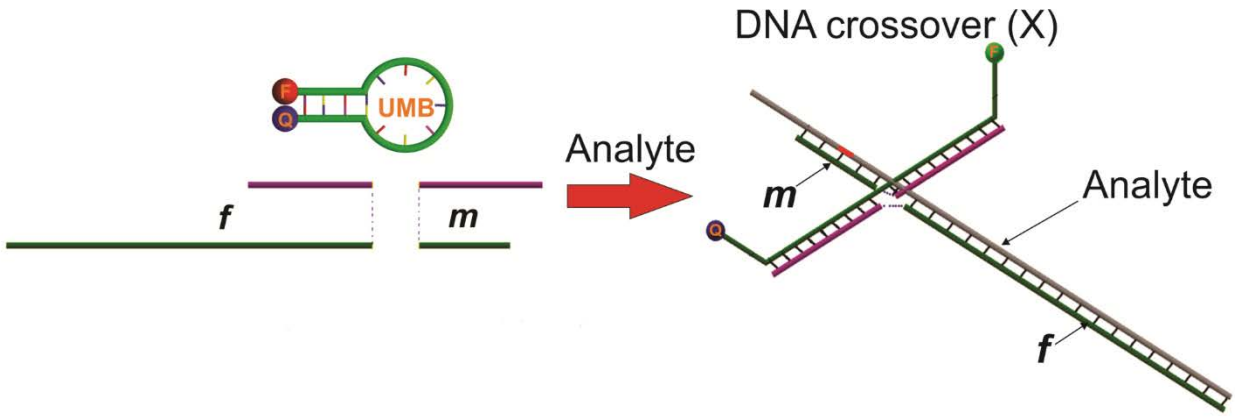

Figure 3. Working mechanism of an X sensor.[16]

The X Sensor uses two adapter strands, m and f, to modulate the hybridization between the analyte and the UMB. The green portions of the m and f strands allow for target recognition, as they bind to the analyte. The pink portions of m and f bind to the UMB, allowing for the fluorescent output only if the analyte is present. The green portion of the f strand is long in length, allowing for strong hybridization and for opening up of any secondary structure present in the analyte. The green portion of the m strand is much shorter, and binds to the SNP site shown in red on the grey analyte. The short length of the m strand allows for selectivity, as an incorrect base-pair greatly destabilizes the hybridization of the m strand with the analyte. This figure was adopted with permission from the PhD thesis of Maria Stancescu.

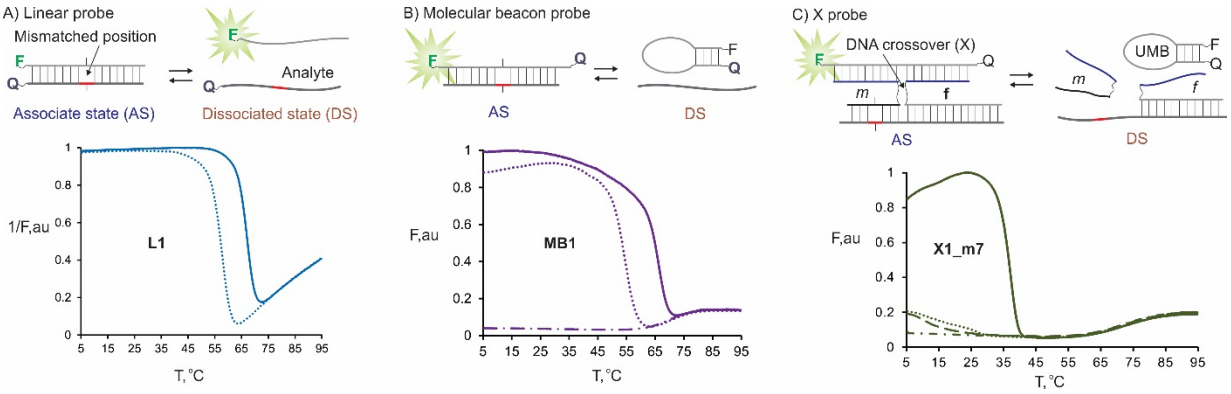

Figure 4. Different types of hybridization probes: design and fluorescent melting profiles for a highly structured analyte.[16]

A) Linear probe. Upper panel: unfolded DNA probe hybridizes to a nucleic acid analyte. The analyte was labeled by a quencher dye (Q), while the probe was conjugated with a fluorophore (F) to enable fluorescent detection of complex formation. Bottom panel: Inverted fluorescence (1/F) of the linear probe L1 in the presence of matched (solid line) and mismatched (dotted line) analytes at different temperatures.

B) MB probe. Upper panel: MB probe upon hybridization to a mismatched target. Lower panel: Fluorescent response of MB1 in the presence of fully matched (solid line) or mismatched (dotted line) at different temperatures. Dash-dotted line is melting of MB1 alone.

C) X1 probe. Upper panel: Strands *m* and *f* bind analyte and a universal MB probe (UMB) to form a fluorescent crossover (X) complex. UMB-binding arms of strands *f* and *m* are in blue. Low panel: Melting temperature for X1 probe (UMB1, f, m7) in the presence of fully complementary (solid line) or mismatched (dotted line). Dash-dotted line corresponds to the melting of UMB1 alone, while dashed line represents the melting of X1 (no target).

This figure and legend was adopted with permission from the PhD thesis of Maria Stancescu.

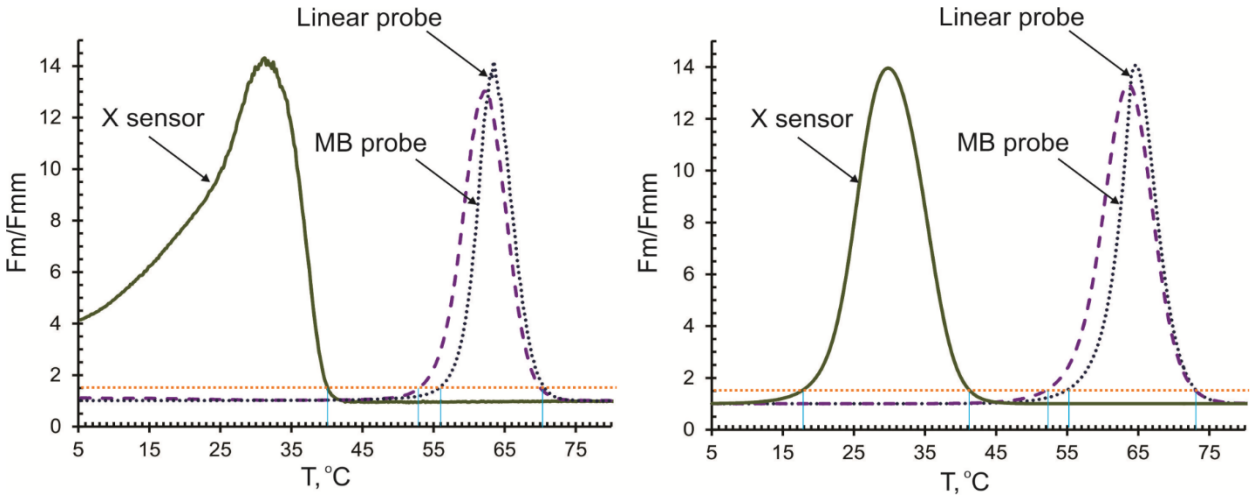

Figure 5. Differentiation range for the three types of hybridization probes for a highly structured analyte is due to nonequilibrium conditions.[16]

A) The ratio of fluorescence produced by each probe in the presence of fully matched analyte (F_m) to that of mismatched analyte (F_{mm}) are plotted against temperature for linear probe (blue dotted line), MB probe (purple dashed line) and X sensor (green solid line). The threshold F_m/F_{mm} ~ 1.5 is indicated by the orange dotted line.

B) Theoretical prediction of the profiles shown in panel B in the assumption of thermodynamic equilibrium shows a shorter temperature range for differentiation. The extension of differentiation into low temperatures is attributed to the sensor behaving and non-equilibrium conditions where a kinetic advantage allows for differentiation in a wider temperature range.

This figure and legend was adopted with permission from the PhD thesis of Maria Stancescu.

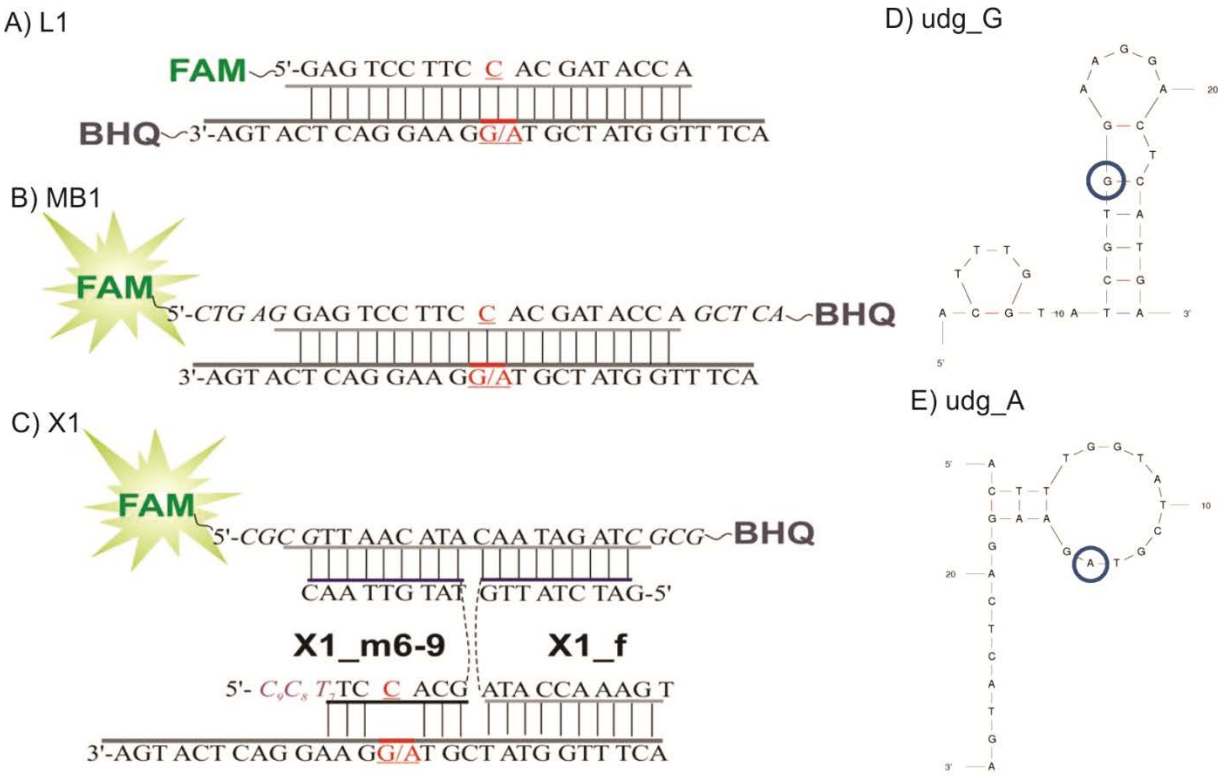

Figure 6. Structures of analyte-probe complexes and the highly structured analyte.[16]

A) L1; B) MB1; C) X1. SNP positions are red underline. Peg linkers are shown as dashed lines in panel C. Purple C7, C8 and T7 indicate nucleotides that are absent in X1_m6 adaptor strand in panel C. Folding of DNA analytes at 10°C under experimental conditions: udg_G (D) and udg_A (E). The position of point mutations in the sequence is blue circled.

This figure and legend was adopted with permission from the PhD thesis of Maria Stancescu.

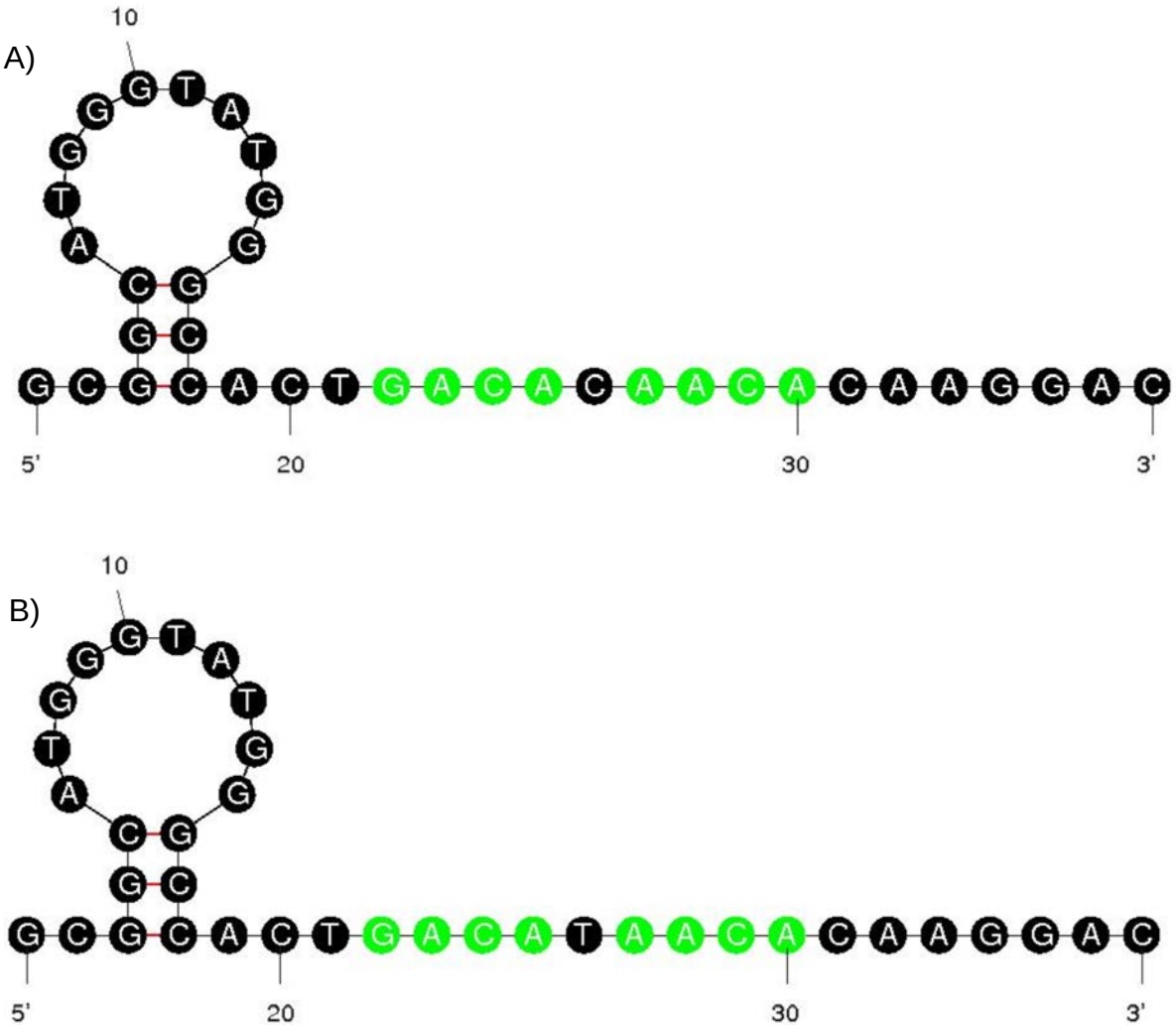

Figure 7. Lowest energy folding of the inhC and inhT analytes shows a nearly linear structure.

The analytes are shown folded by mfold.[22] The green nucleotides indicate the region where P_9 binds. The black nucleotide in the middle of the green region indicates the variable base (mismatch site). The inhC and inhT analytes both have a ΔG= -1.84 kcal/mol.

A) inhC analyte is the wild type of the *inhA* SNP site and has a cytosine in the 26th position.

B) inhT analyte is the mutant version of the *inhA* SNP site and has a thymine in the 26th position.

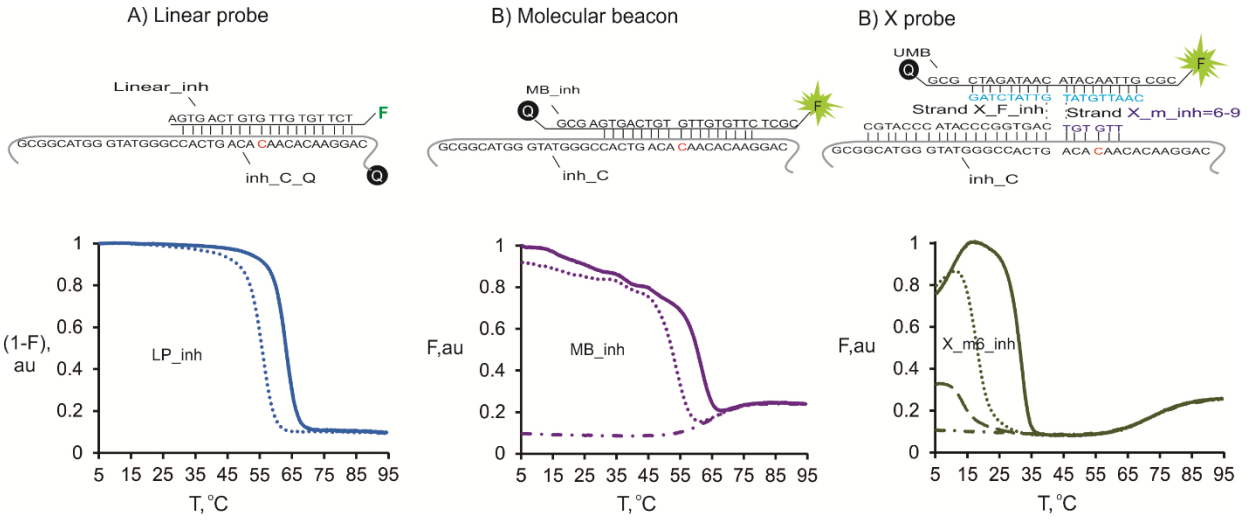

Figure 8. SNP recognition by different types of hybridization probes for a nearly linear analyte show narrow ranges for differentiation.[16]

A) Linear probe. Upper panel: Linear probe hybridized to the matched analyte. The analyte was labeled by a quencher dye (Q), while the probe was conjugated with a fluorophore (F) to enable fluorescent detection of complex formation. Bottom panel: Reverse fluorescence (1-F) of the probe in the presence of matched Inh_C_Q (solid lines) and mismatched (dotted lines) Inh_T_Q analytes at different temperatures. The reverse fluorescence is presented to simplify comparison the data with panels B and C since linear probe, as designed, increased fluorescence upon melting, not decreasing as MB probe and X sensor.

B) Molecular beacon probe. Upper panel MB probe hybridizes to complementary target and produces fluorescent signal. The SNP position is shown in red, and the mutation is C ->T.

C) X sensor. Upper panel: Fluorescent crossover (X) complex formed by strands **X_F_inh** and **X_m_inh** when binding to analyte **Inh_C** and MB probe. MB-binding arms of strands ***f*** and ***m*** are in cyan. Low panel: Melting temperature curves for X sensors with 6-nucleotides long m-analyte binding (**X_m-6_inh** in Table 2).

This figure and legend was adopted with permission from the PhD thesis of Maria Stancescu.

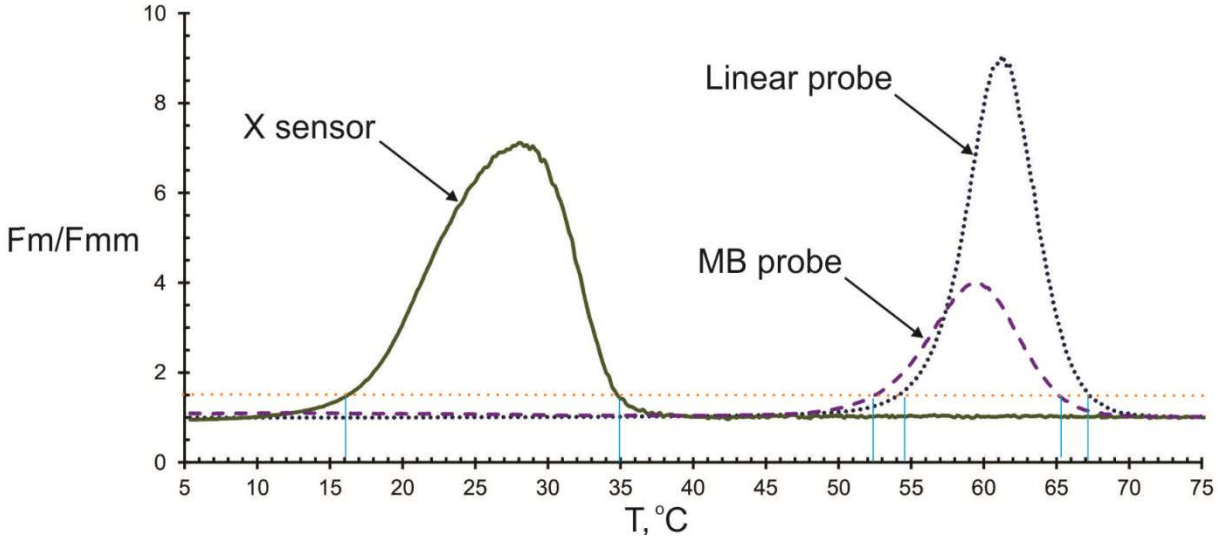

Figure 9. Commercial probes and the X Sensor show limited differentiation range for a nearly linear analyte.[16]

The ratio of fluorescence from Figure 8 melting curves produced by each probe in the presence of fully matched analyte (F_m) to that of mismatched analyte (F_{mm}) are plotted against temperature for LP_inh (blue dotted line), MB_inh probe (purple dashed line) and X_inh sensor (X_m-6_inh, green solid line). The threshold F_m/F_{mm} ~ 1.5 is indicated by orange dotted line.

This figure and legend was adopted with permission from the PhD thesis of Maria Stancescu.

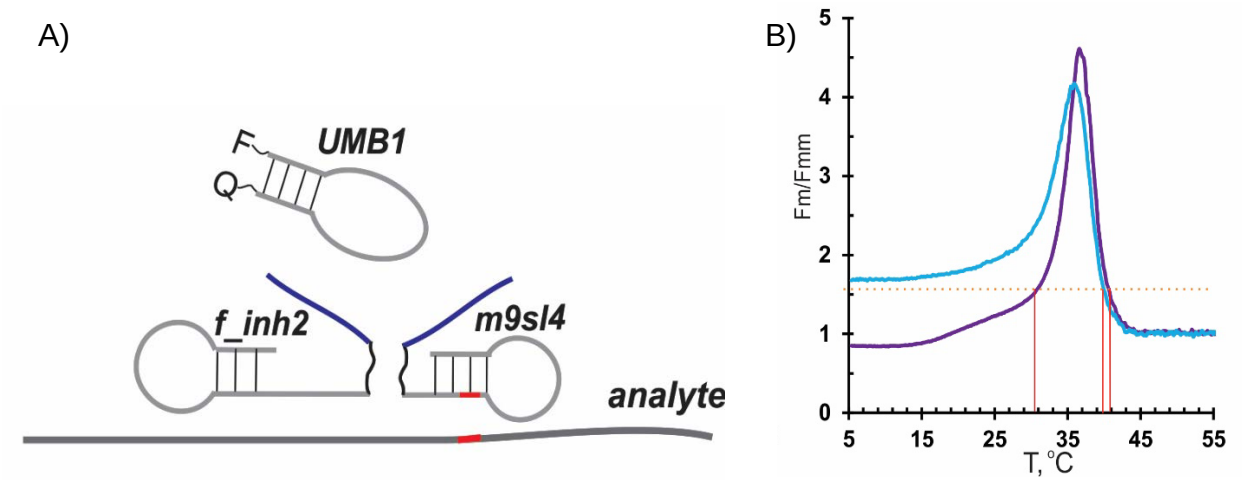

Figure 10. Upon adding conformational constraints, the X Sensor gained differentiation ability for inhC, a nearly linear analyte.[16]

A) Hairpin loops on the X Sensor's analyte binding arms allowed for the extension of the temperature range for differentiation of the matched and mismatched analytes.

B) The purple line shows the range for differentiation with the X Sensor with a stem only in the f strand. The blue line shows a larger range of differentiation after the addition of stem loops to both the m and f adapter strands.

This figure was adopted with permission from the PhD thesis of Maria Stancescu.

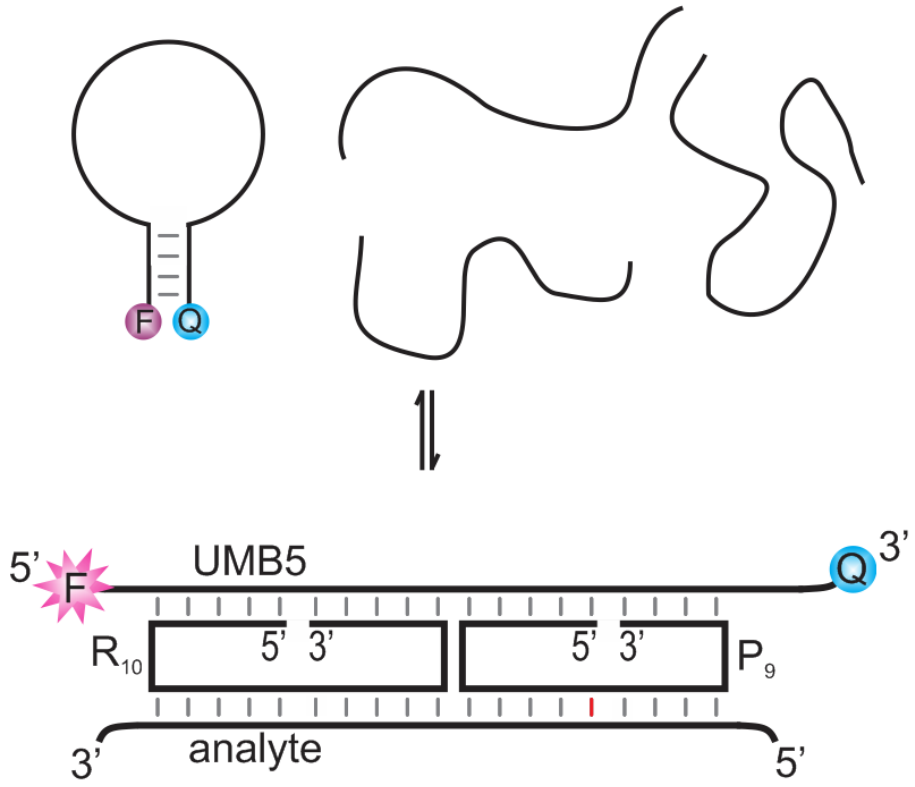

Figure 11. Working mechanism of the Owl Sensor.
In the dissociated state (above), the universal molecular beacon (UMB5) is in its folded, closed state where little fluorescence is absorbed due to quenching. Upon hybridization of the adapter strands to the analyte, UMB5 can hybridize, allowing for separation of the fluorophore from the quencher, producing a fluorescent response. The grey lines indicate hydrogen bonds and the red line indicates the mismatch site, which is located near the middle of the P_9 strand.

CHAPTER 2: OWL SENSOR DESIGN, OPTIMIZATION, AND CHARACTERIZATION

Introduction

In order to find the optimum lengths of R and P strands for discrimination between closely related analytes, a symmetric Owl Sensor adapter strands ranging from 12-8 nucleotides bound to the *inhA* analyte were designed on a mirror plane to allow for combination with all lengths of R to be tested with all lengths of P (Figure 12). Adapter strands are named by their length where an R strand with a 12 nucleotide long analyte binding domain is named R_{12}, and a P strand with a 9 nucleotide long analyte binding domain is named is named P_9. The mismatch site was designed to be roughly in the middle of all of the P probes to provide the greatest energetic penalty for sequence variations.[23] This allows R to act as a stabilizing sequence, as each tested analyte is complimentary to all of the R adapter strands. Unless otherwise indicated, throughout this study the P stramd is specific (perfectly complimentary) to the inhC version of the *inhA* SNP site, and the mutated inhT version is used as the 'mismatched' analyte.

The temperature at which a melting curve has an inflection point is called the T_m and can be used as a quantitative value that suggests the stability of a complex. At the T_m, 50% of the formed complexes have melted. Having a higher T_m indicates that the complex can withstand higher temperatures before the complex falls apart.

Materials and Methods

Reagents

All buffers and stock solutions were made with DNAse/protease-free water purchased from Fisher Scientific Inc. (Pittsburg, PA). All other reagents needed for buffers were purchased from Sigma-Aldrich (St. Louis, MO). UMB5 was custom-made by TriLink Biotechnologies, Inc. (San Diego, CA). All other oligonucleotides (sequences listed in Table 1) were obtained from Integrated DNA Technologies, Inc. (Coraville, IA). The concentrations of nucleic acid strands was determined using the Beer-Lambert law, a 1 cm quartz cuvette (volume of 100 µL), and extinction coefficients determined by using OligoAnalyzer 3.1 software (Integrated DNA Technologies, Inc.). Three independent different amounts of the same oligonucleotide were mixed with water to total volume of 100 µL and tested for their absorbance values at 260 nm using a Perkin-Elmer Lambda 35 UV/Vis spectrometer (San Jose, CA). The average of the concentrations calculated was used with relative standard deviations of each sample less than 10%. Working stock solutions of convenience concentrations were prepared for all sequences and stored frozen at -20°C until use.

Melt curve fluorescent assays

After samples were made, an optical adhesive cover was placed firmly on top of the plate and a tool was used to seal the wells. The plate was flicked to eliminate any formed bubbles, vortexed, and then spun at 660 rcf for 20 s.

The solutions were placed in the QuantStudio™ 6 Flex System and cooled (2°C/s) from room temperature to 5°C where they were annealed for 60 min. The fluorescence of the samples was then read continuously as the samples were heated (0.1°C/s) from 5°C to 50°C. The QuantStudio™ 6 Flex System software allowed for the selection of FAM™ dye to be read as the 'Target' and if ROX was utilized, it was selected as a 'Passive Reference'. The system was routinely calibrated for well factors, background, and dye fluorescence. It is important to note that samples taken after different calibrations of the system showed altered background fluorescence of UMB5 and the Control samples (with no analyte present); thus, depending on the date the experiment was conducted, some variation in fluorescent values between experiments may be observed. The QuantStudio™ Real-Time PCR Software (version 1.1) allows for real-time data analysis for initial processing, but all relevant data was exported to Excel for further analysis. The readings from at least two wells were averaged and replotted to produce the presented figures. The derivative of fluorescence over time was graphed by the QuantStudio™ Real-Time PCR Software and further processed in Excel. The maximum of the derivative plots gives the inflection point of the curve, also called the melting temperature (T_m).

Original fluorescent melt curves

In order to test if the Owl Sensor could bind to the target and differentiate between closely related sequences, preliminary temperature-dependent fluorescence measurements were performed using a QS6 real QuantStudio™ 6 Flex System from Life Technologies (Grand Island, NY). Buffer conditions were originally 50 mM HEPES, pH 7.4, 100 mM $MgCl_2$, 20 mM KCl, 120 mM NaCl, 0.03% Triton X-100, and 1% DMSO. Oligonucleotides

UMB5, R_X, P_X, and analytes inhC or inhT were added to wells in a 96-well plate (30 µL wells, although a 25 µL total volume was used) from stock concentrations so that all final concentrations were 200 nM. The fluorescence of the samples was divided by the fluorescence of UMB5 alone was reported as 'Normalized Fluorescence'.

Optimized fluorescent melt curves

After optimization, the buffer used contained 50 mM Tris-HCl, pH 7.4, 50 mM $MgCl_2$, and 0.1% Tween-20 with UMB5 and ROX (if used), R_X, P_Y, and analyte concentrations at 50 nM, 50 nM, 150 nM, 200 nM, and 100 nM, respectively.

Prior to mixing, stock solutions of oligonucleotides were allowed to thaw to room temperature, vortexed for 5 seconds, and centrifuged on a tabletop minicentrifuge for 10 seconds. A master mix solution containing R_X/P_Y was created such that adding 11.5 µL of the master mix to the samples (to a total volume of 25 µL) would result in R_X and P_Y concentrations of 150 nM and 200 nM, respectively. The master mix was used to make samples with the following names: Control, Mismatched, Matched, and Insertion and Deletion, if tested. The master mix solution (11.5 µL) was added to a 96-well plate (30 µL wells). Next, 1 µL of water, inhT, inhC, inh_del, or inh_ins was added to the plate to make the Control, Mismatched, Matched, Deletion, or Insertion samples, respectively. Another well was filled with 12.5 µL of water to serve as a control named 'UMB5'. A buffer-fluorophore solution containing 2X Buffer, 100 nM UMB5, and either 0 or 100 nM ROX was made. By adding 12.5 µL of the buffer-fluorophore solution, to each sample well, final concentrations of the fluorophores were 50 nM. ROX was used as a passive dye

reference since its fluorescence shows little fluctuation with temperature. Using ROX also allows for correction of well-to-well and plate-to-plate variations in fluorescence detection. Fluorescence was reported as F_{FAM}/F_{ROX}, where F_{FAM} is the fluorescence given off by the fluorophore attached to UMB5 and F_{ROX} is the fluorescence of the ROX reference dye.

Results and Discussion

Symmetric Owl Sensor

Combinations of symmetric Owl Sensors (R_Z/P_Z) were tested (See Figure 1 and 12 for drawings of structures). Owl Sensor adapter strands ranging from 12-8 nucleotides for R and P strands were tested. The pairs (R_{12}/P_{12} through R_8/P_8) were tested in the presence of both matched (inhC) and mismatched analytes (inhT). Results indicate that the R_9/P_9 pair demonstrate the most promising results for differentiating matched vs. mismatched analytes (Figure 13).

The derivative plots (Figure 14) show that the R_{12}/P_{12} pair is the most stable due to it having the highest T_m followed by R_{10}/P_{10}, R_{11}/P_{11}, and R_9/P_9, in that order. It is interesting to note that R_{10}/P_{10} shows a higher T_m than R_{11}/P_{11}, indicating that it forms a more stable structure even though it forms a shorter hybrid with the analyte.

Mismatches typically cause a reduction in T_m, but we see in the results that the R_{12}/P_{12} pair does not demonstrate a change in the T_m when a mismatch is present, indicating that the structure is incredibly stable, and the mismatch is not affecting the complex formation.

R_8/P_8 showed no signal above the background, indicating it is too short to allow for complex formation.

Testing other combinations of R and P to find the most optimum Owl Sensor

In order to determine the best combination of R/P for differentiation of similar nucleic acid sequences, further testing was done. Since the previous experiment revealed R_9/P_9 to be the best combination for symmetric Owl Sensors, all lengths of R were tested with P_9 (Figure 15 and 16); in addition, all lengths of P were tested with R_9, but these combination showed little differentiation ability, indicating that the shorter 9 nucleotide length analyte binding region must be in the P strand, to allow for the differentiation (Figure 17).

Results show that the best combination for differentiation of inhT and inhC is R_{10}/P_9 (Figure and Table 2). The matched analyte (inhC) shows significantly higher signal than both the control (no analyte) and a mismatched analyte (inhT) up to temperatures greater than 30°C. R_{11}/P_9 also shows some promise for correctly differentiating analytes, but the signal of the matched analyte becomes the same as that of the controls at a lower temperature (about 24°C) than for R_{10}/P_9 (32°C). Since R_{10} was shown to combine well with P_9, all lengths of P were tested with R_{10}. Results in Figure 18 show that R_{10}/P_9 was indeed the best combination of R and P for differentiation of matched and mismatched analytes is R_{10}/P_9.

The goal for selective biosensors is to have high signal above the background for the correct analyte and no signal above the background if the incorrect analyte is present. Therefore, in order to improve the performance of the Owl Sensor, buffer conditions, and oligonucleotide concentrations were altered to improve performance (Figure 19 and 20). Further characterization of the Owl Sensor continues in Chapters 3-6.

It is important to note that here, the Owl Sensor complementary to inhC and mismatched with inhT was tested. The resultant mismatched complex has a Guanine:Thymine base pair, commonly referred to as a “wobble” base pair as two hydrogen bonds can still form when G hydrogen bonds with T. For this reason, a G:T mismatch does not provide as large of a thermodynamic penalty as other mismatches, and can be difficult for other sensor types to differentiate between matched and mismatched analytes in a broad range of temperatures. Figure 21 shows X Sensor’s performance when the mismatched complex has a wobble base pair (Figure 21A) and when the mismatched complex has a C:A base pair, which results in a much larger thermodynamic penalty (Figure 21B). Results show the range for differentiation for a complex with a G:T mismatch is significantly lower than that for a C:A mismatch. However, Figures 19 and 20 show that the Owl Sensor has no problem distinguishing a wobble base pair as a mismatched analyte, as little signal above the background is observed.

Owl Sensor differentiation of SNVs

For some applications, nucleotide sequence discrepancies can include more than just the substitution of the correct base for an incorrect nucleotide (a mismatch). In addition,

nucleotide insertions and deletions can occur when one extra nucleotide is present, or missing, respectively. Mismatches, insertions, and deletions are referred to collectively as single nucleotide variations (SNVs). Figure 22 shows the ability of the Owl Sensor to differentiate insertions and deletions, revealing that the differentiation range for the R_{10}/P_9 Owl Sensor spans to 32.8°C for all the SNVs tested (mismatch, insertion, and deletion).

Owl Sensor specific to inhT

All previous results showed the Owl Sensor specific to inhC, in which P_9 binds to inhT with a G:T mismatch. When diagnosing SNVs, it can be important for practitioners to know which variation of a SNV is occurring in a patient sample. For this reason, an P strand specific to inhT was created (P_{9_A}) so that inhC would behave as a mismatched analyte, with a C:A mismatch. Results show that the Owl Sensor specific to inhT performs similarly as the R_{10}/P_9 variation (Figure 23A). Although there is a slightly higher signal for the SNV analytes, the differentiation ability is not compromised (Figure 23B), as $\Delta T_{1.5}$ extends from 5-32.4°C for all SNVs.

Figures and tables

Table 1: Sequences for all oligonucleotides in this study.

Name	Sequence	Purification
inhT (DNA)	5′–GCG GCA TGG GTA TGG GCC ACT GAC ATA ACA CAA GGA C	SD
inhC (DNA)	5′–GCG GCA TGG GTA TGG GCC ACT GAC ACA ACA CAA GGA C	SD
inhT (RNA)	5′–GCG GCA UGG GUA UGG GCC ACU GAC AUA ACA CAA GGA C	SD
inhC (RNA)	5′–GCG GCA UGG GUA UGG GCC ACU GAC ACA ACA CAA GGA C	SD
inh_ins	5′–GCG GCA TGG GTA TGG GCC ACT GAC ACCA ACA CAA GGA C	SD
inh_del	5′–GCG GCA TGG GTA TGG GCC ACT GAC AA ACA CAA GGA C	SD
inhT_Q	5′–GCG GCA TGG GTA TGG GCC ACT GAC ATA ACA CAA GGA C/BHQ1/	HPLC
inhC_Q	5′–GCG GCA TGG GTA TGG GCC ACT GAC ACA ACA CAA GGAC/BHQ1/	HPLC
Linear Probe	5′–/FAM/TCT TGT GTT GTG TCA GTG A	HPLC
MB Probe	5′–/FAM/CGCTC TTG TGT TGT GTC AGT GAGCG/BHQ1/	HPLC
UMB5	5′–/FAM/CGCG TTAA CATA CAAT AGAT CGCG/BHQ1/	SD
R_{12}	5′–CTATTG AGTGG CCCATA CGCGATC	SD
P_{12}	5′–AACGCG TTGTGT TGTGTC TATGTT	SD
R_{11}	5′–TATTG AGTGG CCCATA GCGATC	SD
P_{11}	5′–TAACGC TGTGTT GTGTC TATGT	SD
R_{10}	5′–TATTG AGTGG CCCAT CGATC	SD
P_{10}	5′–TAACG GTGTT GTGTC TATGT	SD
R_9	5′–TATTG AGTGG CCCA GATC	SD
P_9	5′–TAAC TGTT GTGTC TATGT	SD
P_{9_A}	5′–TAAC TGTT GTATC TATGT	SD
R_8	5′–ATTG AGTG GCCC ATCT	SD
P_8	5′–TTAA GTTG TGTC TATG	SD
A_{10}	5′–CGATC TATTG/peg/AGTGG CCCAT	SD
B_{11}	5′–TG TGTT GTGTC/peg/TATGT TAAC GC	SD
B_{10}	5′–G TGTT GTGTC/peg/TATGT TAAC G	SD
B_9	5′–TGTT GTGTC/peg/TATGT TAAC	SD
B_8	5′–GTT GTGTC/peg/TATGT TAA	SD
R_{12h}	5′–CTATTG AGTGGC TCATAC CGCGAT	SD

Name	Sequence	Purification
R_{11h}	5′–TATTG AGTGG TCCATA GCGATC	SD
R_{10h}	5′–TATTG AGTGG TCCAT CGATC	SD
$R_{10\_o\text{-}peg}$	5′–TATTG AGTGG CCCAT/peg/CGATC	SD
$P_{9\_i\text{-}peg}$	5′–TAAC TGTT GTGTC/peg/TATGT	SD
$P_{9\_o\text{-}peg}$	5′–TAAC/peg/TGTT GTGTC TATGT	SD
miDNA99a	5′–AA CCCGT AGATC CGATC TTGT G	SD
miDNA100	5′–AA CCCGT AGATC CGACC TTGT G	SD
miRNA99a	5′–AA CCCGU AGAUC CGAUC UUGU G	SD
miRNA100	5′–AA CCCGU AGAUC CGACC UUGU G	SD
R_{12_mi}	5′– CTTATTG GATCTA CGGGTT CGCGATC	SD
R_{11_mi}	5′–CTTATTG GATCTA CGGGT GCGATC	SD
R_{10_mi}	5′–TTATTG GATCT ACGGG CGATC	SD
$P_{9\_mi\_99a}$	5′–TAAC ACAA GATCG TATGT	SD
$P_{9\_mi\_100}$	5′–TAAC ACAA GTTCG TATGT	SD

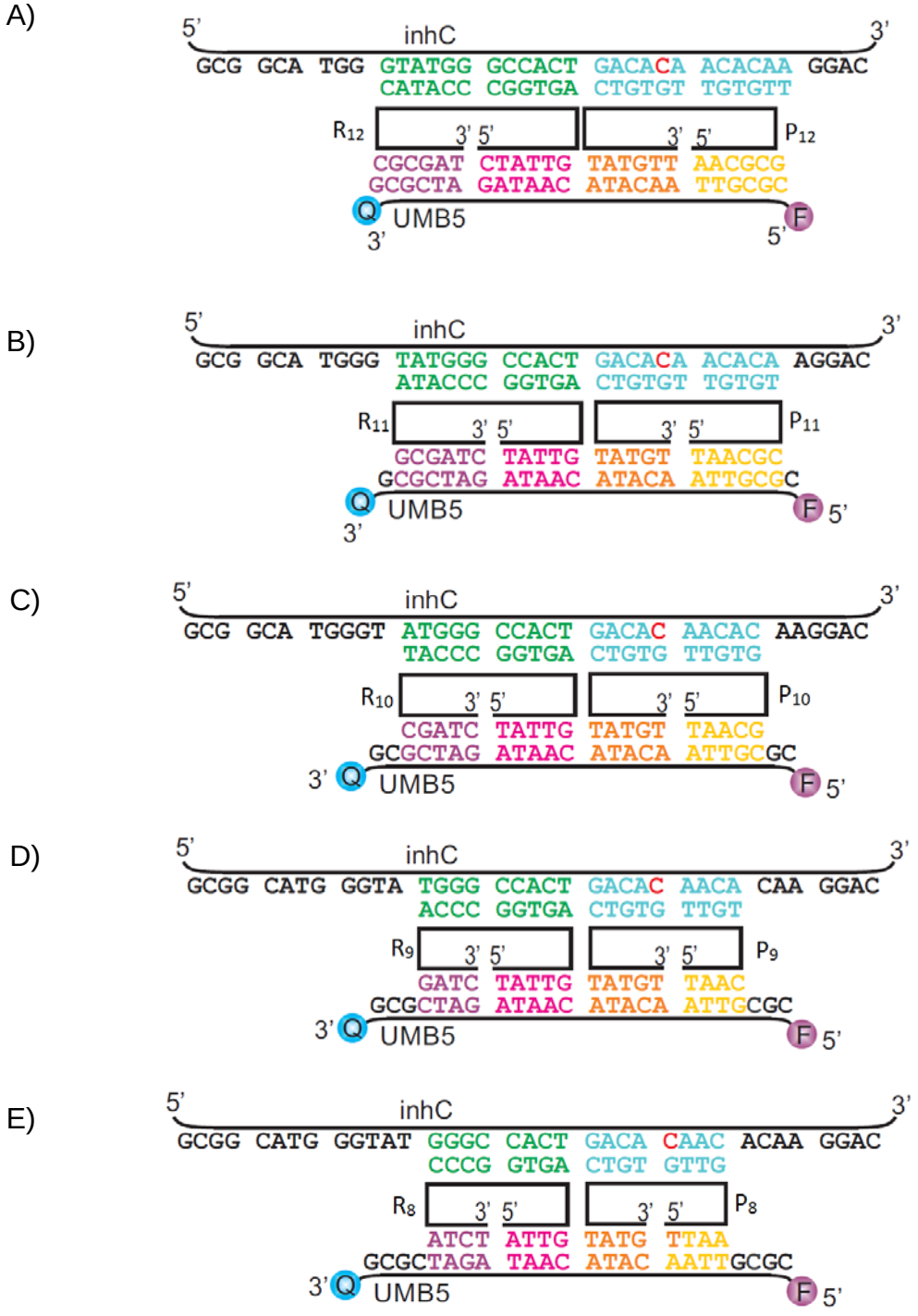

Figure 12. Drawings of the symmetric Owl Sensors.
Sequence hybridization of the symmetric Owl Sensor. A-E show R and P lengths 12-8, respectively.

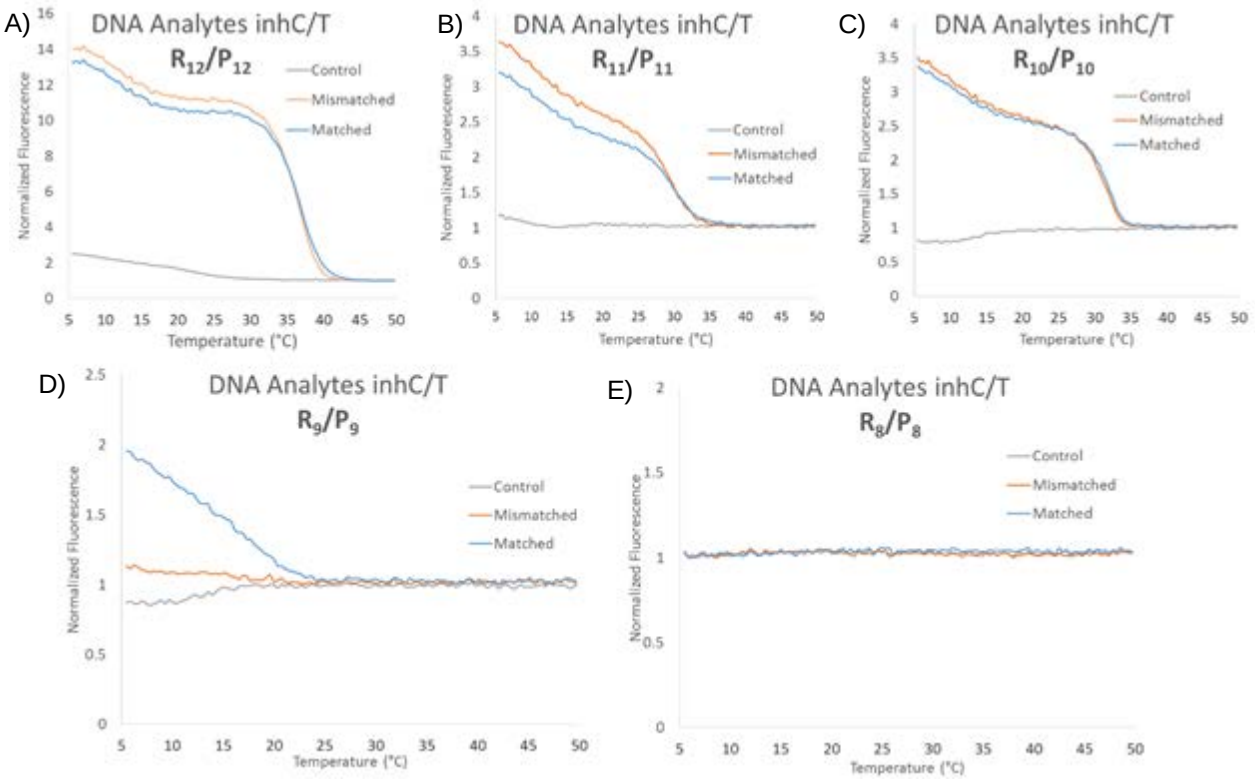

Figure 13. Melting curves for symmetric Owl Sensors (R_Z/P_Z) show that only R_9/P_9 is able to differenitate matched and mismatched analytes.

Lines indicate the Fluorescence of the sample divided by the fluorescence of UMB5. Blue, orange, and grey lines indicated matched, mismatched, and no analyte, respectively.

A-C) Owl sensors with 12-10 nucleotides for both R and P (R_{12}/P_{12}, R_{11}/P_{11}, and R_{10}/P_{10}) showed no ability to differentiate matched and mismatched analytes.

D) The combination of R_9/P_9 was found to show promise for differentiating matched and mismatched analytes, as the signal produced by the matched analyte complex was significantly higher than that of the msimatched up to about 20°C.

E) The combination of R_8/P_8 showed no signal above the control with no analyte present, indicating that 8 nucleotide analyte binding domains on each side are too short for any complex formation.

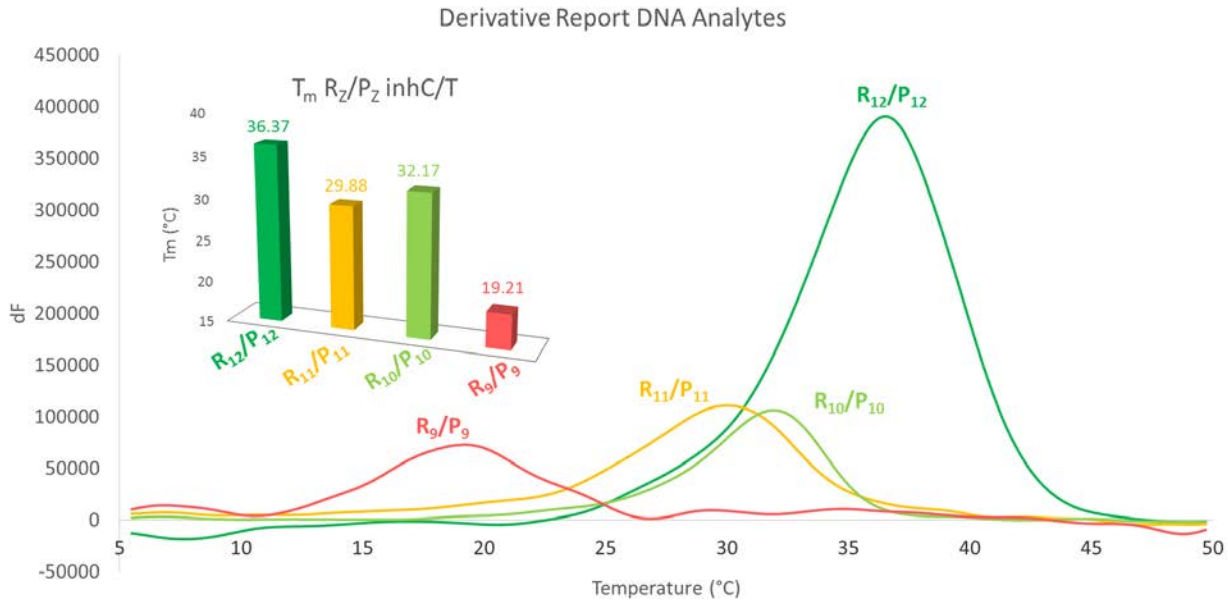

Figure 14: Derivative plots and T_m of symmetric Owl Sensors show that R_{10}/P_{10} is more stable than R_{11}/P_{11}.

The derivative plots of the symmetric Owl Sensors. Complex stabilities, which correlate with the melting temperatures (found from the peak maximums), rank from strongest complex to weakest by adapter strands lengths as follows: 12, 10, 11, and 9. The inset shows the melting temperatures (T_m) of each set.

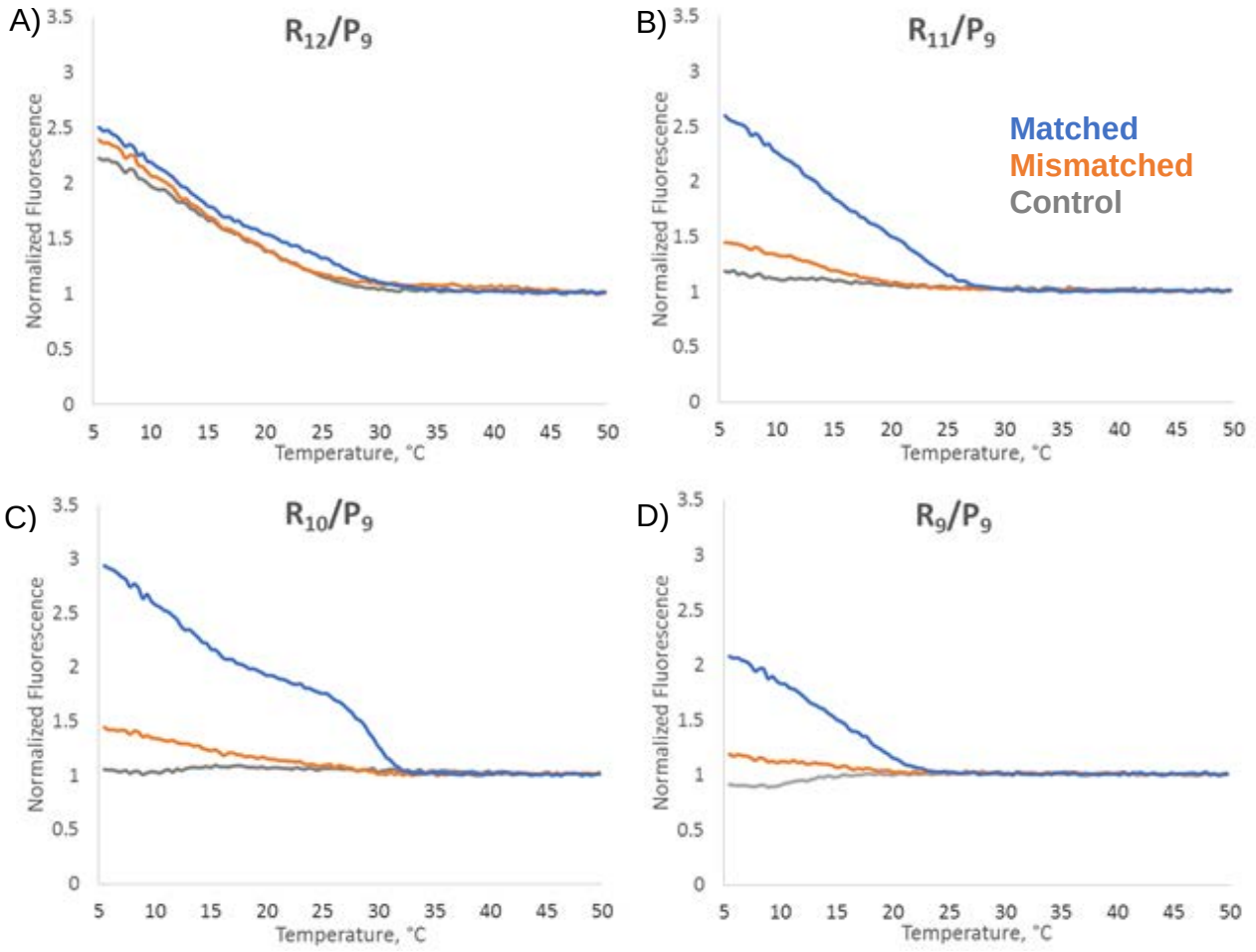

Figure 15: Melt curves for R_X/P_9 show that R_{10} is the best combination with P_9 for differentiation of matched and mismatched analytes

Lines indicate the Fluorescence of the sample divided by the fluorescence of UMB5. Blue, orange, and grey lines indicated matched, mismatched, and no analyte, respectively.

A) The R_{12}/P_9 combination did not differentiate between matched and mismatched analytes.

B) The R_{11}/P_9 shows decent differentiation between matched and mismatched analytes, with differentiation stopping at 24°C.

C) R_{10}/P_9 shows the most promise as a selective sensor. With high signal for the matched analyte and minimal signal for the mismatched analyte, differentiation continues up to 31°C.

D) As tested previously in Figure 13, R_9/P_9 can differentiate matched and mismatched analytes up to 18°C.

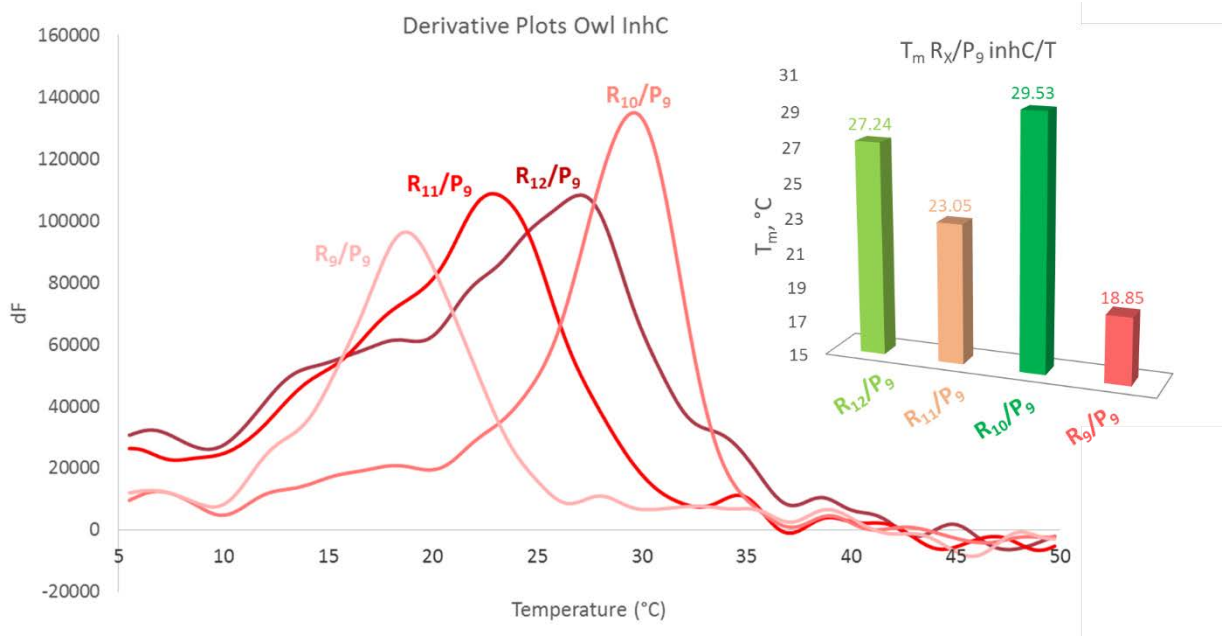

Figure 16. Derivative plot for R_X/P_9 shows that the most stable R strand with P_9 is R_{10}.

The derivative plots of the asymmetric Owl Sensors when all lengths of R were combined with P_9. Complex stabilities, which correlate with the melting temperatures (found from the peak maximums), rank from strongest complex to weakest as follows: R_{10}, R_{12}, R_{11}, R_9 . The inset shows the melting temperatures (T_m) of each set.

.

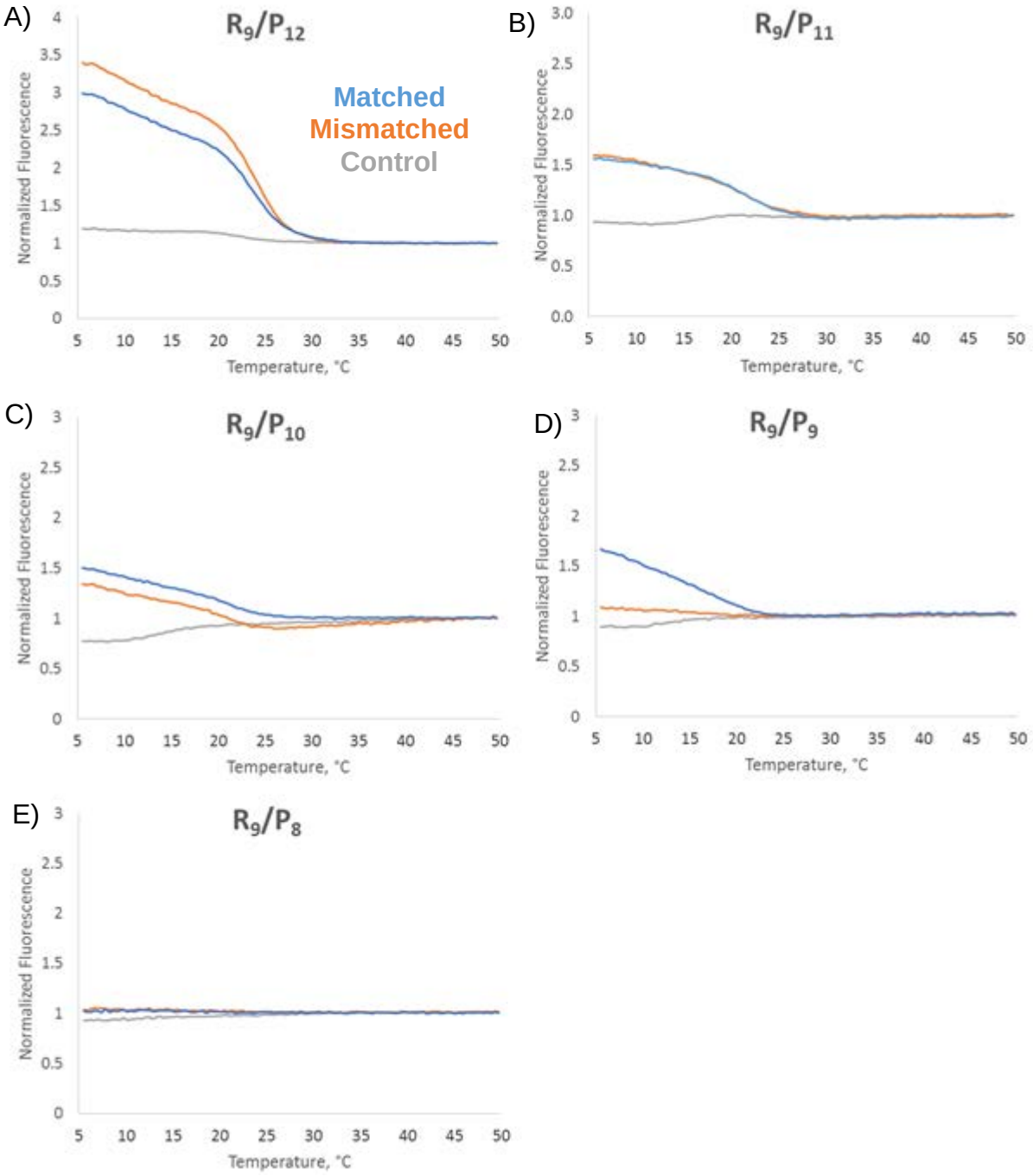

Figure 17. Testing all lengths of P with R_9 found resulted in poor differentiation bettween matched and mismatched analytes.

Results show that there is poor differentiation except for the case of R_9/P_9, as was shown in previous experiments. It can be concluded that R_9 is a less than optimum length for the R strand, further validating that the best combination is R_{10}/P_9 for the Owl Sensor specific detecting DNA analytes.

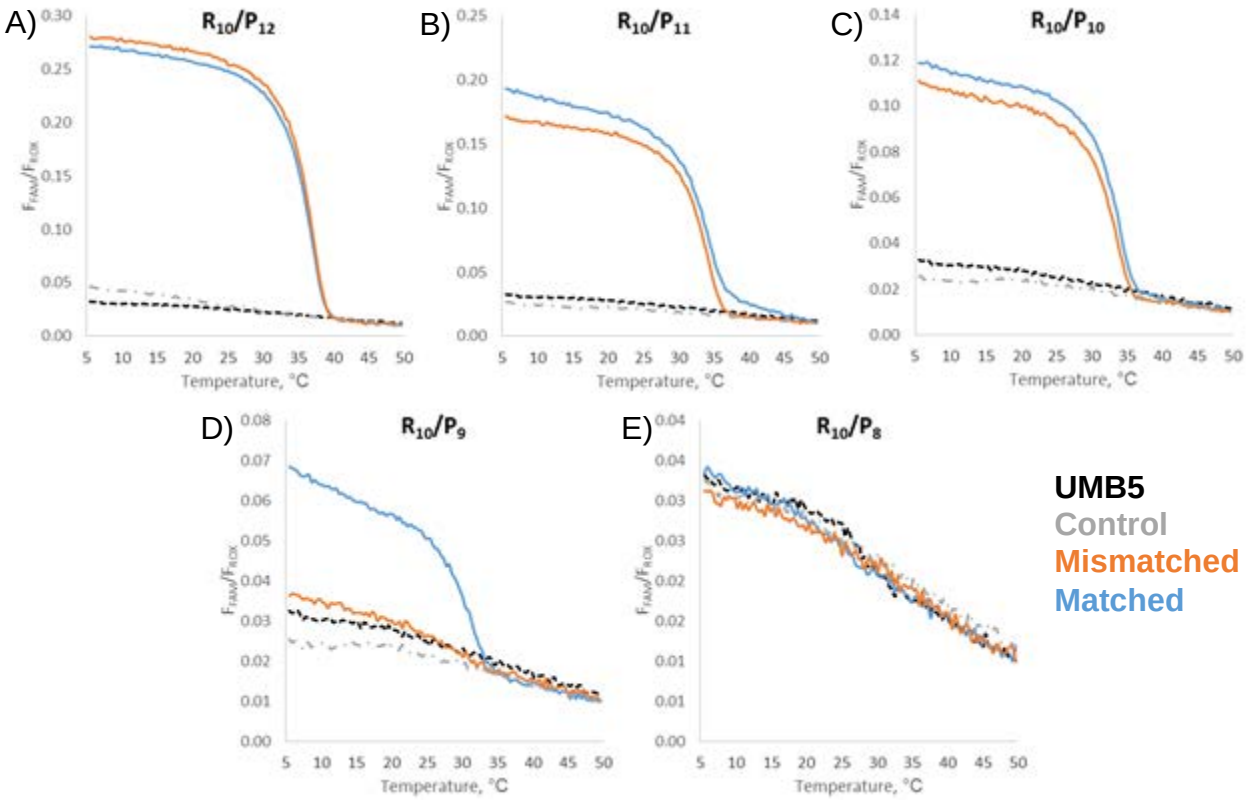

Figure 18. Testing all lengths of P with R_{10} affirms that the best combination for differentiation is R_{10}/P_9.

Results show that there is poor differentiation except for the case of R_{10}/P_9, as was shown to be a good combination in previous experiments.

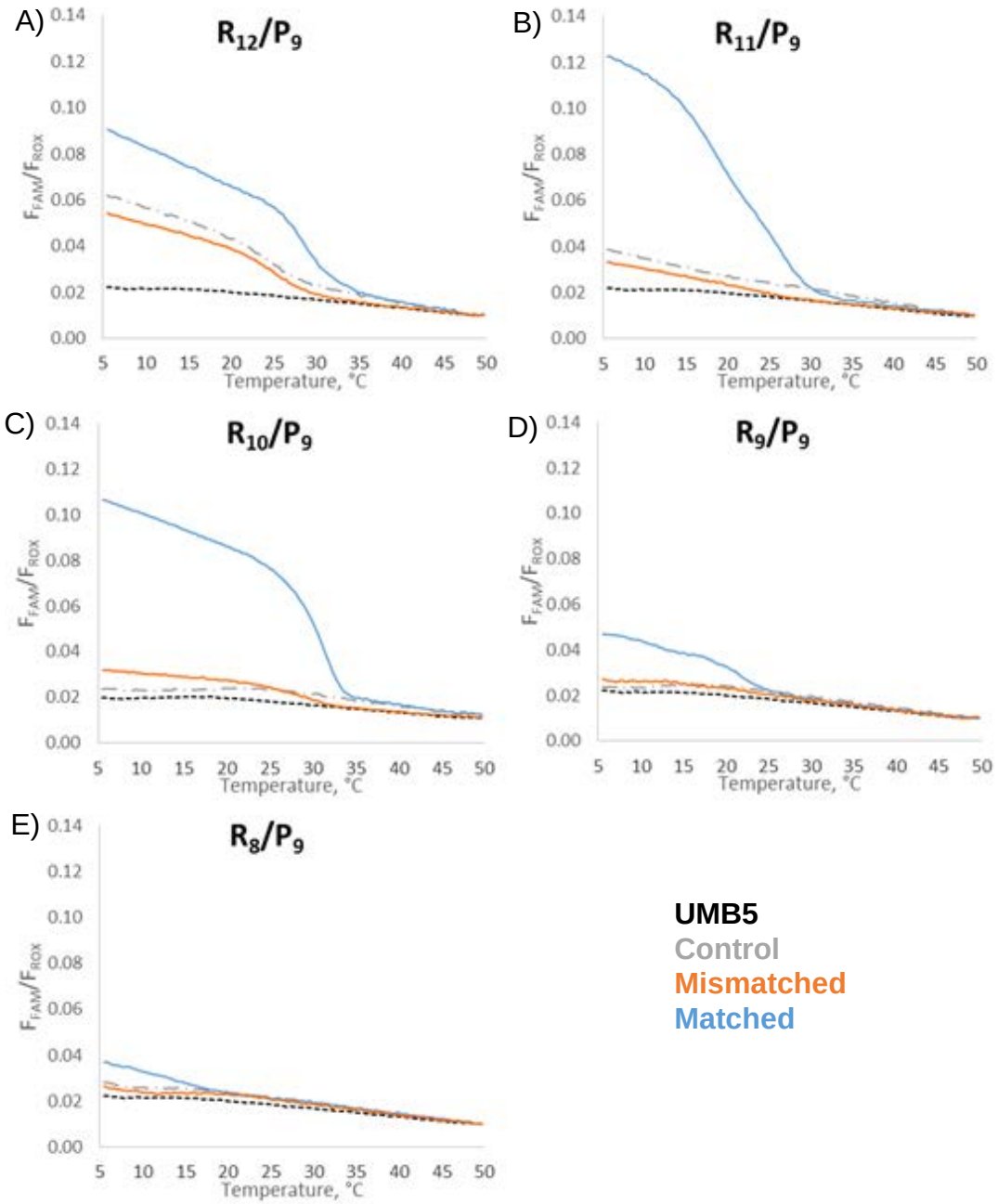

Figure 19. Optimized melt curves of R_X/P_9 show that R_{11} and R_{10} have improved signal for the matched analyte with mismatched analytes showing only background fluorescence with.

The optimized conditions uses a different buffer (now 50 mM Tris-HCl, pH 7.4, 50 mM $MgCl_2$, and 0.1% Tween-20) with altered strand concentrations (now 50 mM, 100 nM, 50 nM, 150 nM, and 200 nM for ROX, analyte, UMB5, R, and P, respectively).

A) Little differentiation between matched and mismatched analytes is observed.

B-C) Excellent differentiation between matched and mismatched analytes

D) Differentiation is observed, but it does not extend to higher temperatures, and a low signal is seen.

E) No signal above the background is seen for R_8/P_9.

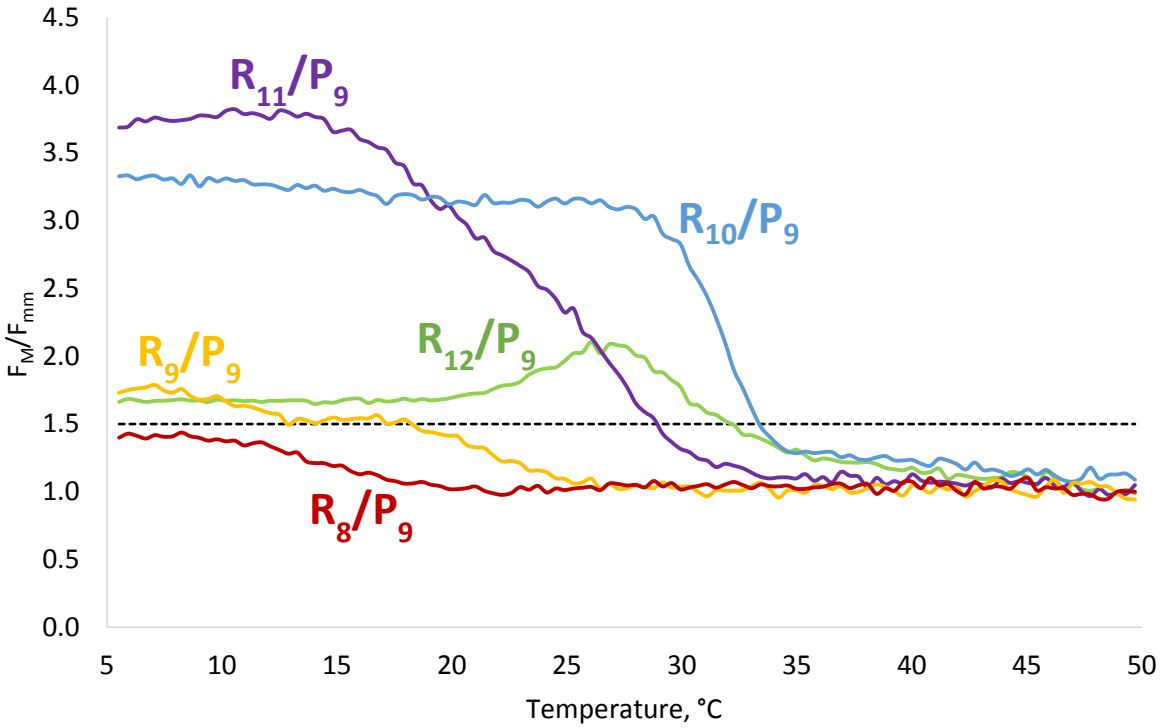

Figure 20. Temperature differentiation range for R_X/P_9 Owl Sensors.

By dividing the fluorescence of the matched analyte by the fluorescence of the mismatched analyte (F_M/F_{mm}) from Figure 19, the differentiating power can be quantified. The green, purple, blue, yellow, and maroon lines represent P_9 in combination with R_{12}, R_{11}, R_{10}, R_9, and R_8, respectively. Here we see that R_{10}/P_9 shows the largest temperature range for differentiation, spanning 5-33°C. The horizontal line labeled $\Delta T_{1.5}$ indicates the line being used to determine differentiability.

Table 2: Differentiation Ranges for Owl Sensor R_X/P_9 shows the largest temperature range for differentiation is R_{10}/P_9.

x	$\Delta T_{1.5}$	Temperature Range (°C)
12	26.9	5.0-31.9
11	23.8	5.0-28.8
10	27.0	5.0-33.0
9	12.9	5.0-17.9
8	0.0	--

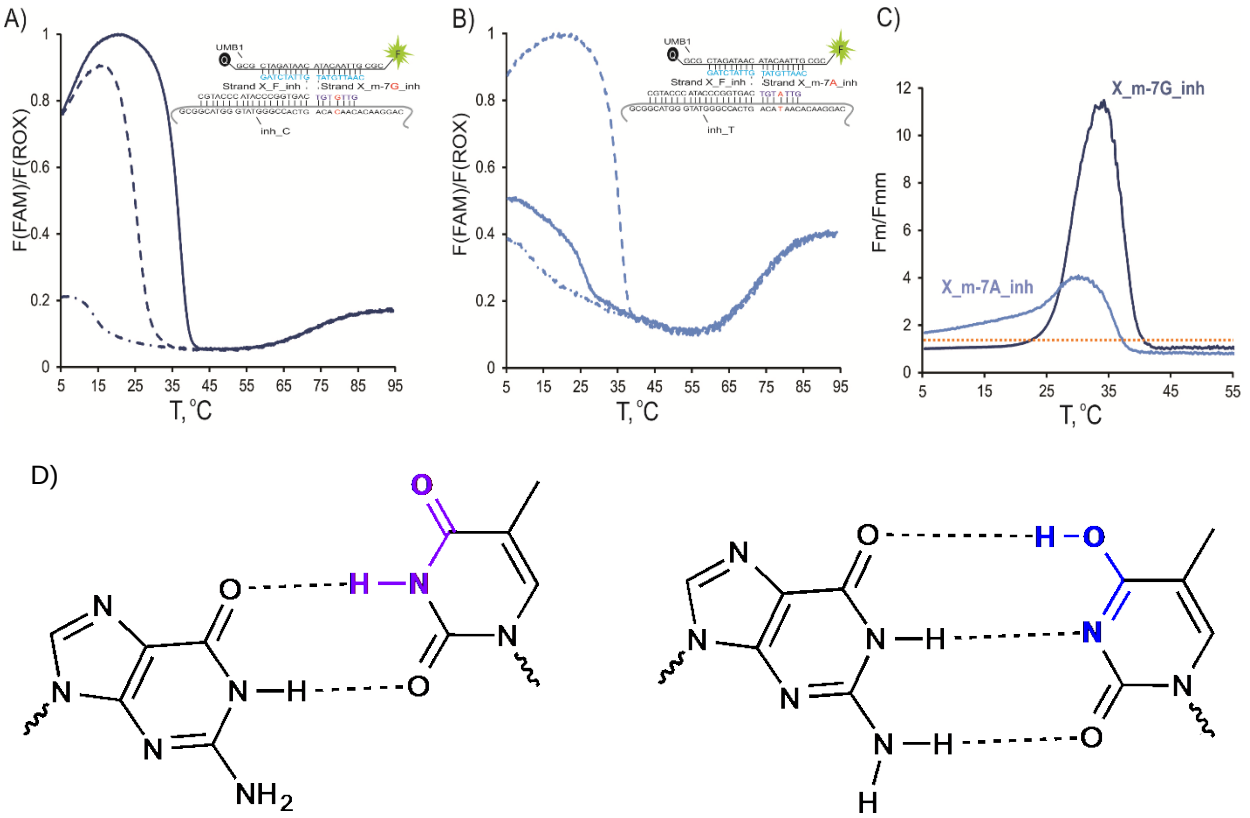

Figure 21. Limited differentiation ablity of X sensor to a C→T mutation.[16]

A) Melting curves of X sensor in complex with the inhC fully matched analyte (solid line) and inhT mismatched (dashed line) analyte. A schematic of the complex formed with the fully matched analyte is shown in the inserted figure.

B) The X Sensor shows better melting curve performance when the fully matched analyte to the mutated analyte, inhT. Therefore, the mismatched base is a C:A base pair, which provides for a larger thermodynamic penalty, and improved differentiation.

C) Ratio of fluorescence responses of X sensors to the presence of corresponding fully matched (F_m) to mismatched (F_{mm}) analytes. The threshold F_m/F_{mm} ~ 1.5 is indicated by orange dotted line. Results show that limited differentiation is observed when analyzing a G:T mismatch caused by a C→T mutation.

D) The Guanine:Thymine "wobble" base pair shows two possible hydrogen bonds when thymine is in the keto form and three hydrogen bonds when the thymine goes is in the enol tautomer, shown on the right. For this reason, it can be difficult for many probes to distinguish G:T mismatches in a wide range of temperatures.

Part of this figure and legend was adopted with permission from the PhD thesis of Maria Stancescu.

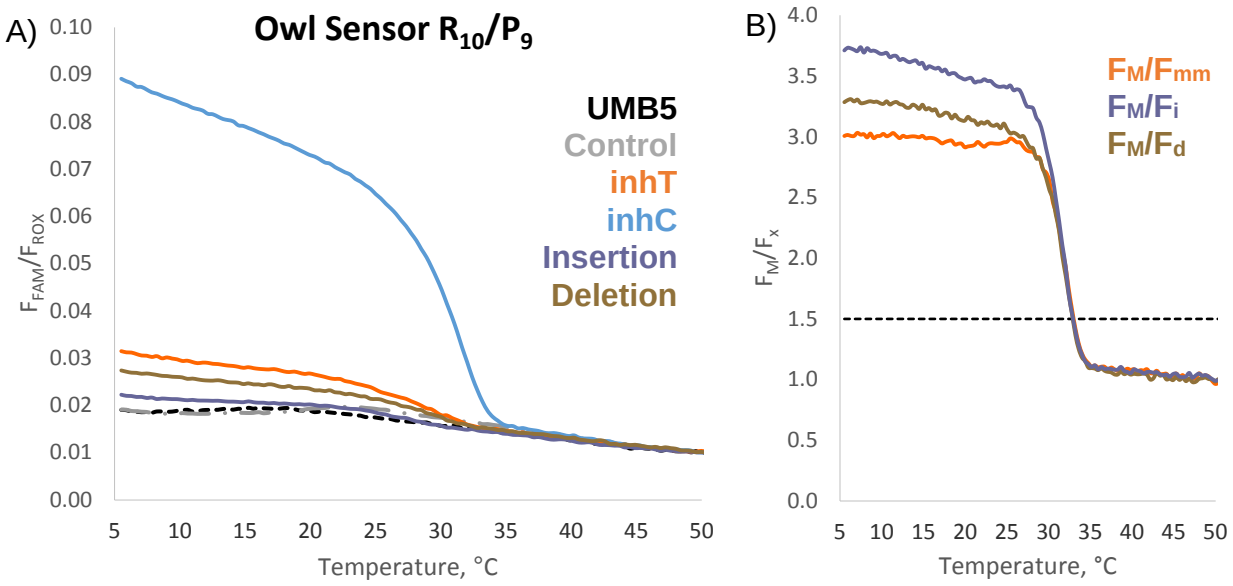

Figure 22. The Owl Sensor shows excellent differentiation of SNVs when analyzing DNA analytes.

A) Melt Curve for R_{10}/P_9 with DNA analytes shows high signal for the matched analyte (blue) with minimal signal for insertion (purple line), deletion (brown line), and mismatched (orange) analytes. The signal from UMB5 alone is represented by the black dashed line, and the signal from the control (UMB5 with R_{10} and P_9) is represented by the grey dotted dashed line.

B) Differentiation ability for R_{10}/P_9 with DNA analytes shows the Owl Sensor can be assessed by graphing F_M/F_{mm}. Results show that differentiation is achieved up to 32.8°C for all SNVs tested.

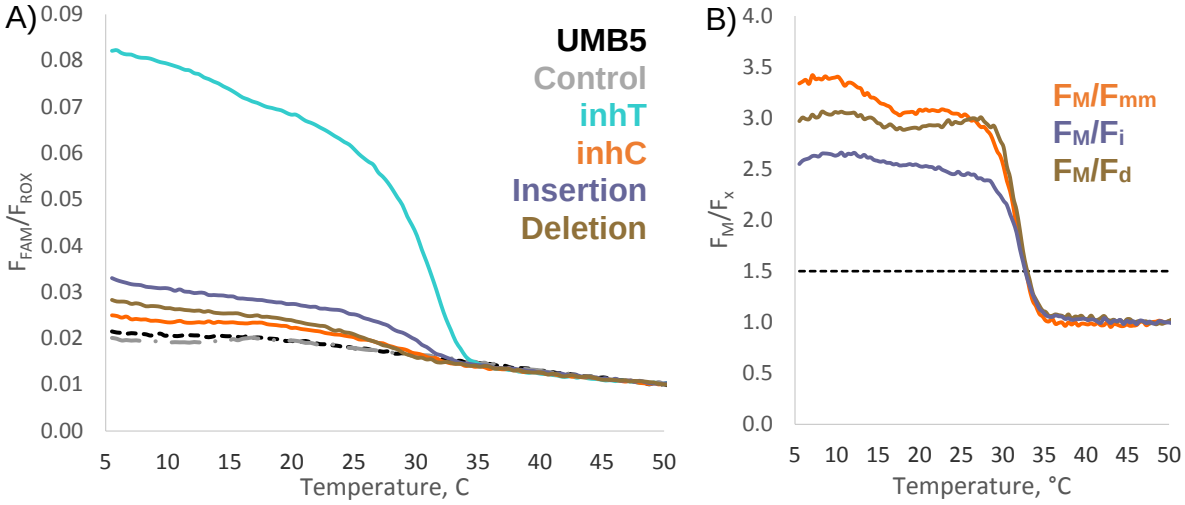

Figure 23. Owl Sensor specific to inhT DNA shows excellent performance.

A) Melt Curve for R_{10}/P_{9_A} with DNA analytes shows high signal for the matched analyte (teal) with minimal signal for insertion (purple line), deletion (brown line), and mismatched (orange) analytes. The signal from UMB5 alone is represented by the black dashed line, and the signal from the control (UMB5 with R_{10} and P_{9_A}) is represented by the grey dotted dashed line.

B) Differentiation ability for R_{10}/P_{9_A} with DNA analytes shows the Owl Sensor can be assessed by graphing F_M/F_{mm}. Results show that differentiation is achieved up to 32.6°C for all SNVs tested.

CHAPTER 3: HELICITY MATTERS

Introduction

The field of DNA Nanotechnology has utilized knowledge about the helicity of DNA to fold DNA strands into various shapes including triangles, smiley faces, tiles, and flasks (Figure 24). Because hybridization of DNA is known and predictable, DNA strands can be designed to fold in ways not found in nature to create shapes. To hold these structures together, small DNA strands are designed to jump from one helix to another, forming four way junctions (4WJ) that bind together parallel helices (Figure 25). In order to ensure that 2D shapes are indeed flat, these structures must be carefully designed so that the strands that hold together these structures enter and exit a helix with the same angle, allowing for planar structures (Figure 26). Typically planar shapes utilize strands with 21 bp portions, roughly 2 full helical turns of binding, allowing the strand to enter and exit the helix at the same angle, which reduces strain on the complex and the junction.[26,27] In order to fold DNA into a curved or warped shape, binding portions shorter or longer than 21 bp allow for nonplanar structures that exhibit strain to curve the parallel helices into 3D shapes.[27]

The dogma of common hybridization probes based on the nearest neighbor model[24] states that as more nucleotides are added, the stronger hybridization becomes due to more nucleotides being available for stacking interactions, and subsequently a more negative ΔG. When it comes to differentiating SNVs, a longer adapter strand allows for stronger hybridization, but additional length comes at the cost of losing differentiability, as if enough nucleotides are present, the energy penalty from the incorrect nucleotide can

be compensated for by additional nucleotides.[25] For this reason, the LP probes, MB probes, and the X Sensor all require length optimization to allow for optimum selectivity.

As such, the Owl Sensor was originally designed with adapter strand lengths from 8-12 nucleotides for both R and P to allow for testing of the most optimum length. It was expected that the longer the adapter strands, the more stable complex that would be formed with the matched analyte. However, when examining the derivative plots of symmetric R_Z/P_Z Owl Sensors, the R_{10}/P_{10} sensor showed to be more stable than R_{11}/P_{11} (Figure 14). This led us to believe that the helicity of DNA may be influencing the stability of these complexes. DNA-DNA hybrids typically adopt the B-DNA conformation as shown in Figure 27 where one helical turn takes 10.4 base pairs (bp). The Owl Sensor was designed so that the middle of the adapter strands bind easily to the analyte, but can only bind to UMB5 by folding around to adopt a constrained confirmation. By utilizing an R adapter strand whose analyte binding portion has the same length as one full helical turn of DNA, binding to UMB5 can be accomplished with less strain on the strand. At one helical turn, the binding arms that bind to UMB5 will exit the analyte:R helix with the same angle. A longer analyte binding portion results in an analyte:R helix with greater than one full helical turn, causing strain on the MB binding arms due to their different exiting trajectories from the helix. A shorter analyte binding domain results in a helix with less than one helical turn, adding strain to the system in a similar fashion. For this reason, it is believed that R_{10} provides the most stabilization for the Owl Sensor, as it is the probe whose length allows for a duplex closest to one full helical turn.

In addition, the helicity of DNA can provide a reason why P_9 is the best for differentiating SNVs. It is hypothesized that if a stable R is present, the analyte:P_9 portion of the helix can also bind if the fully matched analyte is present even though it may be helically strained. Since mismatches, deletions, and insertions cause DNA to unwind to accommodate imperfect base pairing, any variation in sequence in the analyte results in a complex with much larger helical strain, destabilizing the complex and resulting in little fluorescent response.

For this reason, R_{10}/P_{10} can be thought of as the “Perfect Structure”, as both its adapter strands will exit the analyte helix at nearly the same angle, allowing for easier binding of UMB5. However, in this perfect structure, imperfections such as SNVs can be tolerated. Just like a stable bridge can absorb stress such as a semi-trailer running into a support truss, the R_{10}/P_{10} nanostructure was shown to absorb the free energy penalty due to a sequence variation. Similar to how an already strained bridge can collapse when a stress is introduced, the R_{10}/P_9 Owl Sensor cannot withstand additional stresses or strains introduced by SNVs due to its already slightly strained nature. For this reason, R_{10}/P_9 allows for high complex formation when the correct analyte is present, while SNVs show little to no signal after 1 hour of incubation at 5˚C (Figure 22).

To demonstrate this, further experiments were conducted to provide evidence for the hypothesis that helicity contributes to the Owl Sensor’s ability to differentiate SNVs.

Materials and Methods

Reagents

All buffers and stock solutions were made with DNAse/protease-free water purchased from Fisher Scientific Inc. (Pittsburg, PA). All other reagents needed for buffers were purchased from Sigma-Aldrich (St. Louis, MO). UMB5 was custom-made by TriLink Biotechnologies, Inc. (San Diego, CA). All other oligonucleotides (sequences listed in Table 1) were obtained from Integrated DNA Technologies, Inc. (Coraville, IA). The concentrations of nucleic acid strands was determined using the Beer-Lambert law, a 1 cm quartz cuvette (volume of 100 µL), and extinction coefficients determined by using OligoAnalyzer 3.1 software (Integrated DNA Technologies, Inc.). Three independent different amounts of the same oligonucleotide were mixed with water to total volume of 100 µL and tested for their absorbance values at 260 nm using a Perkin-Elmer Lambda 35 UV/Vis spectrometer (San Jose, CA). The average of the concentrations calculated was used with relative standard deviations of each sample less than 10%. Working stock solutions of convenience concentrations were prepared for all sequences and stored frozen at -20°C until use.

Melt Curve Fluorescent Assays

Prior to mixing, stock solutions of oligonucleotides were allowed to thaw to room temperature, vortexed for 5 s, and centrifuged on a tabletop minicentrifuge for 10 seconds. A master mix solution containing R_X/P_Y was created such that adding 11.5 µL of the master mix to the samples (to a total volume of 25 µL) would result in R_X and P_Y

concentrations of 150 nM and 200 nM, respectively. The master mix was used to make samples with the following names: Control, Mismatched, Matched, and Insertion and Deletion, if tested. The master mix solution (11.5 µL) was added to a 96-well plate (30 µL wells). Next, 1 µL of water, inhT, inhC, inh_del, or inh_ins was added to the plate to make the Control, Mismatched, Matched, Deletion, or Insertion samples, respectively so that the final concentration of the analyte was 100 nM. Another well was filled with 12.5 µL of water to serve as a control named 'UMB5'.

The buffer used contained 50 mM Tris-HCl, pH 7.4, 50 or 10 mM $MgCl_2$, and 0.1% Tween-20 with UMB5 and ROX (if used). A buffer-fluorophore solution containing 2X Buffer, 100 nM UMB5, and either 0 or 100 nM ROX was made. By adding 12.5 µL of the buffer-fluorophore solution, to each sample well, final concentrations of the fluorophores were 50 nM. ROX was used as a passive dye reference since its fluorescence shows little fluctuation with temperature. Using ROX also allows correction for well-to-well and plate-to-plate variations in fluorescence detection. Fluorescence was reported as F_{FAM}/F_{ROX}, where F_{FAM} is the fluorescence given off by the fluorophore attached to UMB5 and F_{ROX} is the fluorescence of the ROX reference dye.

After samples were made, an optical adhesive cover was placed firmly on top of the plate and a tool was used to seal the wells. The plate was flicked to eliminate any formed bubbles, vortexed, and then spun at 660 rcf for 20 s.

The solutions were placed in the QuantStudio™ 6 Flex System and cooled (2°C/s) from room temperature to 5°C where they were annealed for 60 min. The fluorescence of the samples was then read continuously as the samples were heated (0.1°C/s) from 5°C to 50°C. The QuantStudio™ 6 Flex System software allowed for the selection of FAM™ dye to be read as the 'Target' and if ROX was utilized, it was selected as a 'Passive Reference'. The system was routinely calibrated for well factors, background, and dye fluorescence. It is important to note that samples taken after different calibrations of the system showed altered background fluorescence of UMB5 and the Control samples (with no analyte present); thus depending on the date the experiment was conducted, some variation in fluorescent values between experiments may be observed. The QuantStudio™ Real-Time PCR Software (version 1.1) allows for real-time data analysis for initial processing, but all relevant data was exported to Excel for further analysis. The readings from at least two wells were averaged and replotted to produce the presented figures. The derivative of fluorescence over time was calculated by the QuantStudio™ Real-Time PCR Software. The maximum of the derivative plots gives the inflection point of the curve, also called the melting temperature (T_m).

Results and Discussion

The Perfect Structure: R_X/P_{10}

Previous results showed that P_9, a strained P stand due to its P:analyte duplex being less than one full helical turn, provided the best length for distinguishing SNVs. The hypothesis is that P_9 is stable enough to allow for complex formation when the matched analyte is

present, but that an imperfection in base-pairing caused by an SNV in the analyte causes the strained nanostructure to collapse, resulting in low fluorescent output. To show that a constrained P strand is necessary for differentiation, all lengths of R were tested with P_{10}, an unstrained P strand whose length allows for 1 full helical turn in the analyte:P helix. Results show that P_{10} does not support good differentiation between matched and mismatched analytes, indicating that a P strand with optimum helicity can accommodate a mismatch in the analyte (Figure 28). The derivative plot revealed that R_{10}/P_{10} is the most stable combination of R with P_{10}, indicating that strands with optimum helicity result in more stable nanostructures (Figure 29). While this experiment provided evidence as to why P_9 is the most optimum adapter strand, the next two experiments will provide evidence as to why R_{10} is the most optimum adapter strand for DNA analytes.

A mismatch in the R strand

While 10 nucleotides is the best for stabilizing the R strand, if a mismatch was present in the region the R hybridizes with the analyte, poorer performance is expected. A large decrease in performance will especially occur if the mismatch unwinds the DNA hybrid, making it adopt a conformation with less optimum exit trajectory. If a mismatch unwinds a helix with greater than one full helical turn, making it adopt a more optimum exit trajectory than it did before, then a mismatch will not cause as large of a decrease in sensor performance.

Here, a mismatch in the R strand is indicated by adding an ‘h’ to the name of the strand (for example R_{10h}). Figure 30C shows that a mismatch is not tolerated in the R_{10h}/P_9 Owl

Sensor as there is a great reduction in signal when a mismatch is introduced into the R strand, as seen in the light blue line. However, as seen in Figure 30B, a slightly longer probe, R_{11h} can accommodate a mismatch in the R strand, as it does not shows minimal reduction in the signal of the matched analyte (inhC). An 11 bp hybridization is lightly longer than the 10.4 bp required for on full turn of DNA. It is possible that a mismatch in the 11 nucleotide long R strand may slightly unwind the helix, still allowing for decent hybridization with the inhC analyte. This indicates that the mismatch may be slightly unwinding the 11 bp helix so that it does not show a great reduction in complex formation.

The Owl Sensor for RNA Analytes

RNA-DNA hybrids typically adopt a different helical conformation called A-DNA that has 11.1 bp/turn. When testing all the lengths of R with P_9 on RNA analytes, results how that the R_{11}/P_9 is the best combination for differentiating SNVs for RNA analytes, further indicating that the helicity of the complex matters in order for proper complex formation (Figure 32). R_{10}/P_9 does not form a complex with the correct RNA analyte, suggesting that having a probe much shorter than one full helical turn does not favor complex formation. Not only does this study show that the Owl Sensor can be used to analyze RNA products, it suggests that the optimal length of the analyte:R duplex occurs when the length of R is closest to the length of on full helical turn. The R_{11}/P_9 Owl Sensor differentiated between matched and mismatched analytes in a temperature range of 5-27.35°C (Figure 32B). The R_{11}/P_{9_A} Owl Sensor performed similarly, with maintained differentiation from 5-27.37°C (Figure 32C and D).

Figures and Tables

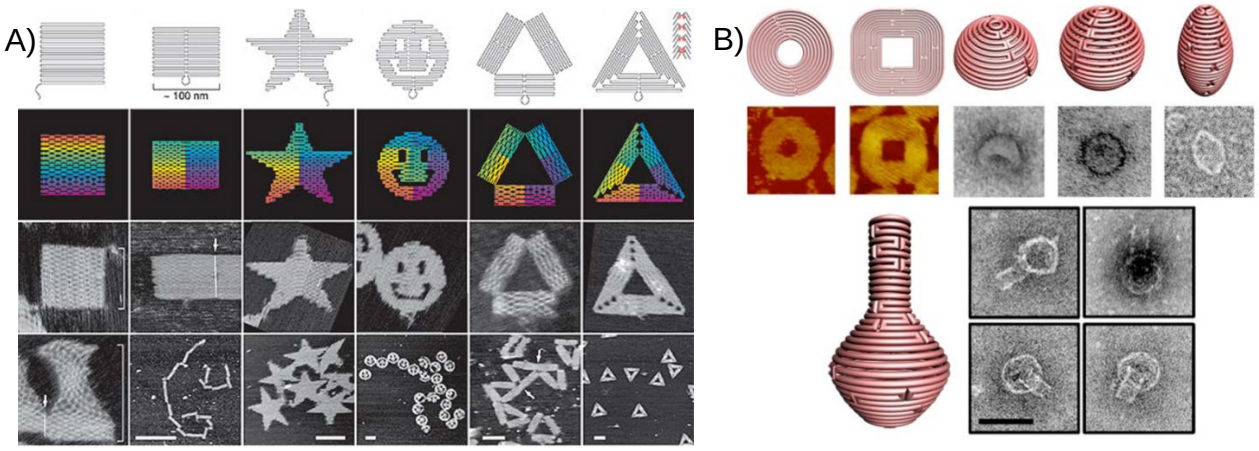

A) Adapted by permission from Macmillan Publishers Ltd: Nature. Rothemund, PWK. *Folding DNA to create nanoscale shapes and patterns*. Nature, 2006. 440: p. 297-302., copyright 2006.
B) From Han, D., Pal, S., Nangreave, J. Deng, Z. Liu, Y., and Yan, H. *DNA Origami with Complex Curvatures in Three-Dimensional Space*. Science, 2011. 332: p. 342-346. Reprinted with permission from AAAS.

Figure 24: DNA Origami folds DNA strands into complex 2D[26] and 3D[27] shapes.

With predictable sequence complementarity, it is easy to design structures of desired shapes. These images demonstrate the ability to intricately control the folding of DNA into predetermined nanostructures.
A) 2D shapes made by Rothemund.[26]
B) 3D shapes made by Yan and colleagues.[27]

Figure 25. Four Way Junction picutred shows the strain involved from jumping helices.

The blue and red strands jump from one helix to another. Strain can be seen in the crossover, as the nucleotides reach to complete their base pairs.

Image from http://www.lifesci.dundee.ac.uk/groups/nasg/research.php

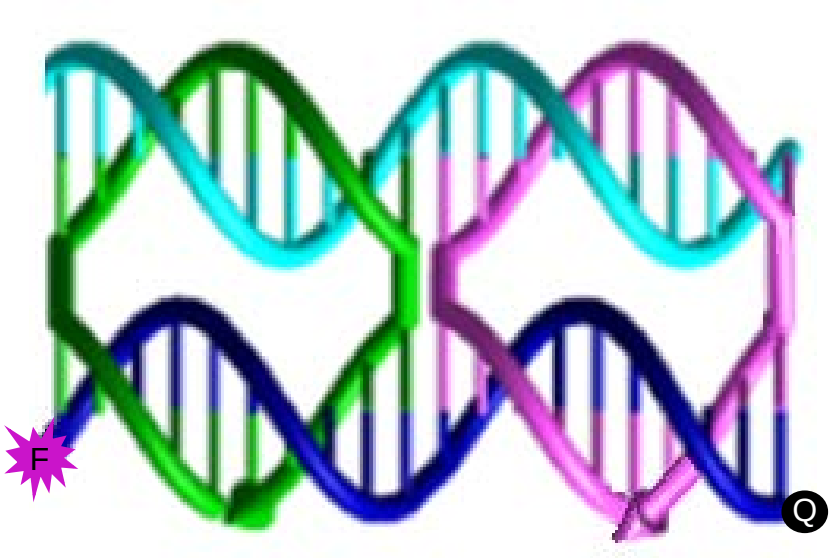

Figure 26. Helical turns for a DNA Crossover motif.

Figure adapted from Zadegan and Norton.[28]
DNA complex shows a DNA Crossover motif in the Owl Sensor. The cyan strand represents the analyte of interest and the dark blue strand represents UMB5 in its open conformation where high fluorescence is observed.The green strand represents a R_{10} strand where one full helical turn is achieved allowing for similar exit trajectory of the MB binding arms. The pink strand represents P_{10}. If a shorter P strand such as P_9 was used, it is evident that it would be more difficult for the UMB5 binding arms to bind to UMB5, especially in the presence of a mismatch.

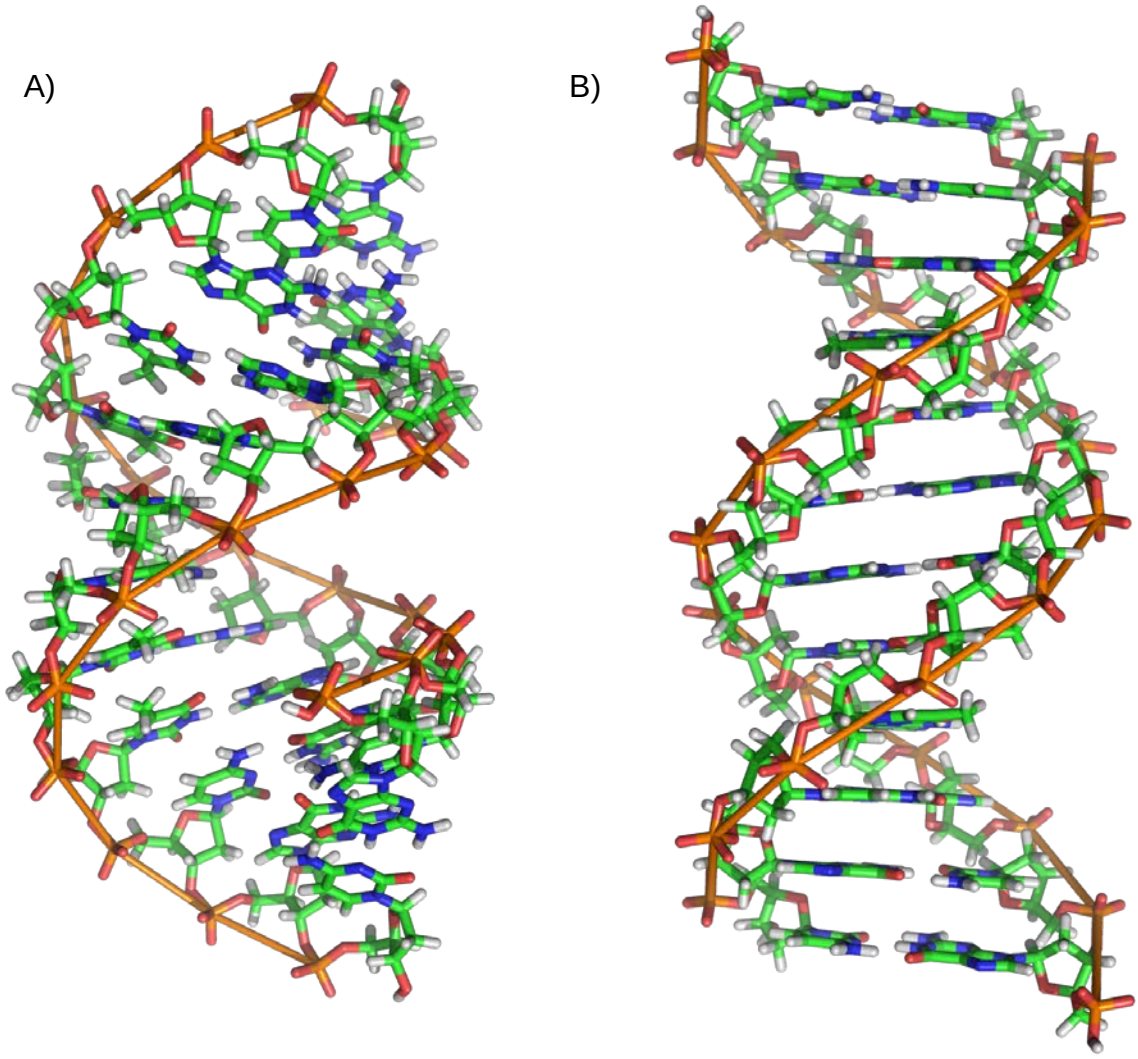

Figure 27. Helical turn of A and B DNA.

A) A-DNA. Helical turn is 11.1 base pairs (bp) per turn. RNA-DNA hybrids have a similar helical conformation

B) B-DNA with helical turn is 10.4 bp/turn, which is typical for DNA-DNA hybrids.

Image from https://en.wikipedia.org/wiki/Z-DNA#/media/File:A-DNA,_B-DNA_and_Z-DNA.png

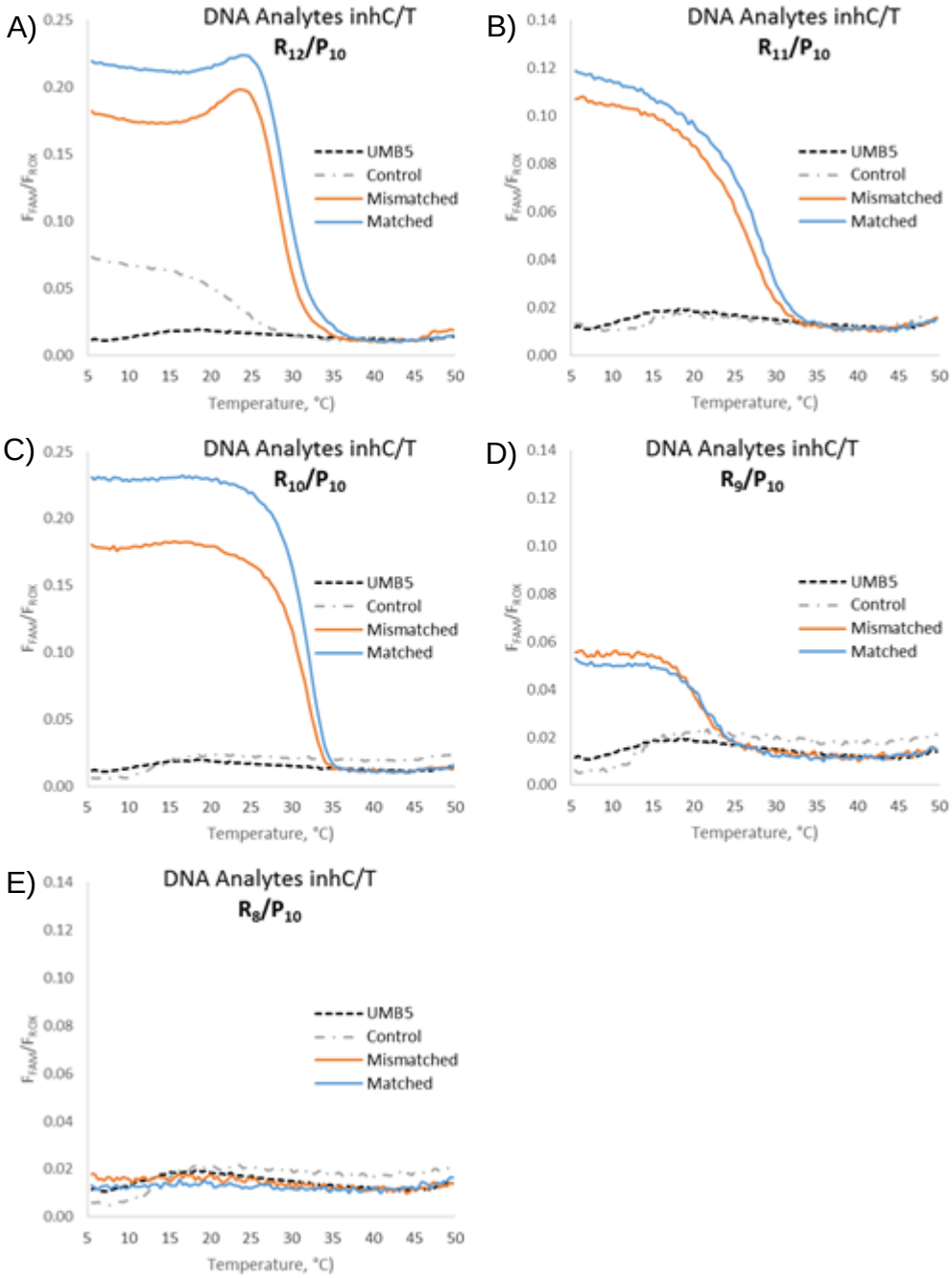

Figure 28. Melt curves with R_X/P_{10} show that a mismatch can be tolerated with P_{10}.

Although complex formation is good for these R length 12-9 in combination with P_{10}, little differentiation between matched and mismatched analytes is observed, indicating that a 10 nucleotide long P strand (one with ~1 full helical turn) can withstand a mismatch in the analyte strand.

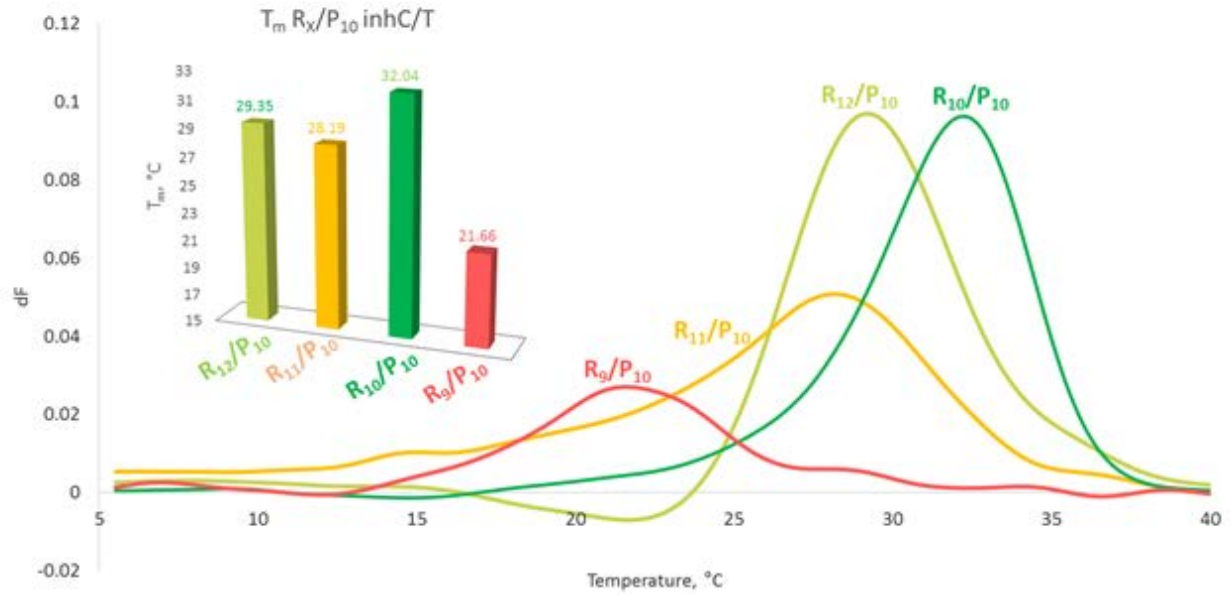

Figure 29. Derivative Plot of R_X/P_{10} Owl Sensors.

The derivative plots of Owl Sensors from Figure 28 when all lengths of R were combined with P_{10}. Complex stabilities rank from strongest complex to weakest: R_{10}, R_{12}, R_{11}, and R_9. The inset shows the T_m of each.

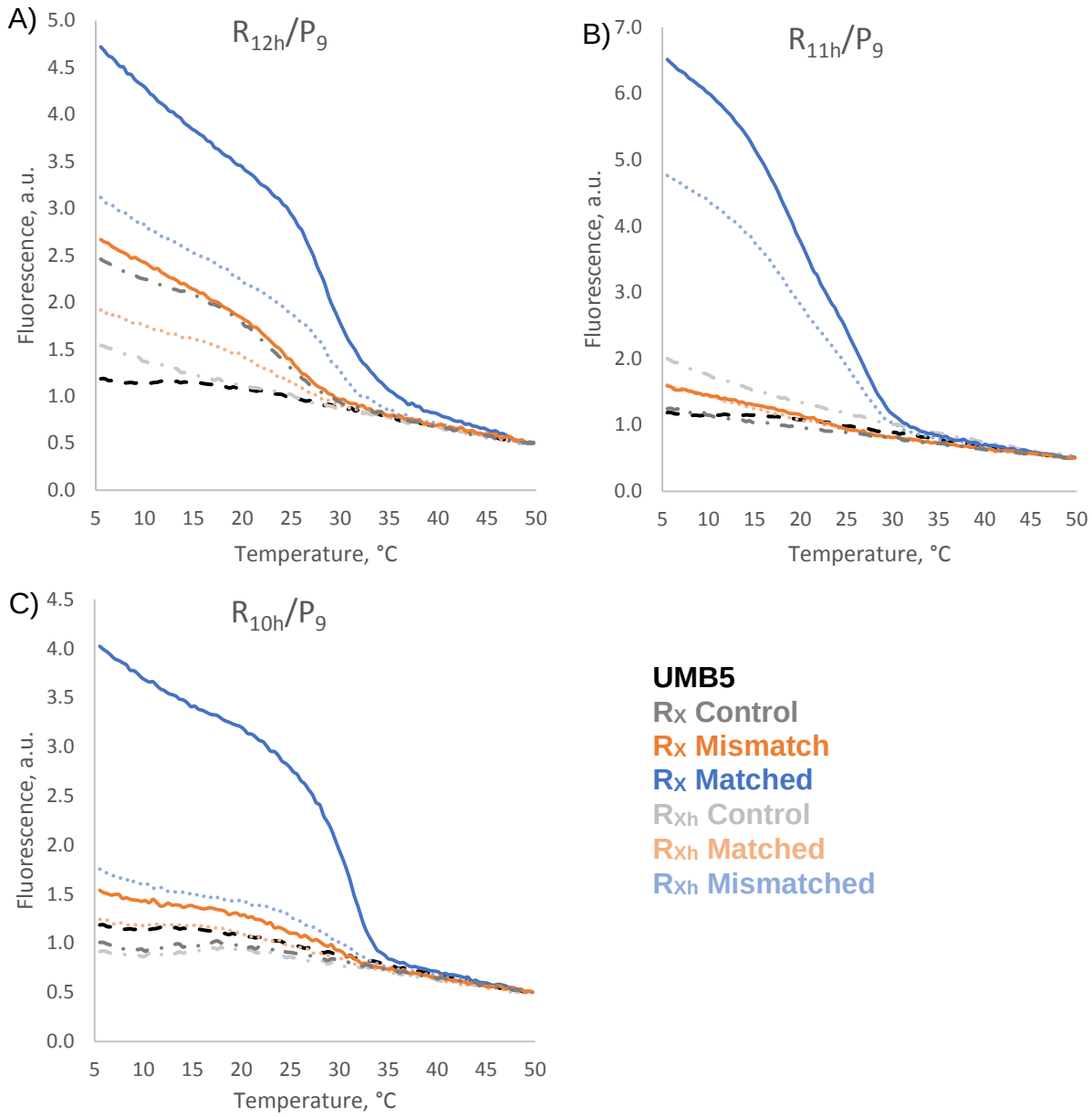

Figure 30. Melt Curves for Owl sensors with a mismatch in the R strand

Darker, solid lines indicate the performance of the regular Owl Sensor, while dotted muted colors show the performance of Owl Sensors with R probes with an incorporated mismatch. Arbitrary fluorescence units are reported.

A) The signal of the control, mismatched, and matched analytes all dropped when a mismatch in the R_{12} strand was introduced (dotted lines). However, when the matched analyte was present (light blue dotted line) still has a significant signal above the background.

B) R_{11h} does the best job of accommodating a mismatch in the R strand, as it maintains over 70% of the fluorescence of its perfectly matched R_{11} strand.

C) R_{10h} is very poor at accommodating a mismatch in the R strand. The light blue dotted line shows a large reduction in the signal when matched with the correct analyte.

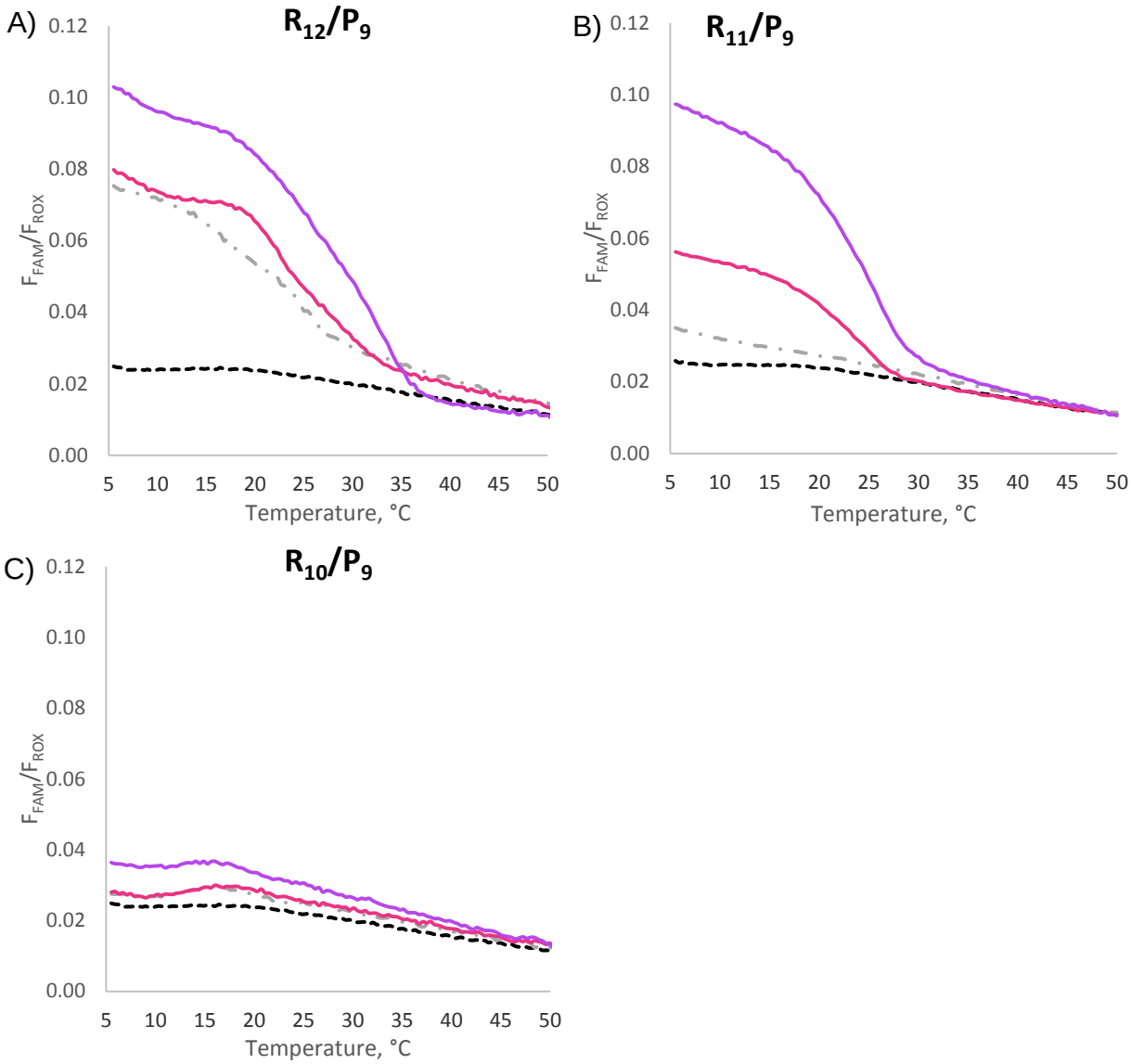

Figure 31. R_{11}/P_9 is the best Owl Sensor for differentiating SNPs in RNA analytes.

A) Melt Curve for R_{12}/P_9 with RNA analytes shows little differentiation.
B) Melt Curve for R_{11}/P_9 with RNA analytes shows the best differentiation for matched and mismatched analytes.
C) Melt Curve for R_{10}/P_9 with RNA analytes shows minimal complex formation.

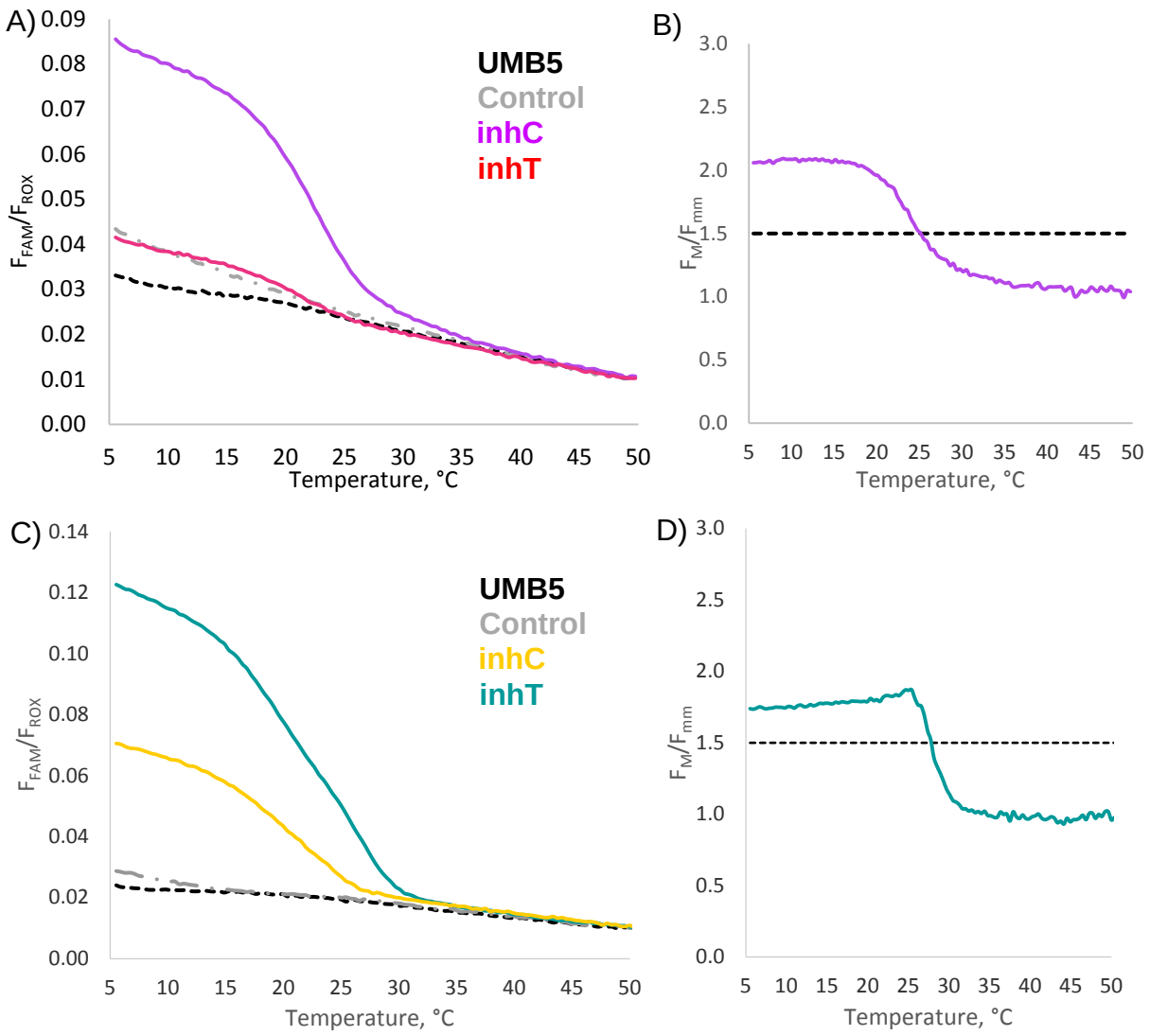

Figure 32. The Owl Sensor is able to differentiate mismatches in RNA analytes.

A) Melt Curve for R_{11}/P_9 with RNA analytes.
B) Differentiation ability for R_{11}/P_9 with RNA analytes extends from 5.0°C to 25.1°C using 10 mM $MgCl_2$.
C) Melt Curve for R_{11}/P_{9_A} with RNA analytes.
D) Differentiation ability for R_{11}/P_{9_A} with RNA analytes extends from 5.0°C to 27.4°C using 50 mM $MgCl_2$.

CHAPTER 4: RIGIDITY MATTERS

Introduction

The structures made by DNA Nanotechnology are rigid in nature, able to withstand elevated temperatures due to the large numbers of base pairs involved. While the Owl Sensor is much smaller in size, it can be thought of as a rigid structure, especially at low temperatures. When fully matched with the correct analyte, the nanostructure containing a four-way junction (4WJ) is nearly planar (4WJ pictured in Figure 33). Because P_9 is shorter than ideal for forming a strong structure where the strand enters and exits at the same trajectory, it is likely causes a distorted structure that flexes slightly out of a 2D plane. However, this designed imperfection is needed to allow for collapse of the structure if an imperfection like a SNV is present.

If flexibility is added into the structure, then the structure will become less stable (as can be seen by a lower T_m value) and differentiation of SNVs will be compromised (as seen by signal above the background for SNV analytes). One way to introduce flexibility into the structure is by adding a spacer where the strands cross from one helix to the other in the form of a polyethylene glycol (peg) linker (Figure 34). Throughout this chapter, the place where the adapter strands switch from hybridizing to the analyte to the UMB5 will be referred to as junctions or crosses. Peg linkers were added between the analyte binding domain and the UMB probe binding arm of $R_{10,}$ the outside of P_9, and the inside junction of P_9, and these strands are called $R_{10\_o\text{-}peg}$, $P_{9\_o\text{-}peg}$, and $P_{9\_i\text{-}peg}$, respectively. “i-peg” indicates the peg linker is on the inside of the Owl Sensor structure (in the 4WJ),

and “o-peg” indicates the peg linker is on the outside of the Owl Sensor (example shown in Figure 34). In addition, peg linkers on both the inside and outside were tested and are referred to as “pegD”.

Materials and Methods

Reagents

All buffers and stock solutions were made with DNAse/protease-free water purchased from Fisher Scientific Inc. (Pittsburg, PA). All other reagents needed for buffers were purchased from Sigma-Aldrich (St. Louis, MO). UMB5 was custom-made by TriLink Biotechnologies, Inc. (San Diego, CA). All other oligonucleotides (sequences listed in were obtained from Integrated DNA Technologies, Inc. (Coraville, IA). The concentrations of nucleic acid strands was determined using the Beer-Lambert law, a 1 cm quartz cuvette (volume of 100 µL), and extinction coefficients determined by using OligoAnalyzer 3.1 software (Integrated DNA Technologies, Inc.). Three independent different amounts of the same oligonucleotide were mixed with water to total volume of 100 µL and tested for their absorbance values at 260 nm using a Perkin-Elmer Lambda 35 UV/Vis spectrometer (San Jose, CA). The average of the concentrations calculated was used with relative standard deviations of each sample less than 10%. Working stock solutions of convenience concentrations were prepared for all sequences and stored frozen at -20°C until use.

Melt Curve Fluorescent Assays

Prior to mixing, stock solutions of oligonucleotides were allowed to thaw to room temperature, vortexed for 5 s, and centrifuged on a tabletop minicentrifuge for 10 s. A master mix solution containing R_X/P_Y was created such that adding 11.5 µL of the master mix to the samples (to a total volume of 25 µL) would result in R_X and P_Y concentrations of 150 nM and 200 nM, respectively. The master mix was used to make samples with the following names: Control, Mismatched, Matched, and Insertion and Deletion, if tested. The master mix solution (11.5 µL) was added to a 96-well plate (30 µL wells). Next, 1 µL of water, inhT, inhC, inh_del, or inh_ins was added to the plate to make the Control, Mismatched, Matched, Deletion, or Insertion samples, respectively so that the final concentration of the analyte was 100 nM. Another well was filled with 12.5 µL of water to serve as a control named 'UMB5'.

The buffer used contained 50 mM Tris-HCl, pH 7.4, 50 mM $MgCl_2$, and 0.1% Tween-20 with UMB5 and ROX (if used). A buffer-fluorophore solution containing 2X Buffer, 100 nM UMB5, and either 0 or 100 nM ROX was made. By adding 12.5 µL of the buffer-fluorophore solution, to each sample well, final concentrations of the fluorophores were 50 nM. ROX was used as a passive dye reference since its fluorescence shows little fluctuation with temperature. Using ROX also allows correction for well-to-well and plate-to-plate variations in fluorescence detection. Fluorescence was reported as F_{FAM}/F_{ROX}, where F_{FAM} is the fluorescence given off by the fluorophore attached to UMB5 and F_{ROX} is the fluorescence of the ROX reference dye.

After samples were made, an optical adhesive cover was placed firmly on top of the plate and a tool was used to seal the wells. The plate was flicked to eliminate any formed bubbles, vortexed, and then spun at 660 rcf for 20 s.

The solutions were placed in the QuantStudio™ 6 Flex System and cooled (2°C/s) from room temperature to 5°C where they were annealed for 60 min. The fluorescence of the samples was then read continuously as the samples were heated (0.1°C/s) from 5°C to 50°C. The QuantStudio™ 6 Flex System software allowed for the selection of FAM™ dye to be read as the 'Target' and if ROX was utilized, it was selected as a 'Passive Reference'. The system was routinely calibrated for well factors, background, and dye fluorescence. It is important to note that samples taken after different calibrations of the system showed altered background fluorescence of UMB5 and the Control samples (with no analyte present); thus depending on the date the experiment was conducted, some variation in fluorescent values between experiments may be observed. The QuantStudio™ Real-Time PCR Software (version 1.1) allows for real-time data analysis for initial processing, but all relevant data was exported to Excel for further analysis. The readings from at least two wells were averaged and replotted to produce the presented figures. The derivative of fluorescence over time was calculated by the QuantStudio™ Real-Time PCR Software. The maximum of the derivative plots gives the inflection point of the curve, also called the melting temperature (T_m).

Results and Discussion

In order to determine how flexibility of the Owl Sensor could be tolerated, different combinations of inside, outside, and double pegs were tested. Results show that by introducing flexibility into the Owl sensor through the addition of peg linkers, differentiation ability and complex stability is compromised. The ability to differentiate the matched analyte from analytes with SNVs is quantitatively assessed by the comparison of $\Delta T_{1.5}$ values, while complex stabilities are represented by the T_m of the matched complex (Figure 35 and Table 3).

Adding peg linkers increases entropy into the adapter strands, especially when unbound, and according to the equation $\Delta G = \Delta H - T\Delta S$, increasing the entropy results in a more negative ΔG and a more stable species. If the peg linker is on the outside of the Owl Sensor complex (not in the 4WJ) as is the case for $R_{10\_o\text{-}peg}$, R_{10_pegD}, $P_{9\_o\text{-}peg,}$ and P_{9_pegD}, not only is the entropy of the reactants increased due to having more flexible free DNA strands, but the entropy of the products increases, as the formed Owl Sensor complex is able to more easily bend out of plane (Figure 34). While the ends of the helices of the regular Owl Sensor are tethered with little flexibility or freedom for movement, the outside peg linkers allow for the helices to adopt non-parallel helices due to the increased flexibility, which is associated with higher energy of the complex (Figure 34).

Contrastingly, the $P_{9\_i\text{-}peg}$ will not significantly increase the flexibility of the system, as the junction is still stabilized by the non-pegylated junction of the R strand. Therefore, adding

flexibility into the Owl Sensor with the addition of $P_{9\_i\text{-}peg}$ will increase the stability of the dissociated state as the entropy of the free strand will increase without adding much entropy into the formed complex, resulting in low complex formation and a greater reduction in the stability, as expressed by a low T_m.

Results show that adding flexibility to the outside junction of P_9 ($P_{9\_o\text{-}peg}$) did not significantly hurt the differentiation ability or complex stability and even slightly increased the fluorescent value at 5°C for the matched analyte when compared to that of R_{10}/P_9 or R_{10}/P_{9_A}. A possible reasoning for this is that the flexibility on the outside of the P_9 strand allows for a reduction in the strain of the complex due to relaxing some of the strain due to nonideal exit trajectories into the flexible peg linker.

Generally, adding flexibility into the system has the greatest differentiation penalty for the insertion analyte. In every case where a pegylated strand was used, a significant signal for the insertion analyte is observed, indicating that a flexible system allows for accommodation of an extra nucleotide in the analyte strand. While it is unclear how to explain the mechanism of complex destabilization and loss of differentiation behind each combination of the R_{10}/P_9 strands, it can be generally stated for the Owl Sensor, a rigid structure is optimum for a large temperature range for differentiation of SNVs (Table 3).

Figures and tables

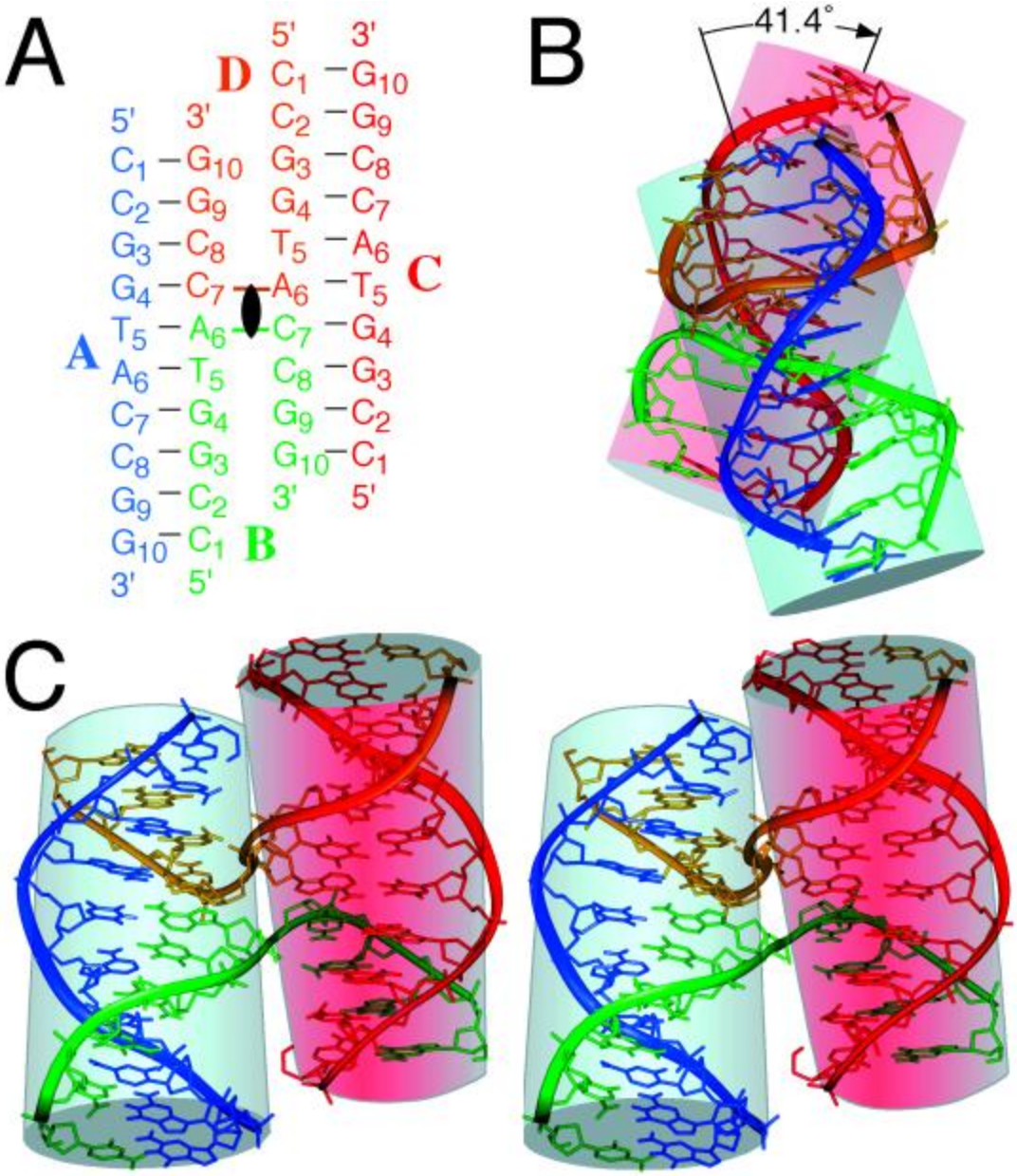

Figure 33. Structure of a Four Way Junction.

Figure from Shing Ho's study of DNA junctions. Copyright (2000) National Academy of Sciences, U.S.A..[29] The crystal structure of DNA complex with a 4WJ, shows offset helices. The complex crystalized has open ends, allowing for DNA strands to twist into their most optimal conformation (41.4° between helices) as shown in B. However, the adapter strands of the Owl Sensor crossover from on helix to another on the outside of the two helices, limiting the ability of the structure to twist and resulting in a nearly planar nanostructure.

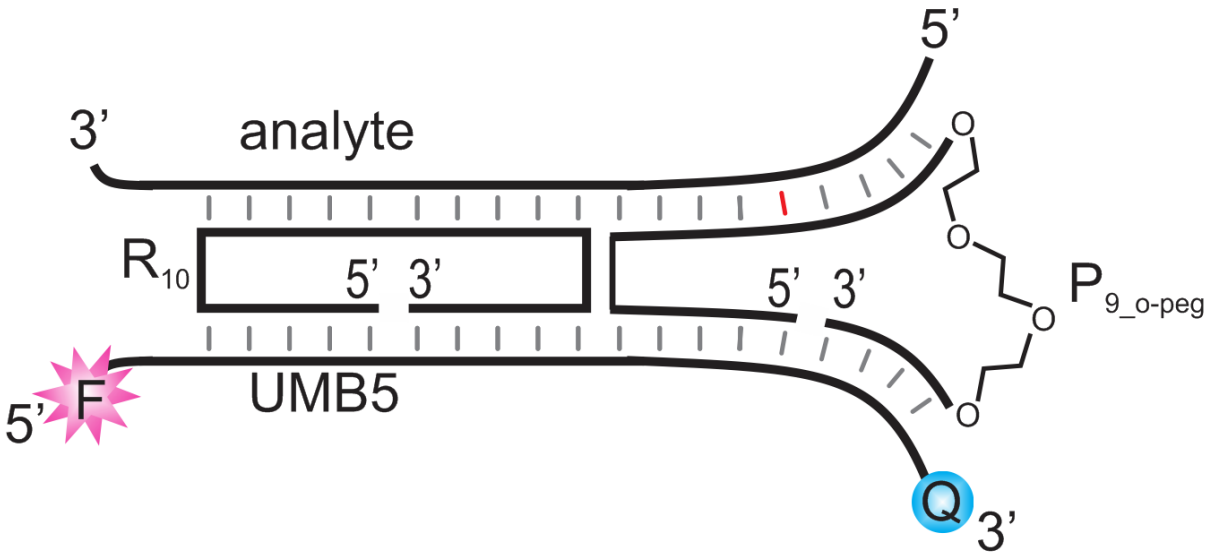

Figure 34. Flexibility introduced from an outside peg linker.
Rather than the helices remaining in a parallel conformation, with a peg linker on an outside junction, the structure can be flexible, which increases the entropy of the Owl Sensor complex.

Table 3: Quantitative assessment of the differentiation ability of the Owl Sensor with and without peg linkers

The 'Strands' column shows which combination of R and P is shown in that row. The T_m column is shaded with high values as green and lower values as red. The standard deviation of $\Delta T_{1.5}$ values was typically under 2°C. The shading of $\Delta T_{1.5}$ shows low values in red and high values in green.

Strands		T_m	T_{low}			T_{high}			$\Delta T_{1.5}$		
R	P	Matched	Mismatch	Deletion	Insertion	Mismatch	Deletion	Insertion	Mismatch	Deletion	Insertion
10	9_A	31.45	5.0	5.0	5.0	32.8	32.9	32.8	27.8	27.9	27.8
10	9	31.64	5.0	5.0	5.0	32.6	32.9	32.6	27.6	27.9	27.6
10	9_o-peg	31.27	5.0	5.0	5.0	33.0	33.3	32.6	28.0	28.3	27.6
10_i-peg	9_i-peg	27.82	5.0	5.0	-	29.0	29.0	-	24.0	24.0	0.0
10_o-peg	9	26.23	5.0	5.0	16.9	28.1	28.4	28.8	23.1	23.4	11.9
10_o-peg	9_o-peg	25.46	6.6	5.6	-	24.7	25.5	-	18.2	19.9	0.0
10	9_i-peg	23.91	5.0	5.0	-	25.0	25.8	-	20.0	20.8	0.0
10_pegD	9_pegD	23.78	5.0	5.0	5.0	24.4	24.4	23.2	19.4	19.4	18.2
10	9_pegD	23.71	-	-	-	-	-	-	0.0	0.0	0.0
10_o-peg	9_i-peg	19.26	5.0	5.3	-	17.1	16.0	-	12.1	10.7	0.0
10_i-peg	9	18.97	5.0	5.0	-	17.4	18.6	-	12.4	13.6	0.0
10_pegD	9	15.56	5.0	5.0	-	13.2	15.5	-	8.2	10.5	0.0

	Melt Curve	Differentiation Ability
R_{10}/P_9	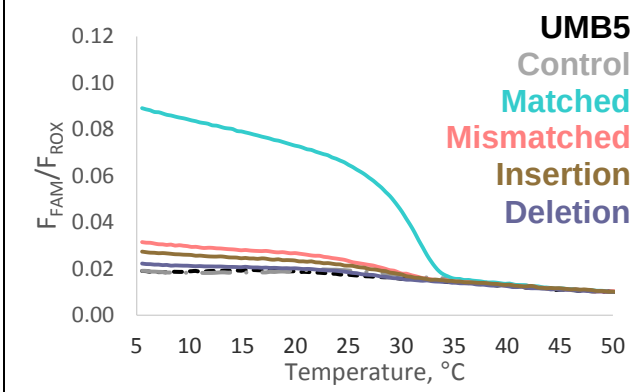	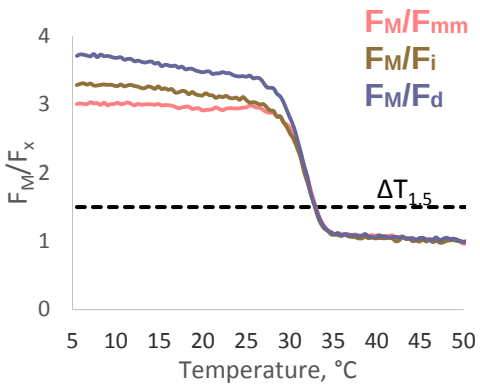
R_{10}/P_{9_A}	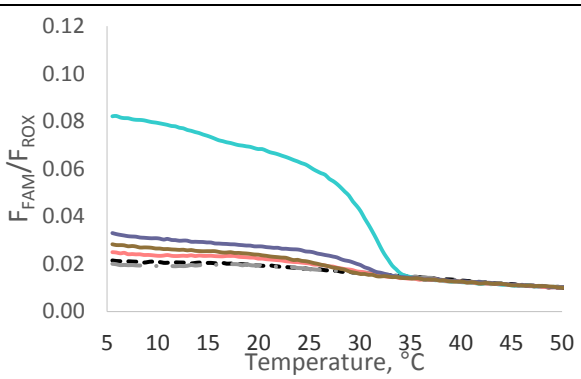	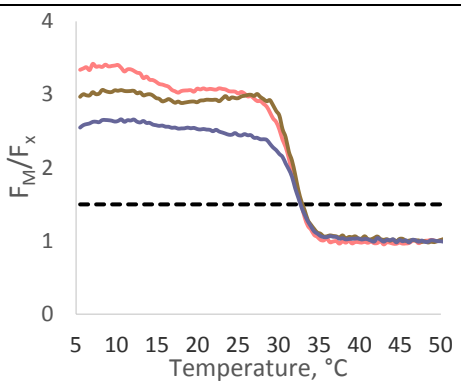
$R_{10}/P_{9\_o\text{-}peg}$	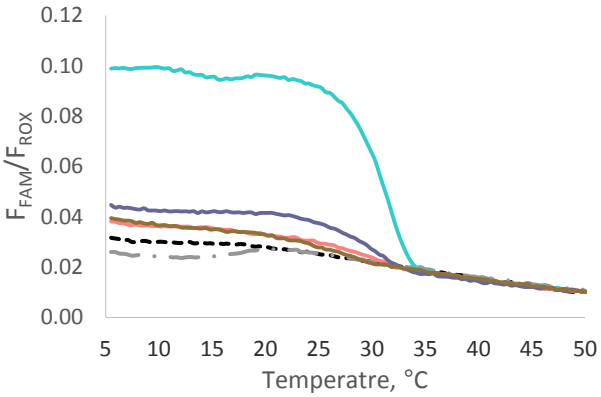	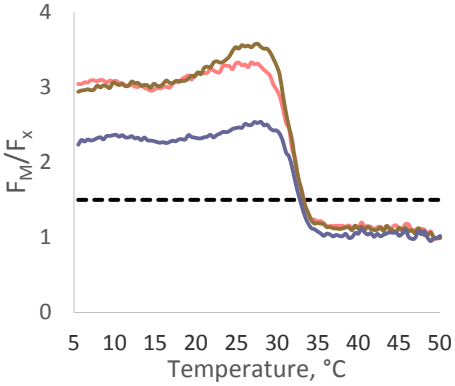

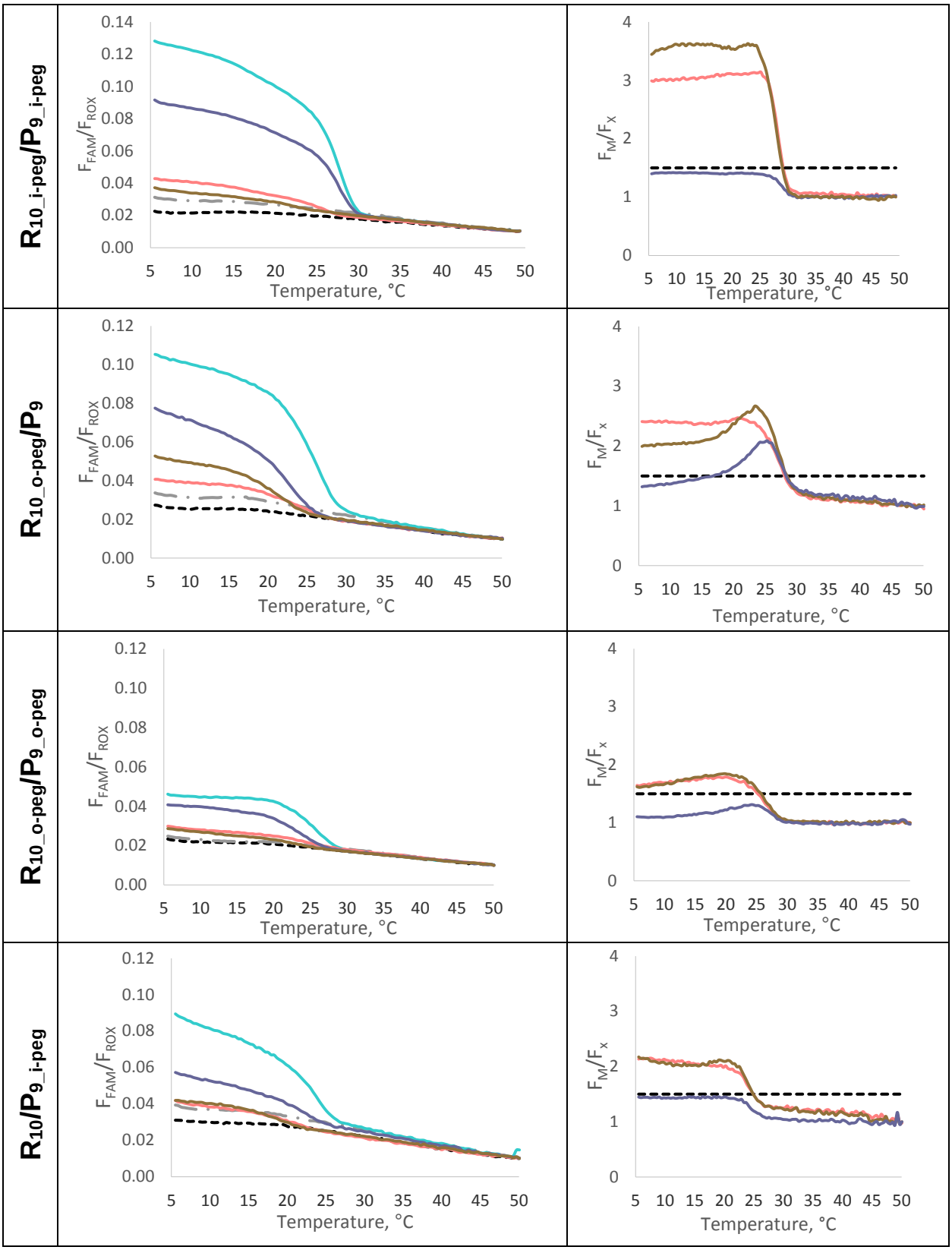
R10_i-peg/P9_i-peg
R10_o-peg/P9
R10_o-peg/P9_o-peg
R10/P9_i-peg
FFAM/FROX
FM/Fx
Temperature, °C

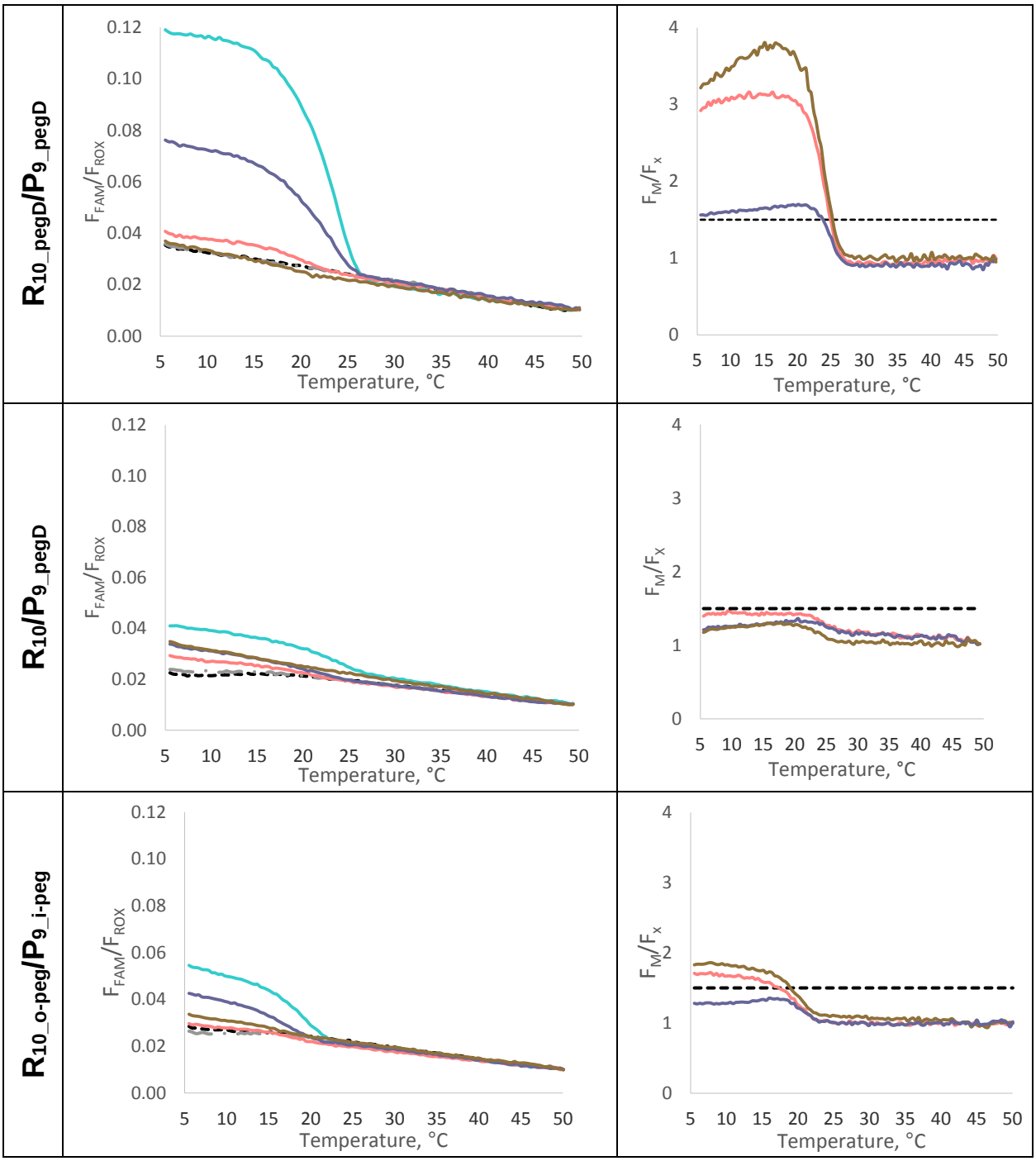
R10_pegD/P9_pegD
R10/P9_pegD
R10_o-peg/P9_i-peg
FFAM/FROX
FM/Fx
Temperature, °C
0.12
0.10
0.08
0.06
0.04
0.02
0.00
4
3
2
1
0
5 10 15 20 25 30 35 40 45 50

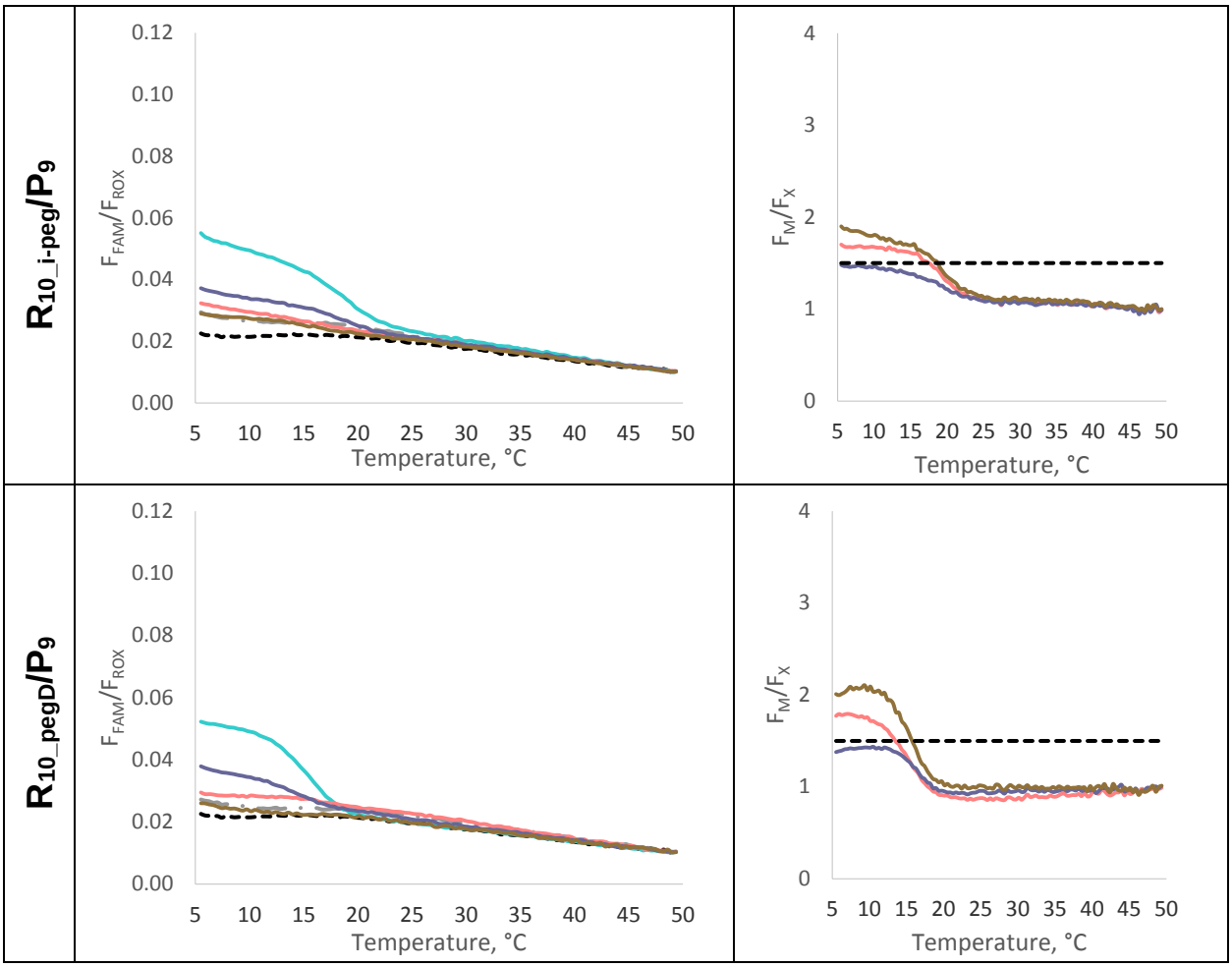

Figure 35. Melting Curves and Differentiation ability of Owl Sensor with and without pegs.

Each row show the melt curve and F_M/F_x graph of a different combination of R_{10} and P_9 adapter strands with and without peg groups. The UMB5, Control, Matched, Mismatched, Insertion, and Deletion graphs are in dashed black, dotted dashed grey, teal, coral, brown, and purple, respectively. The same colors for the Mismatched, Insertion, and Deletion graphs are used for representing differentiation ability as F_M/F_{mm}, F_M/F_i, and F_M/F_d, respectively.

CHAPTER 5: CHARACTERIZATION OF THE PERFECTLY IMPERFECT NONSTRUCTURE

Introduction

Chapters 3 showed that the helicity of the nucleic acid target influences the complex stability, and by having an R strand of ideal length and a strained P strand, differentiation of mismatches can be achieved. In this chapter, further characterization including limit of detection, kinetic behavior, and comparison of the Owl Sensor to other commercial probes will be presented.

Materials and Methods

Reagents

All buffers and stock solutions were made with DNAse/protease-free water purchased from Fisher Scientific Inc. (Pittsburg, PA). All other reagents needed for buffers were purchased from Sigma-Aldrich (St. Louis, MO). UMB5 was custom-made by TriLink Biotechnologies, Inc. (San Diego, CA). All other oligonucleotides (sequences listed in Table 1) were obtained from Integrated DNA Technologies, Inc. (Coraville, IA). The concentrations of nucleic acid strands was determined using the Beer-Lambert law, a 1 cm quartz cuvette (volume of 100 µL), and extinction coefficients determined by using OligoAnalyzer 3.1 software (Integrated DNA Technologies, Inc.). Three independent different amounts of the same oligonucleotide were mixed with water to total volume of 100 µL and tested for their absorbance values at 260 nm using a Perkin-Elmer Lambda 35 UV/Vis spectrometer (San Jose, CA). The average of the concentrations calculated

was used with relative standard deviations of each sample less than 10%. Working stock solutions of convenience concentrations were prepared for all sequences and stored frozen at -20°C until use.

Limit of Detection

The limit of detection (LOD) was determined by conducting fluorescence experiments using a 100 µL quartz in a Perkin-Elmet (San Jose, CA) LS-5S Luminescence Spectrophotometer with a Hamamatsu xenon lamp (excitation at 485 nm, emission at 517 nm). A buffer containing 50 mM Tris-HCl, pH 7.4, 50 mM $MgCl_2$, and 0.1% Tween-20 was used. The concentrations of the DNA strands used are in Table 4. Samples were incubated in 5°C water bath for one hour. Samples were then taken out of the bath and analyzed in the Perkin-Elmet LS-5S Luminescence Spectrophotometer at room temperature. Fluorescent values at 517 nm were recorded. Three independent trials for each sample were averaged and plotted in Excel with error bars indicating one standard deviation. The LOD was determined by calculating the signal of the control (0 nM of analyte) + 3*(standard deviation of the control).

Table 4: Concentrations of DNA strands for LOD

Concentrations (nM)					
Sample Name	UMB5	R_{10}	P_9	inhT (mm)	inhC (M)
UMB5	50	-	-	-	-
Control	50	150	200	-	-
inhC, low R_{10}	50	150	200	-	Varied
inhC, excess R_{10}	50	1,150	200	-	Varied
inhC, excess R_{10} and inhT	50	1,150	200	1,000	Varied

Fluorescence Assay

Prior to mixing, stock solutions of oligonucleotides were allowed to thaw to room temperature, vortexed for 5 s, and centrifuged on a tabletop minicentrifuge for 10 s. A master mix solution containing R_X/P_Y was created such that adding 11.5 µL of the master mix to the samples (to a total volume of 25 µL) would result in R_X and P_Y concentrations of 150 nM and 200 nM, respectively. The master mix was used to make samples with the following names: Control, Mismatched, Matched, and Insertion and Deletion, if tested. The master mix solution (11.5 µL) was added to a 96-well plate (30 µL wells). Next, 1 µL of water, inhT, inhC, inh_del, or inh_ins was added to the plate to make the Control, Mismatched, Matched, Deletion, or Insertion samples, respectively so that the final concentration of the analyte was 100 nM. Another well was filled with 12.5 µL of water to serve as a control named ‘UMB5’.

The buffer used contained 50 mM Tris-HCl, pH 7.4, 50 mM $MgCl_2$, and 0.1% Tween-20 with UMB5 and ROX (if used). A buffer-fluorophore solution containing 2X Buffer, 100 nM UMB5, and either 0 or 100 nM ROX was made. By adding 12.5 µL of the buffer-fluorophore solution, to each sample well, final concentrations of the fluorophores were 50 nM. ROX was used as a passive dye reference since its fluorescence shows little fluctuation with temperature. Using ROX also allows correction for well-to-well and plate-to-plate variations in fluorescence detection. Fluorescence was reported as F_{FAM}/F_{ROX}, where F_{FAM} is the fluorescence given off by the fluorophore attached to UMB5 and F_{ROX} is the fluorescence of the ROX reference dye.

After samples were made, an optical adhesive cover was placed firmly on top of the plate and a tool was used to seal the wells. The plate was flicked to eliminate any formed bubbles, vortexed, and then spun at 660 rcf for 20 s.

The solutions were placed in the QuantStudio™ 6 Flex System and cooled (2°C/s) from room temperature to 5°C where they were annealed for 60 min. The fluorescence of the samples was then read continuously as the samples were heated (0.1°C/s) from 5°C to 50°C. The QuantStudio™ 6 Flex System software allowed for the selection of FAM™ dye to be read as the ‘Target’ and if ROX was utilized, it was selected as a ‘Passive Reference’. The system was routinely calibrated for well factors, background, and dye fluorescence. It is important to note that samples taken after different calibrations of the system showed altered background fluorescence of UMB5 and the Control samples (with

no analyte present); thus depending on the date the experiment was conducted, some variation in fluorescent values between experiments may be observed. The QuantStudio™ Real-Time PCR Software (version 1.1) allows for real-time data analysis for initial processing, but all relevant data was exported to Excel for further analysis. The readings from at least two wells were averaged and replotted to produce the presented figures. The derivative of fluorescence over time was calculated by the QuantStudio™ Real-Time PCR Software. The maximum of the derivative plots gives the inflection point of the curve, also called the melting temperature (T_m).

Kinetic Studies

Cooling and Heating

The concentration of X and Owl Sensor strands were the same as previously mentioned for fluorescent assays. Here, f is analogous to R and m is analogous to m. For the MB and LP probe, analyte cocnetnration was 100 nM and probe concentration was 50 nM. Buffer conditions for all probes were 50 mM Tris-HCl, 50 mM $MgCl_2$ and 0.1% Tween-20. The slowest continuous temperature ramping rate that can be programmed with the QS6 instrument is 0.02°C/s. In order to achieve slower temperature rates for kinetic studies, a stepwise method for raising and lowering temperature was utilized where each °C temperature was held for a set amount of time. This procedure utilized two PCR stages bordered at the beginning and end with a Hold Stage. In the first Hold Stage, the temperature was brought up from 25°C to 95°C (1.6°C/s). The system was then cooled to 76°C at a rate of 1.6°C/s. Seventy-one cycles cooled the samples at 1°C temperature

increments from 75°C to 5°C stopping at each temperature degree for a select amount of time: 20, 60, 600, or 1800 s. After cooling, the temperature was heated from 5°C to 75°C at the same equilibration time as the cooling stage. At each temperature, a fluorescent reading was recorded. These equilibration times correspond to 0.05, 0.0167, 0.00167, and 0.000556°C/s rates of temperature change, respectively. The last Hold stage ramps the temperature back down to 25°C (1.6°C/s). Fluorescent data was exported, analyzed, and graphed in Excel. To allow for proper comparison of samples in a set, correction for well-to-well variation was done by setting the first fluorescence reading (75°C) to the same value to make the background fluorescence for all samples in a trial set equal.

Isothermal Kinetics

The concentration of Owl Sensor strands were the same as previously mentioned for fluorescent assays. To see how the Owl Sensor behaves over 24 hrs at one temperature, an altered protocol was required. Because more change in fluorescence is observed right after mixing, data was collected every 20 or 30 s for the first 1-2 hours. After that, longer periods of time were given between fluorescent readings (20 to 30 min) until 24 hrs had passed. This was achieved through 2 PCR stages. The first stage cooled the samples from 25°C to the desired temperature at 1.6°C/s. The temperature was then kept constant as the system repeatedly recorded fluorescent readings at short intervals (20 to 30 s between readings). The second PCR stage remained at the same temperature as the first and fluorescent readings were repeatedly recorded at slower intervals (20 to 30 min). Data was exported to Excel and analyzed.

Results and Discussion

Limit of Detection

Characterization of the Owl Sensor is imperative to understanding its behavior. Sensitivity studies including limit of detection (LOD) allow for researchers to determine the lowest concentration a sensor can confidently detect the presence of an analyte.

Experiments were conducted in order to determine the minimum concentration of matched analyte required for detection. Results in Figure 36 show that in the same concentration of strands used in previous melt curves, the LOD is 6.1 nM, which is comparable to the detection limit of molecular beacons.[30]

In order to determine if the sensor can still specifically recognize fully matched analyte in the presence of high concentrations of a mismatched analyte, 1 μM of inhT was introduced into each sample. This increased the signal of the control (0 nM of inhC), only slightly raising the LOD to 9.4 nM (blue line in Figure 36). This shows that the P_9 strand did not hybridize large amounts of excess nonspecific analyte, and shows that the correct analyte can be detected even with mismatched analyte at over 100 times excess concentrations. Since R_{10} binds to an unchanged region of the *inhA* analyte (its analyte binding domain is fully complementary to inhC and inhT), high concentrations of R_{10} were used (1,150 nM) so that enough R_{10} was available to bind both inhC and the large excess of inhT. For comparison, LOD with 1,150 nM of R_{10} was also found to be 4.9 nM (grey line Figure 36).

Comparison of mismatch differentiation of Owl Sensor with conventional probes

In order to market the Owl Sensor for general use, it must be able to compete with the commonly used probes, which include the MB and Linear Probe (see drawings of these sensors in Figure 37). For this reason, melting curves were used to determine the differentiation range for a Linear Probe (Figure 38), a MB Probe (Figure 39), and the X Sensor with the same adapter strand lengths as the Owl Sensor specific to inhC (Figure 40) and compared to the Owl Sensor (Figure 22). Differentiation was analyzed by dividing the fluorescence of the matched analyte by that of the mismatched analyte and graphed all together with the Owl sensor for comparison (Figure 41) The Owl Sensor showed the widest range for differentiation and has the advantage of being able to differentiate at room temperatures, an essential trait for PoC diagnostic tests (Table 5).

Kinetic analysis of hybridization

Kinetic studies allow for the understanding of how fast complex formation occurs, allowing for insight into the mechanism of hybridization. Isothermal as well as temperature ramping kinetic studies were performed for this purpose.

Cooling and Heating

When ΔG=0, a system is at equilibrium. Because $\Delta G = -RTlnK$, at a given temperature, a system at equilibrium will always have the same K, where $= \frac{[products]}{[reactants]}$. For the Owl Sensor, the signal observed is due to a product, i.e. the fully formed complex. Therefore,

at a given temperature, if the system is at equilibrium, the same fluorescent signal should be produced no matter the path taken to get to the temperature (cooling or heating).

High temperatures were used to denature any pre-formed DNA hybrids, samples were cooled stepwise, decreasing 1°C at a time and allowed to equilibrate for a set amount of time, followed by a fluorescent reading. After annealing, the temperature was increased by 1°C at a time and given the same amount of time for equilibration as for the cooling process. If the time was enough for the system to come into equilibrium, then the fluorescent readings on cooling and on heating would be equal, producing symmetric graphs with no hysteresis observed. If the temperature ramping occurred too fast for the system to fully equilibrate, then the cooling and heating profiles would appear asymmetric with hysteresis showing greater complex formation later in the experiment (on heating), after longer time for equilibration at low temperatures has occurred. These heating and cooling curves were conducted by equilibrating for 20, 60, 600, and 1800 s/°C for the MB probe (Figure 42), the X Sensor (Figure 43), and the Owl Sensor (Figure 44).

Results show that the MB probe can come to equilibrium even with only 20 s of equilibration at each temperature degree, suggesting quick binding of the simple sensor (Figure 42A). The X Sensor takes slightly longer for equilibrium to be achieved, with hysteresis observed with 20 and 60 s equilibration times, while longer equilibration results in symmetric cooling and heating curves (Figure 43).

Hybridization of the Owl Sensor was shown to be a very slow process, as even after equilibrating for 1800s/°C, hysteresis in the cooling and heating curves are observed (Figure 44D). As the equilibration time increases, the signal of both the matched and mismatched analytes continue to increase as complex formation accumulates given longer equilibration times. This suggests that when using simple melt curve analysis with short incubation times (1 hr), the complex is far from equilibrium, allowing for kinetic resolution to provide minimal signal for the mismatched analyte at the time of reading.

Figure 45 shows the signals of the controls, inhT, and inhC analytes at the peak of the cooling-heating curves (5°C). Results show the MB Probe and X Sensor gain signal very fast followed by a levelling out for the signal, indicating the system reaching equilibrium. However, the Owl Sensor continues to gain signal as equilibration time increases, further showing the slow hybridization kinetics.

Isothermal Kinetics

In order to visualize the kinetics of the Owl Sensor at various temperatures, isothermal kinetic studies were performed, with fluorescent reads taken regularly over a 24 hr period. Figure 46 reveals that at 10°C, both the matched and mismatched analytes continue to gain signal over time. However, the matched analyte gains signal much faster than the mismatched analyte, allowing for kinetic resolution. When the samples are made and incubated at 10°C for 1 hour, the kinetic studies show that the mismatched analyte does not show significant signal above the control sample, while the matched analyte shows a relatively high signal. For this reason, a large differentiation is observed when the

samples' fluorescence is read at a 1 hour time point. At a slightly higher temperature of 19°C, the mismatched analyte never gains significant signal above the background, while the matched signal comes into equilibrium after 10 hours of incubation. However 50% of the maximum fluorescence is achieved after 90 minutes and 75% of the maximum fluorescence is achieved after 3.5 hours. Figure 46D shows the signal to background ratio for the isothermal kinetic studies at 10, 19, and 25°C.

Figures and Tables

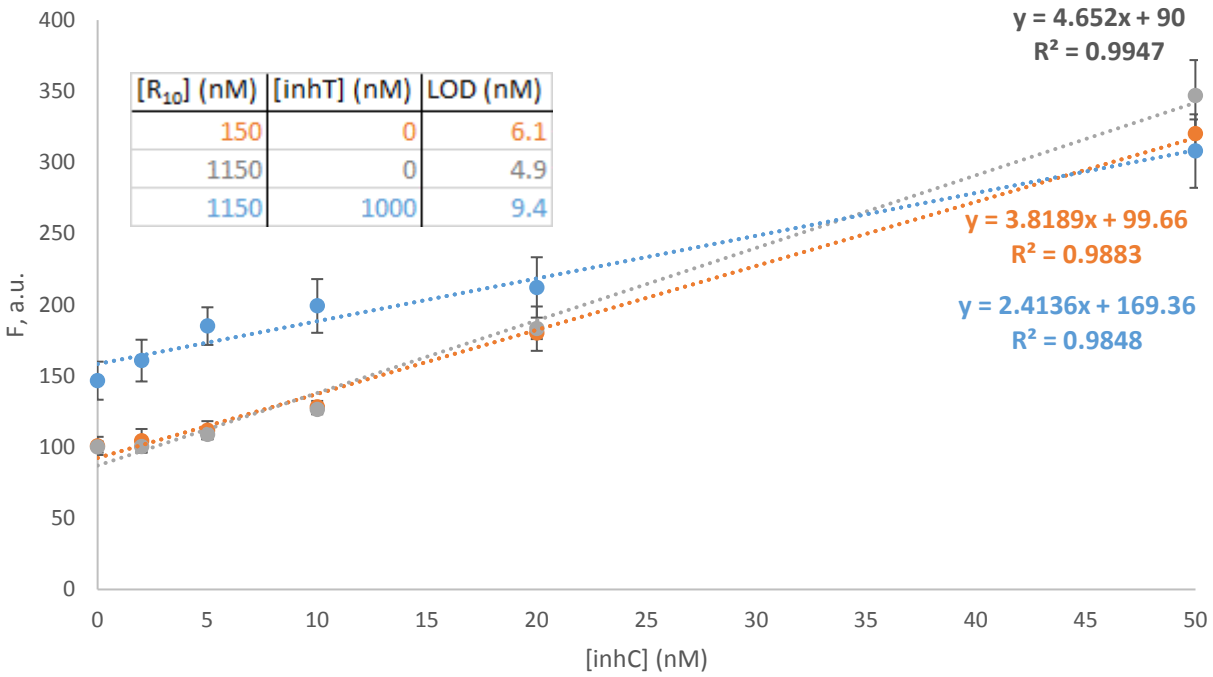

Figure 36. Limit of Detection for the R_{10}/P_9 Owl Sensor.

Limit of Detection of the Owl Sensor. The inset shows the concentratin of R_{10}, inhC, and inhT and the LOD for each of the three samples. The orange line represents the LOD for the previously optimized concentrations of oligonucleotides (the same samples seen in the melt curves after optimization). The blue line shows the LOD for the Owl Sensor when a large excess inhT (mismatched) analyte is present. For comparison, the grey line shows the LOD for the Owl Sensor when a higher concentration of R_{10} is used.

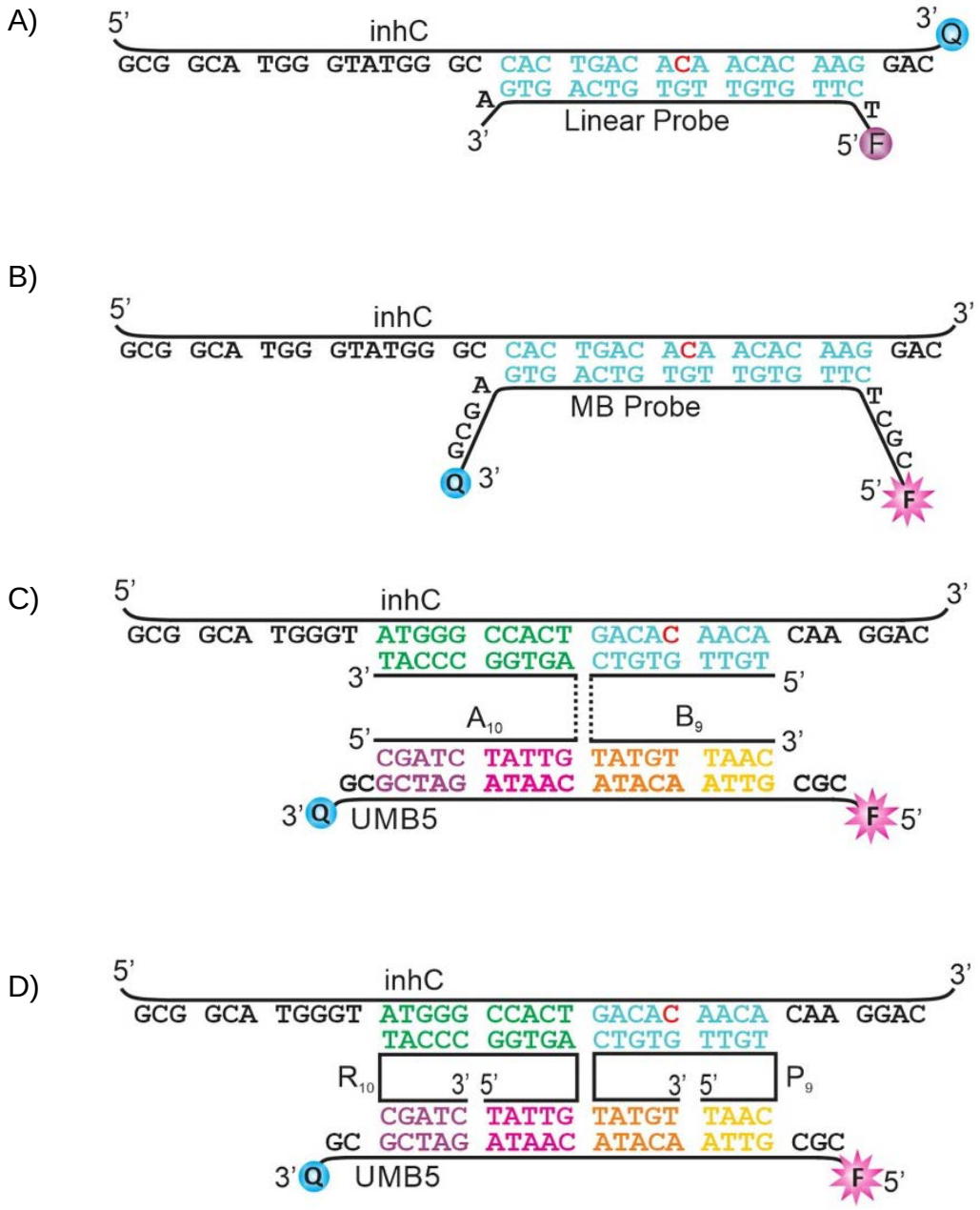

Figure 37: Hybridization probes with sequences.

The inhC analyte is shown here bound to different hybridization probes; the red letter is the location of the variable site where the inhT has a thymine. A) Linear Probe. B) Molecular Beacon Probe. C) X Sensor. Dashed lines indicate peg linkers. D) R_{10}/P_9 Owl sensor. The central portion of each adapter strand binds to the analyte, and the flanking ends must wrap around to bind to UMB5. No additional nucleotides or spacers are present in R/P adapter strands.

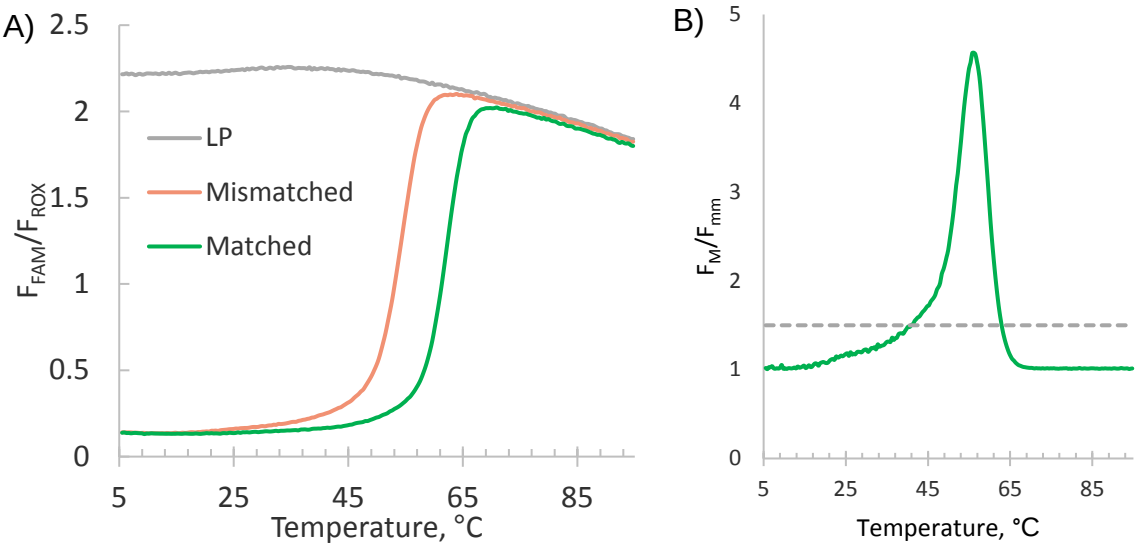

Figure 38. Linear Probe performance.

A) Melt curve for the linear probe with matched, mismatched, and no analyte present in green, orange, and grey, respectively.

B) Differentiation ability for the linear probe shows a limited range for differentiation far from ambient temperatures.

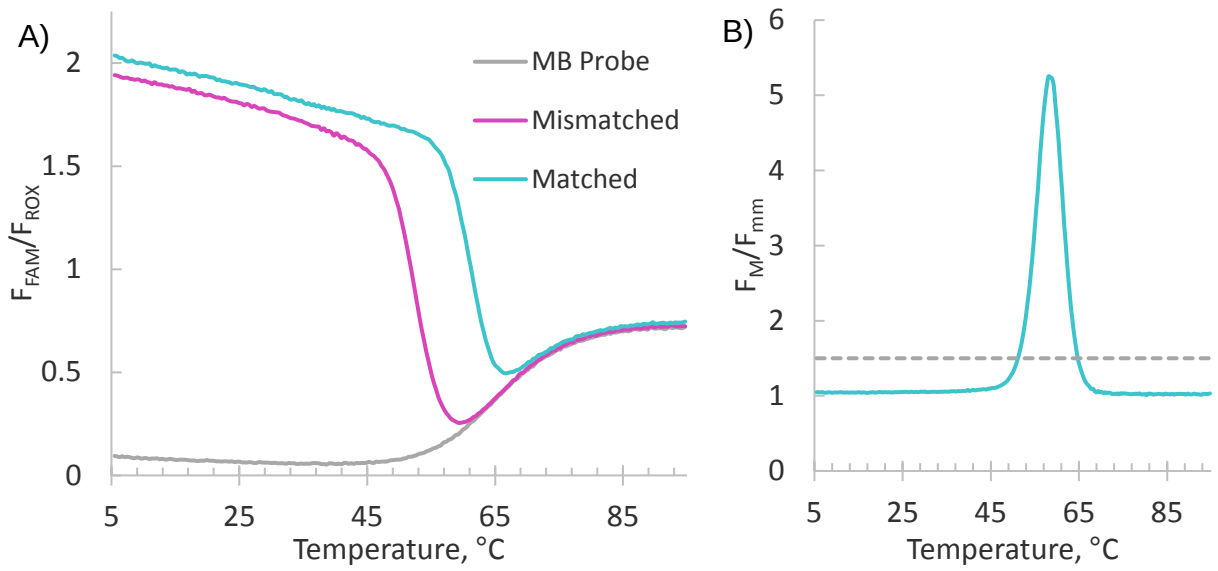

Figure 39. MB Probe performance.

A) Melt curve for the molecular beacon with matched, mismatched, and no analyte present in teal, magenta, and grey, respectively.

B) Differentiation ability for the MB probe shows a limited temperature range for differentiation that does not include ambient temperature.

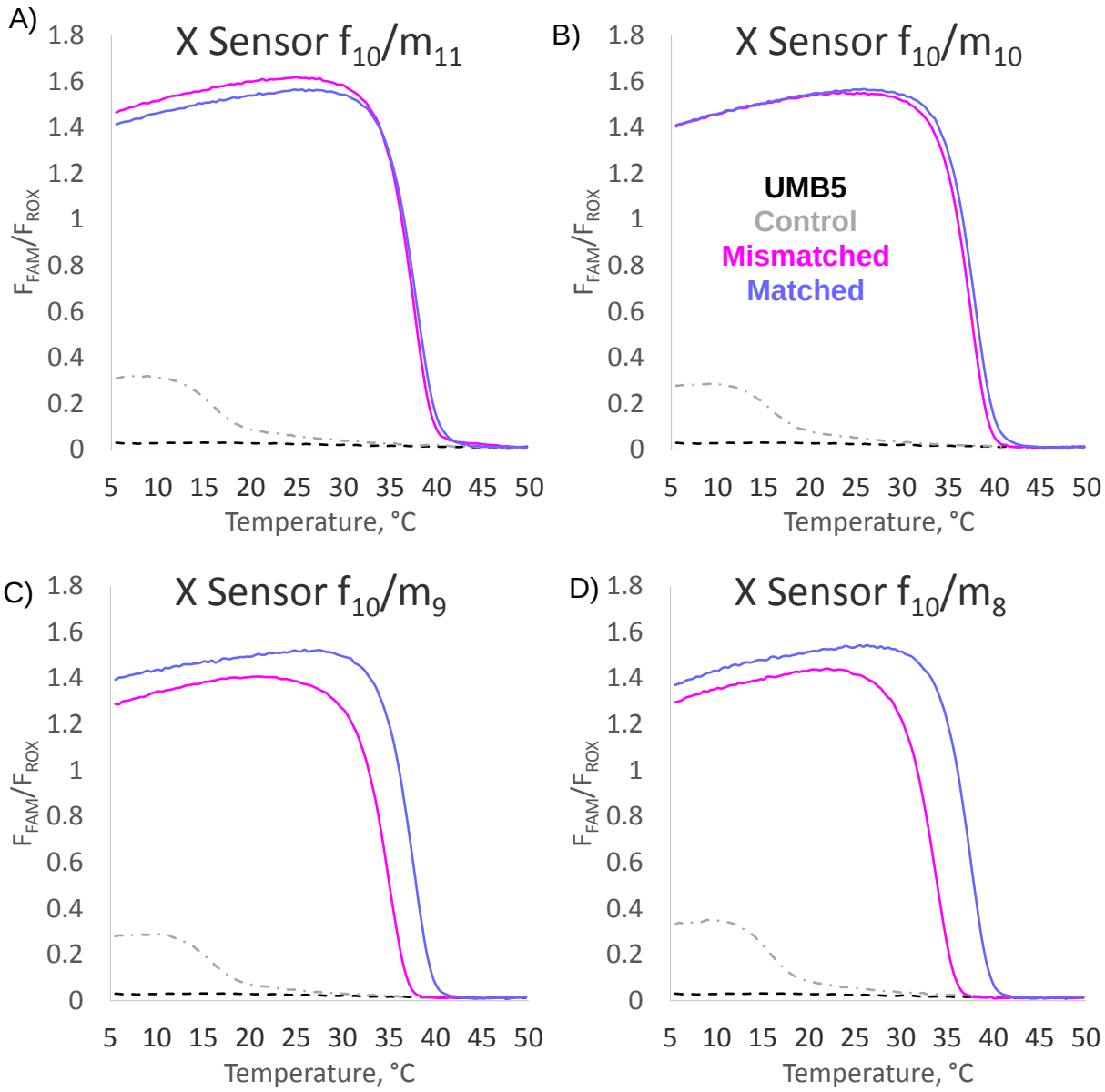

Figure 40. X Sensor performance melt curves

Melt curves for the X sensor with a 10 nucleotide long f strand and m lengths ranging from 11-8.

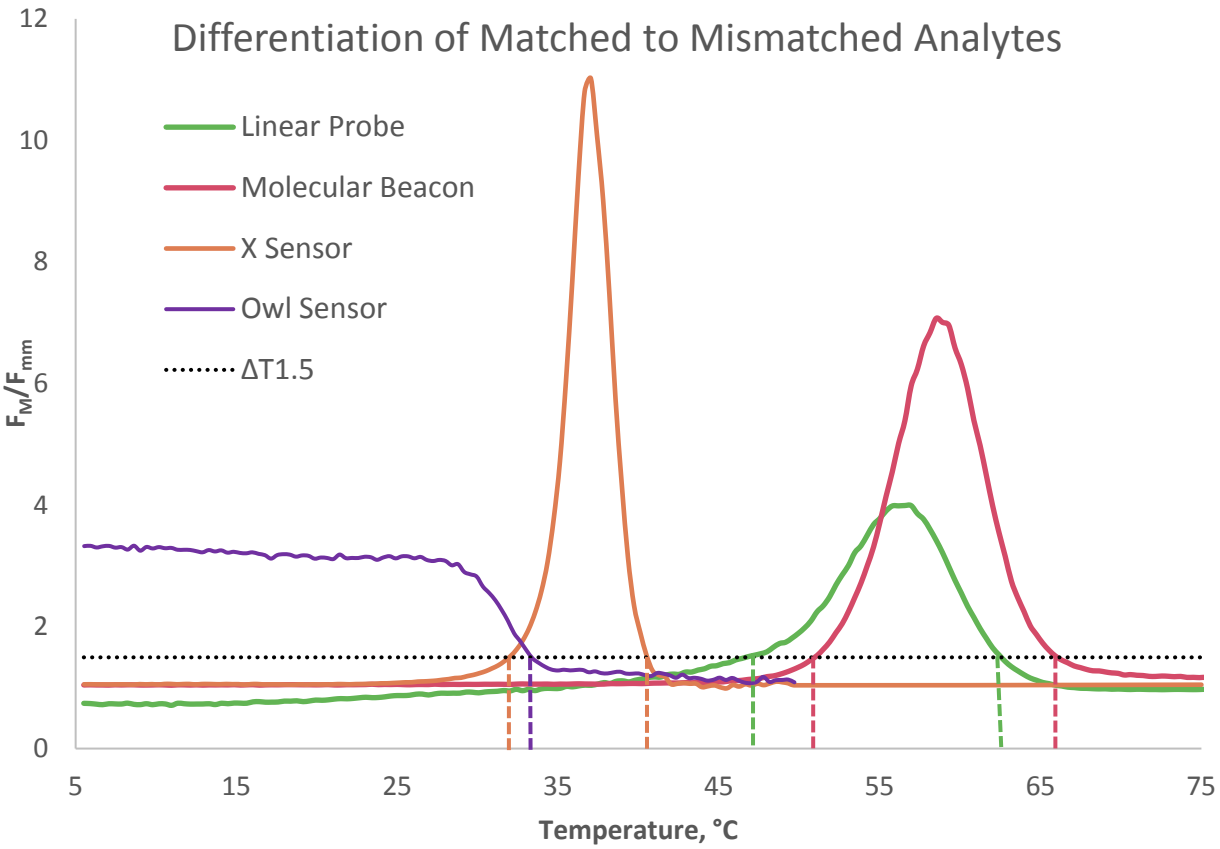

Figure 41. Comparison of the Owl Sensor with commercial Probes.
The differentiation range for the Owl, X, MB, and LP sensors is shown in purple, orange, green, and red colors, respectively. When comparing, the Owl Sensor provides for the largest temperature range for differentiation and is the only one to include ambient temperatures.

Table 5. Quantitation comparison of Owl Sensor with Commercial Probes.
The differentiation by each of the sensors. The $\Delta T_{1.5}$ column is shaded with high numbers in green and low numbers in red.

Probe	T_{low}	T_{high}	$\Delta T_{1.5}$
Linear Probe	46.8	62.4	15.6
Molecular Beacon	51.1	65.9	14.8
Owl Sensor	5.0	33.0	28.0
X Sensor	32.0	40.5	8.5

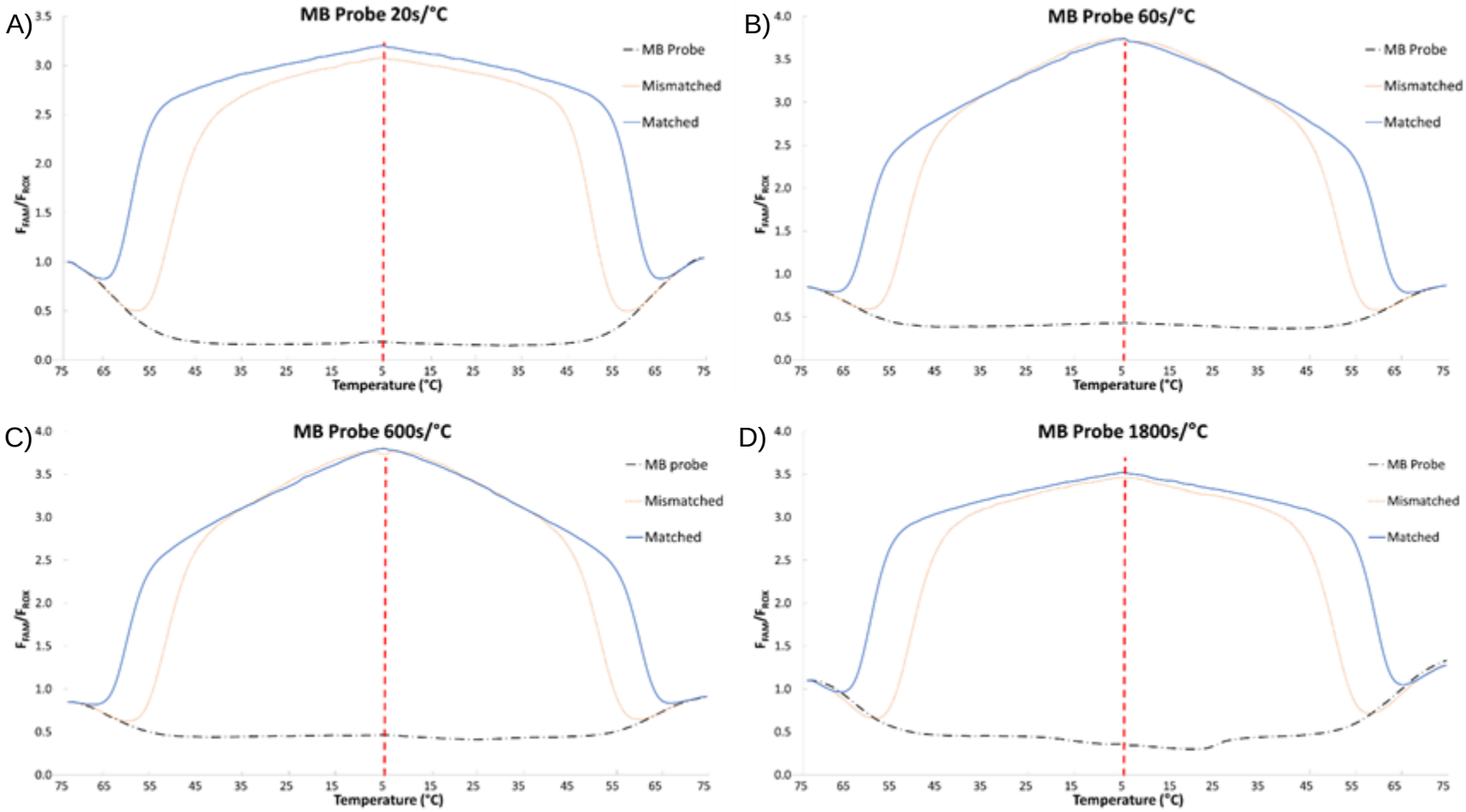

Figure 42: MB Probe Cooling and Heating Curves

Cooling-heating curves of MB Probe. Different equilibrium times were used: 20 s, 60 s, 600 s, and 1800 s. The solid blue lines represent the fully matched complex, dotted orange lines represent the mismatched complex, the dashed grey line represents the control with no analyte present, and the dotted dashed black line represents UMB5 alone. The vertical red dashed line shows the boundary between cooling (left side) and heating (right side) portions of the thermal profiles.

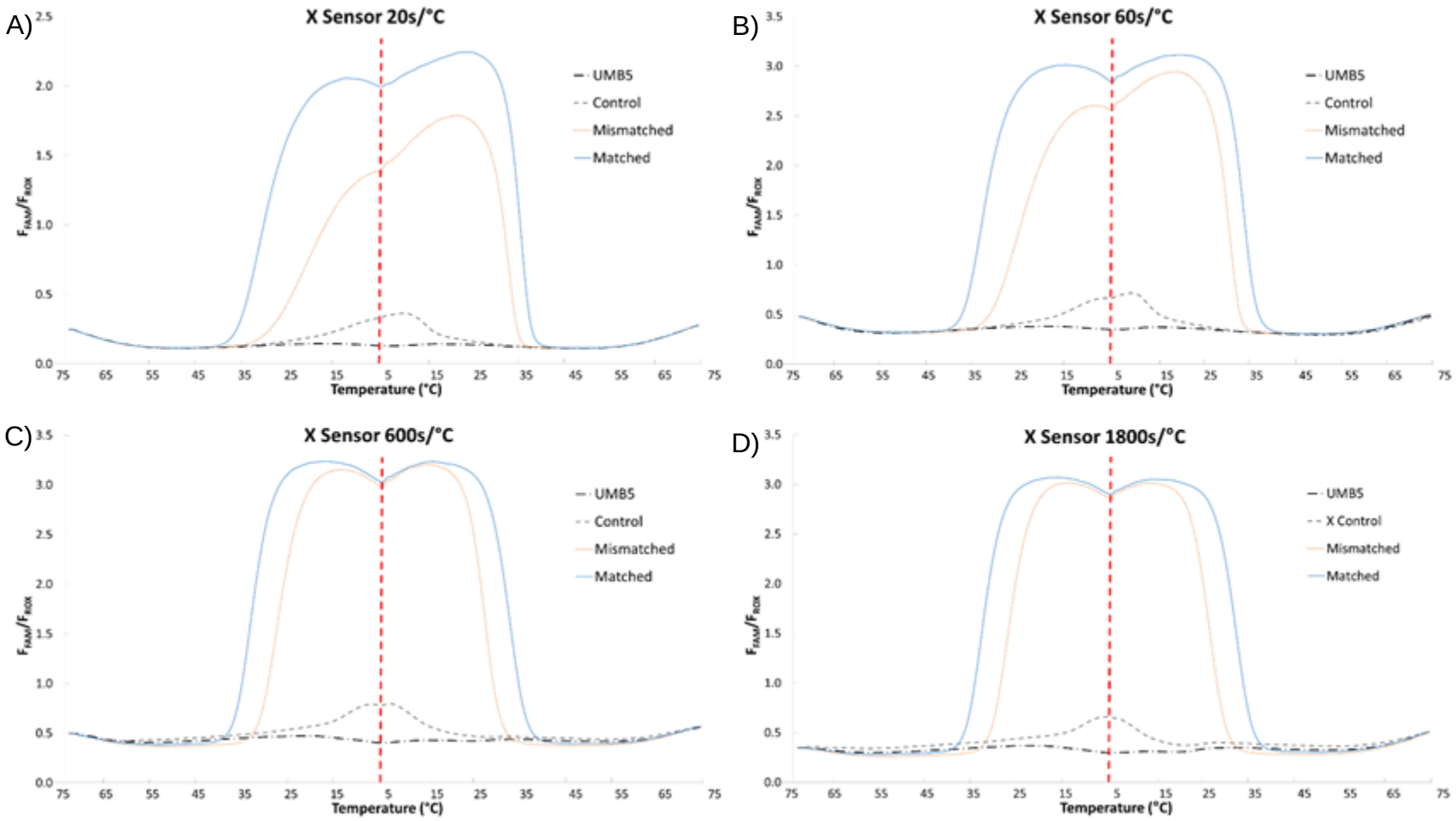

Figure 43: X Sensor Cooling and Heating Curves

Cooling-heating curves of m_{10}/f_9 Owl Sensor. Different equilibrium times were used: 20 s, 60 s, 600 s, and 1800 s. The solid blue lines represent the fully matched complex, dotted orange lines represent the mismatched complex, the dashed grey line represents the control with no analyte present, and the dotted dashed black line represents UMB5 alone. The vertical red dashed line shows the boundary between cooling (left side) and heating (right side) portions of the thermal profiles.

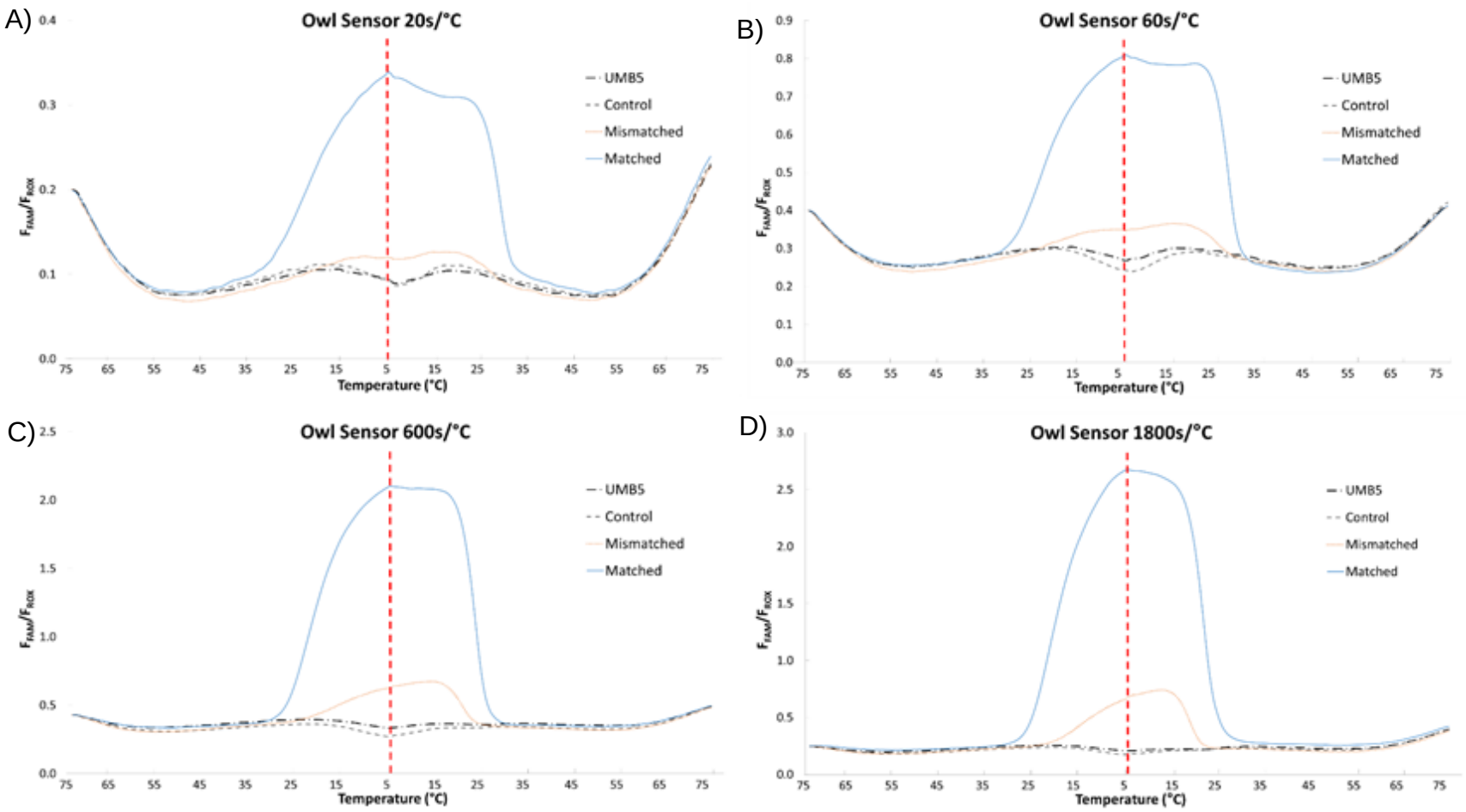

Figure 44: Owl Sensor Cooling and Heating Curves

Cooling-heating curves of R_{10}/P_9 Owl Sensor. Different equilibrium times were used: 20 s, 60 s, 600 s, and 1800 s. The solid blue lines represent the fully matched complex, dotted orange lines represent the mismatched complex, the dashed grey line represents the control with no analyte present, and the dotted dashed black line represents UMB5 alone. The vertical red dashed line shows the boundary between cooling (left side) and heating (right side) portions of the thermal profiles.

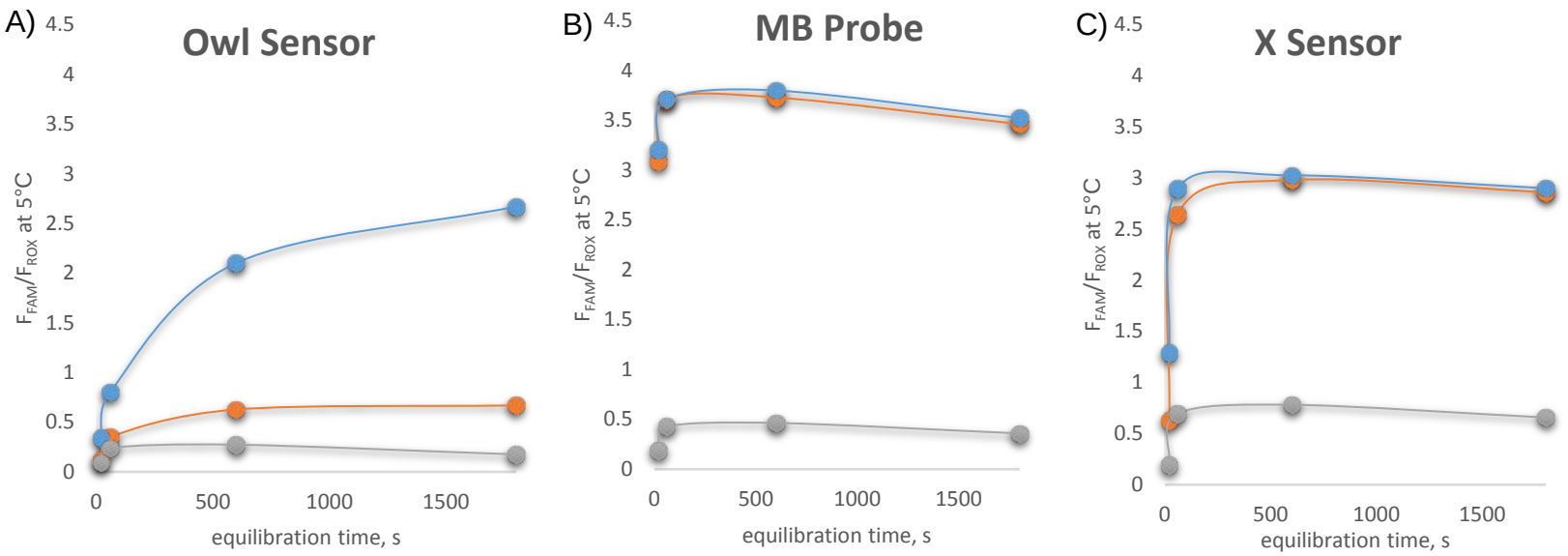

Figure 45. Kinetics at 5°C from cooling and heating curves.
The fluorescence at 5°C was taken from each of the cooling and heating curves from Figures 42-44 and graphed by their equilibration times.

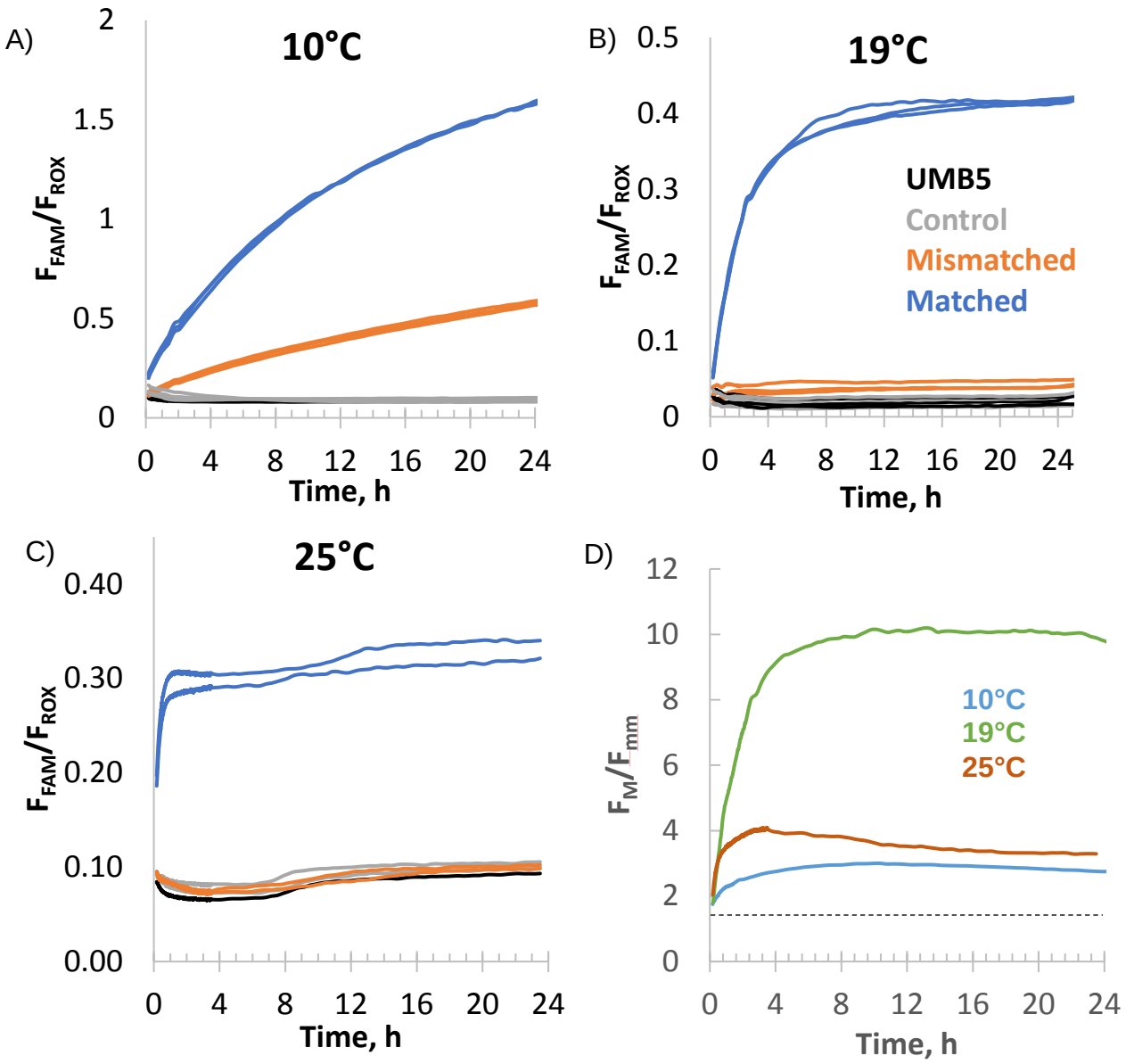

Figure 46. Isothermal Kinetics of the Owl Sensor.

A-C) Isothermal Kinetics of the R_{10}/P_9 Owl Sensor complementary to in the inhC analyte. Figures A-C are represent the sensor incubated at different temperatures: 10, 19, and 25°C. The readings for UMB5, Control, Mismatched, and Matched analytes are shown in black, grey, orange, and blue colors, respectively. D) Differentiation ability of represented by F_M/F_{mm} for 10, 19, and 25°C in blue, green, and brown lines, respectively. The dashed black line represents the differentiation line for $\Delta T_{1.5}$.

CHAPTER 6: THE OWL SENSOR DESIGN IS GENERAL, AS EVIDENCED BY RECOGNITION OF ANOTHER ANALYTE

Introduction

In order to prove general usefulness and versatility, new biosensors designs must not only be specific to different variations of the same analyte (for instance inhC and inhT), but they must also be easily designed and effective for various DNA/RNA analyte sequences. For this reason a miRNA sequence was chosen for analysis. MiRNAs are roughly 21 nucleotide long RNAs that act as regulatory units by binding to the 3' untranslated region of mRNAs. Their binding blocks translation of the mRNA sequence into the protein product and speeds up the degradation of the Poly-A tail, shortening the lifetime of the transcript by signaling it for degradation. Interestingly, miRNAs do not require perfect complementarity to bind to a mRNA and can therefore regulate hundreds of different mRNAs.

The miRNA sequences chosen are miRNA99a and miRNA100 which differ by a single nucleotide. Altered expression of these miRNA have been shown to be influential in various cancers including breast cancer.[32] Owl Sensors specific to both versions of the target were created to target both a DNA mimic (referred to as miDNA) and RNA targets. R strands ranging from 12-10 nucleotides were tested to see if the R_{10}/P_9 pair is indeed best for DNA and R_{11}/P_9 best for RNA analytes. R strands are named R_{11_mi}, for example, to distinguish them from the R strands specific to *inhA* analytes. P strands are named $P_{9\_mi\_99a}$ and $P_{9\_mi\_100}$ to indicate they are specific to miRNA99a and miRNA100, respectively (See Figure 47 for drawings).

The *inhA* analytes are nearly linear, and the region the P_9 adapter strand of the Owl Sensor binds to them is completely linear according to mFold analysis (Figure 7).[22] The Owl Sensor is itself very constrained due to the requirement that the UMB5 binding arms fold back on themselves in order for a signal to be produced. Since the miRNA analyte is predicted to fold in a small stem loop conformation (Figure 48), care must be taken when designing R and P strands. The adapter strands must bind in a way to allow for proper opening of the stem loop. In addition, higher concentrations of probes will be used to drive the process toward complex formation.

Materials and Methods

Reagents

All buffers and stock solutions were made with DNAse/protease-free water purchased from Fisher Scientific Inc. (Pittsburg, PA). All other reagents needed for buffers were purchased from Sigma-Aldrich (St. Louis, MO). UMB5 was custom-made by TriLink Biotechnologies, Inc. (San Diego, CA). All other oligonucleotides (sequences listed in Table 1) were obtained from Integrated DNA Technologies, Inc. (Coraville, IA). The concentrations of nucleic acid strands were determined using the Beer-Lambert law, a 1 cm quartz cuvette (volume of 100 µL), and extinction coefficients determined by using OligoAnalyzer 3.1 software (Integrated DNA Technologies, Inc.). Three independent different amounts of the same oligonucleotide were mixed with water to total volume of 100 µL and tested for their absorbance values at 260 nm using a Perkin-Elmer Lambda 35 UV/Vis spectrometer (San Jose, CA). The average of the concentrations calculated

was used with relative standard deviations of each sample less than 10%. Working stock solutions of convenience concentrations were prepared for all sequences and stored frozen at -20°C until use.

Melt Curve Fluorescent Assays

Prior to mixing, stock solutions of oligonucleotides were allowed to thaw to room temperature, vortexed for 5 s, and centrifuged on a tabletop minicentrifuge for 10 s. A master mix solution containing R_X/P_Y was created such that adding 11.5 µL of the master mix to the samples (to a total volume of 25 µL) would result in R_X and P_Y concentrations of 1,000 nM and 200 nM, respectively. The master mix was used to make samples with the following names: Control, Mismatched, Matched, and Insertion and Deletion, if tested. The master mix solution (11.5 µL) was added to a 96-well plate (30 µL wells). Next, 1 µL of water, miRNA99a, or miRNA100 was added to the plate to make the Control, Mismatched, or Matched, samples so that the final concentration of the analyte was 100 nM. Another well was filled with 12.5 µL of water to serve as a control named ‘UMB5’.

The buffer used contained 50 mM Tris-HCl, pH 7.4, 40 or 50 mM $MgCl_2$, and 0.1% Tween-20 with UMB5 and ROX. A buffer-fluorophore solution containing 2X Buffer, 100 nM UMB5, and either 100 nM ROX was made. By adding 12.5 µL of the buffer-fluorophore solution, to each sample well, final concentrations of the fluorophores were 50 nM. ROX was used as a passive dye reference since its fluorescence shows little fluctuation with temperature. Using ROX also allows for correction of well-to-well and plate-to-plate variations in fluorescence detection. Fluorescence was reported as F_{FAM}/F_{ROX}, where

F_{FAM} is the fluorescence given off by the fluorophore attached to UMB5 and F_{ROX} is the fluorescence of the ROX reference dye.

After samples were made, an optical adhesive cover was placed firmly on top of the plate and a tool was used to seal the wells. The plate was flicked to eliminate any formed bubbles, vortexed, and then spun at 660 rcf for 20 s.

The solutions were placed in the QuantStudio™ 6 Flex System and cooled (2°C/s) from room temperature to 5°C where they were annealed for 60 min. The fluorescence of the samples was then read continuously as the samples were heated (0.1°C/s) from 5°C to 50°C. The QuantStudio™ 6 Flex System software allowed for the selection of FAM™ dye to be read as the 'Target' and if ROX was utilized, it was selected as a 'Passive Reference'. The system was routinely calibrated for well factors, background, and dye fluorescence. It is important to note that samples taken after different calibrations of the system showed altered background fluorescence of UMB5 and the Control samples (with no analyte present); thus depending on the date the experiment was conducted, some variation in fluorescent values between experiments may be observed. The QuantStudio™ Real-Time PCR Software (version 1.1) allows for real-time data analysis for initial processing, but all relevant data was exported to Excel for further analysis. The readings from at least two wells was averaged and replotted to produce the presented figures. The derivative of fluorescence over time was calculated by the QuantStudio™ Real-Time PCR Software. The maximum of the derivative plots gives the inflection point of the curve, also called the melting temperature (T_m).

Results and Discussion

Results show that, for DNA analytes, R_{10_mi} is the best length for differentiation between matched and mismatched analytes. The Owl Sensor specific to miDNA100 performed better than the sensor specific to miDNA99a, as a lower signal was produced for the mismatched analyte. Initial results use 50 mM Mg^{2+} in the buffer and show significant signal for the mismatched analyte (Figure 49). When the magnesium ion concentration was dropped to 40 mM Mg^{2+}, the performance of the sensor greatly improved (Figure 50). Differentiation between matched and mismatched analytes extends from 5°C to 22.44°C and 23.22°C for the Owl Sensor specific to miDNA99a and miDNA100, respectively (Figure 50B and D). When testing on RNA analytes, R_{11_mi} proved to be the best for differentiation between matched and mismatched analytes (Figure 51). Differentiation was achieved from 5°C to 24.10°C for the sensor specific to miRNA99a and from 5°C to 25.70°C for the sensor specific to miRNA100 (Figure 52). Kinetic studies at 10°C showed that the Owl Sensor reaches equilibrium much faster with miDNA analytes than with *inhA* analytes (Figure 53).

Conclusion

Unlike other sensors with adapter strands such as the X Sensor and the OC Sensor,[13-15,33] the Owl Sensor does not need any optimization for the lengths of the adapter strands. For two different analytes, it has been shown that 10 nucleotides for the R strand and 9 nucleotides for the P strand are ideal for DNA analytes. For RNA analytes, in both cases, 11 nucleotides was ideal for R and again 9 nucleotides was ideal for P. Chapters 3 suggests that the helicity of DNA and RNA influence their need for different lengths of R,

making the Owl Sensor the only sensor to use DNA's innate helical properties to bind selectively to a specific sequence, eliminating the need to try different lengths of adapter strands.

For optimal Owl Sensor design, mismatched analytes have produced little to no signal above the control sample when using the standard melt curve procedure (1 hour incubation at 5°C followed by temperature ramping). The Owl Sensor has been proven to be versatile by working effectively for two different analyte sequences and being able to select for either variation of sequence for the same analyte (inhT/inhC or miDNA99a/100). Chapter 5 showed that limits of detection for the Owl Sensor are in the low nM range, making them comparable with Molecular Beacon technology. Chapter 5 also showed that the Owl Sensor achieves its differentiation by taking advantage of non-equilibrium conditions.

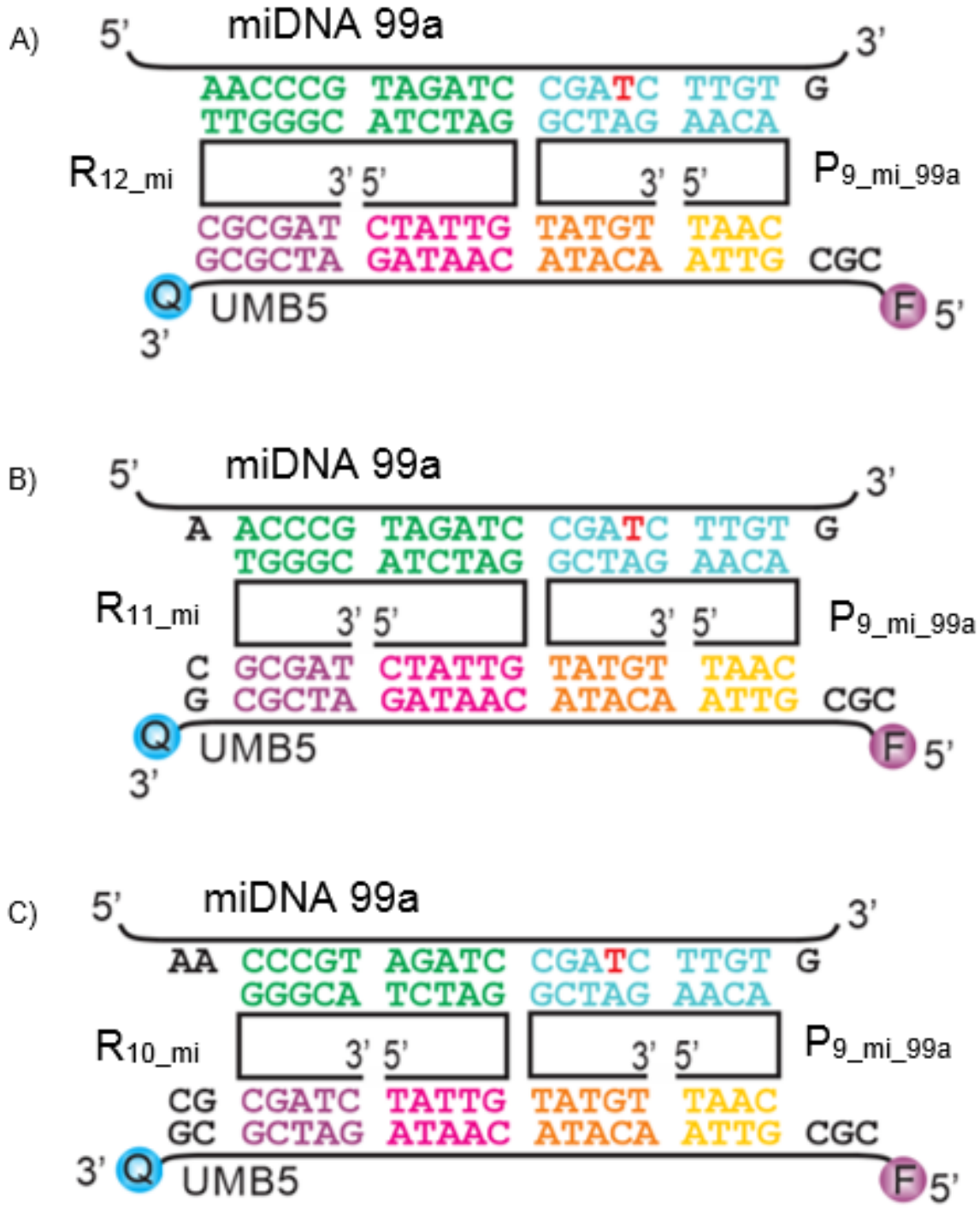

Figure 47. Owl Sensor specific to miDNA analytes.

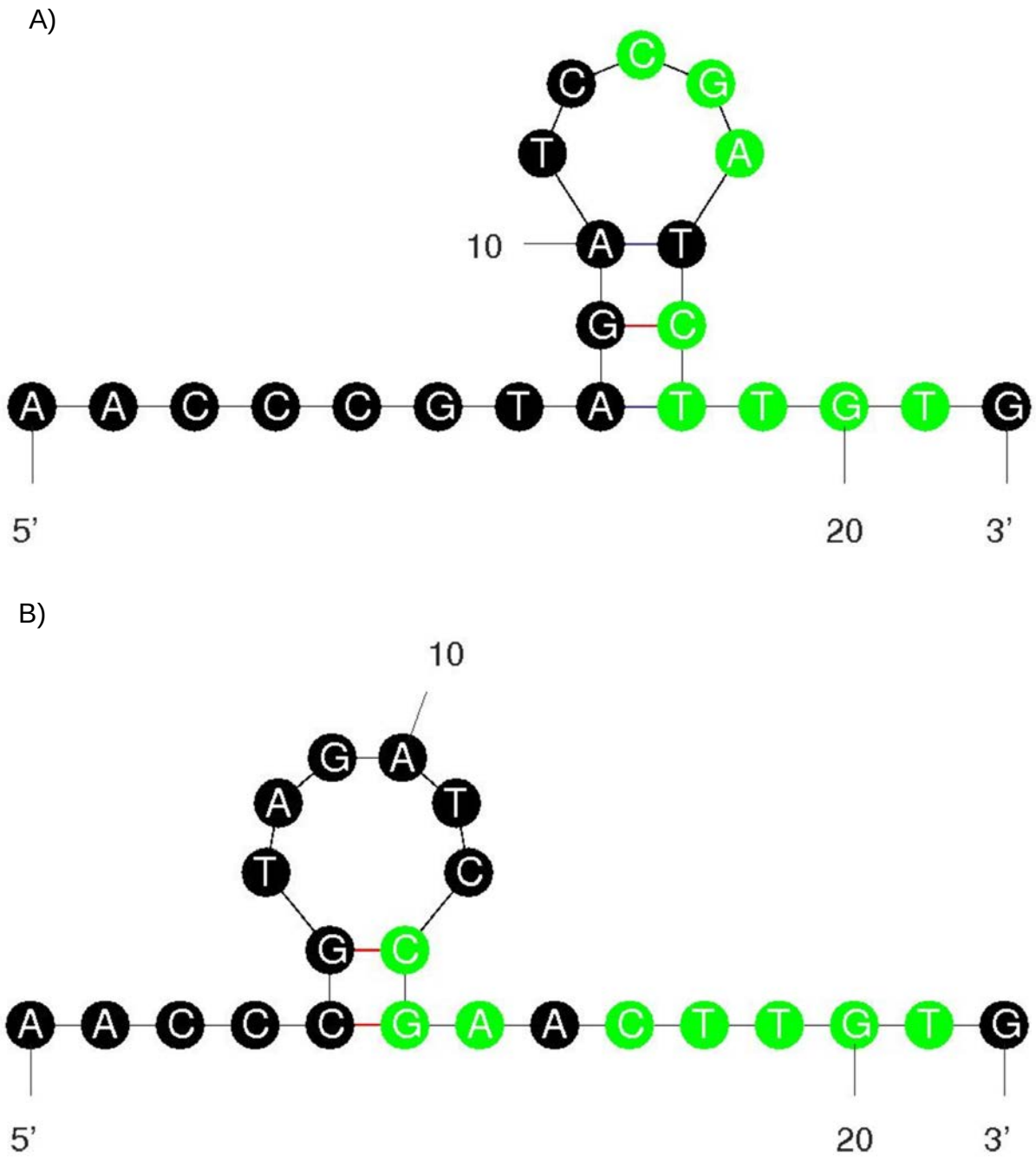

Figure 48. Secondary structures of miDNA analytes

The A) miDNA99a (ΔG= -0.91 kcal/mol) and B) miDNA100 (ΔG= -0.14 kcal/mol) analytes are shown folded by mfold.[22] The green nucleotides indicate the region where P_{9_mi} binds. The black nucleotide in the middle of the green region indicates the variable base.

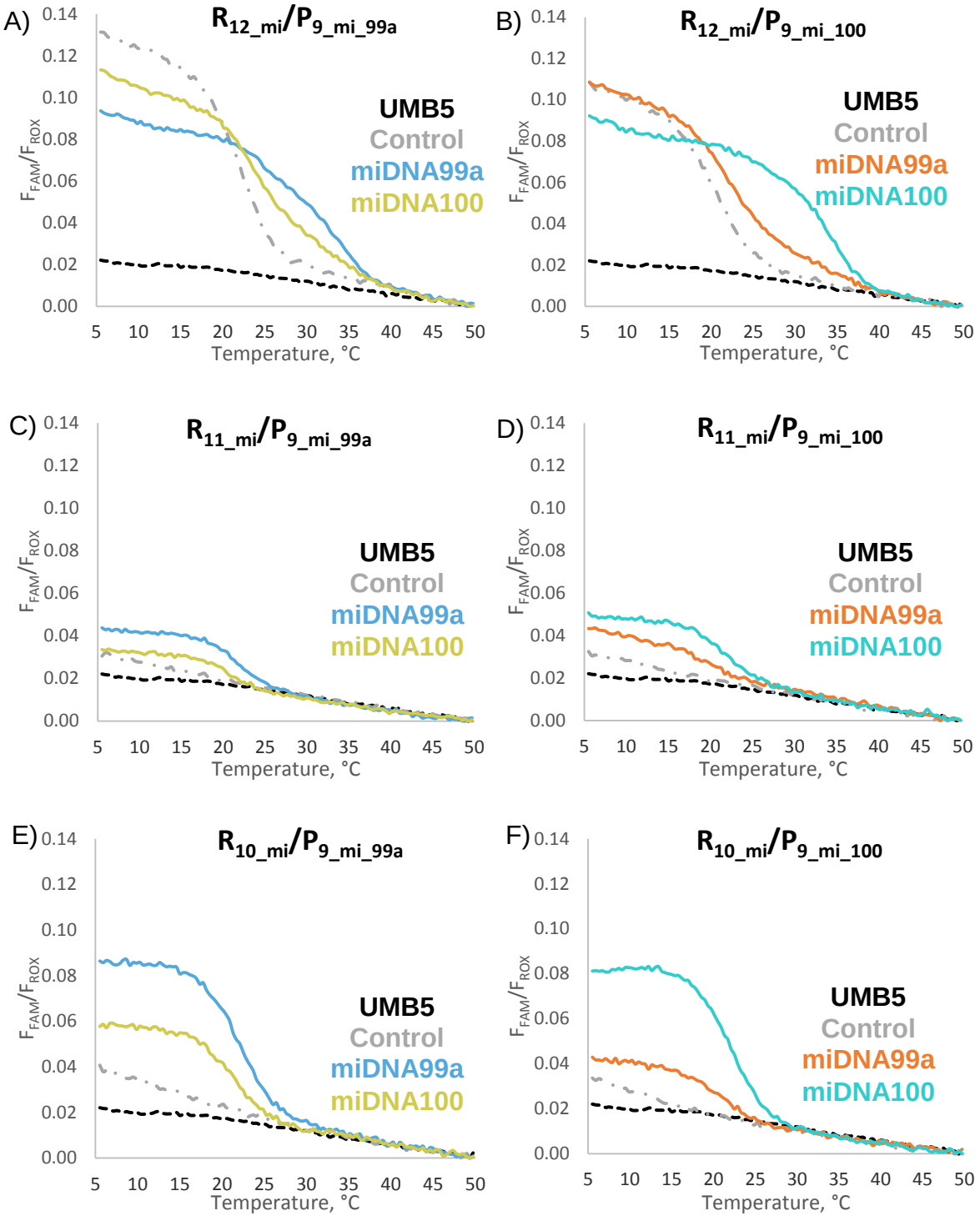

Figure 49. Melt curves for Owl Sensor specific to miDNA.

Figures A, C, and E show melt curves for an R strand with 12-10 nucleotides with a P_9 specific to miDNA99a.

Figures B, D, and F show differentiation for an R strand with 12-10 nucleotides for R paired with a P_9 specific to miDNA100.

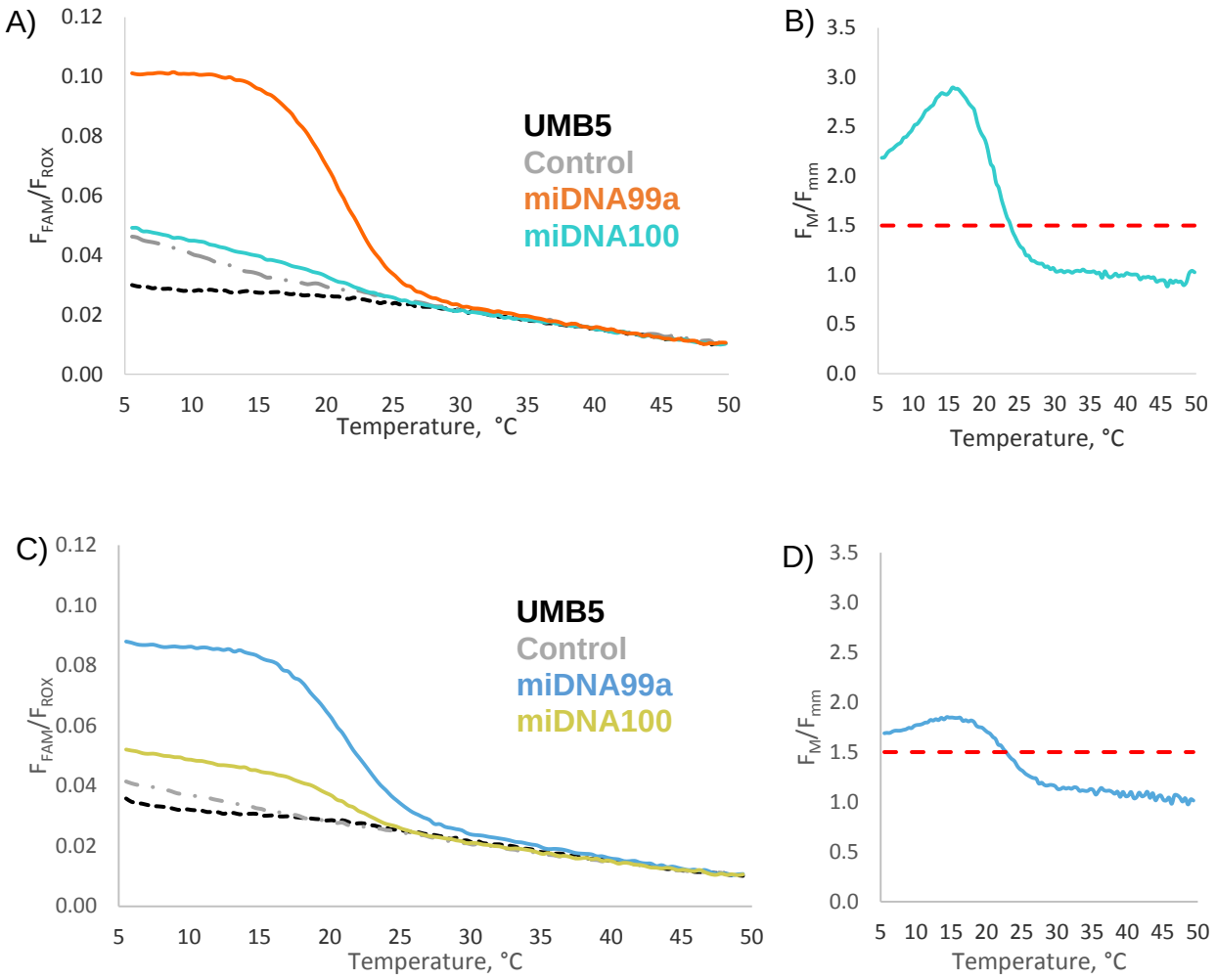

Figure 50. Optimized melt curves and Differentiation of DNA Analytes with the $R_{10\_mi}/P_{9\_mi\_100}$ and $R_{10\_mi}/P_{9\_mi\_99a}$.

A) The melt curve for $R_{10\_mi}/P_{9\_mi\_100}$ Owl Sensor. UMB5, the Control, miDNA99a, and miDNA100 are represented by the black dashed, grey dotted dashed, orange, and teal lines, respectively.

B) The differentiation range extends from 5-23.2°C for Owl Sensor $R_{10\_mi}/P_{9\_mi\_100}$ Owl Sensor with DNA analytes.

C) The melt curve for $R_{10\_mi}/P_{9\_mi\_99a}$ Owl Sensor. UMB5, the Control, miDNA99a, and miDNA100 are represented by the black dashed, grey dotted dashed, blue, and mustard lines, respectively.

D) The differentiation range extends from 5-22.4°C for Owl Sensor $R_{10\_mi}/P_{9\_mi\_99a}$ Owl Sensor with DNA analytes.

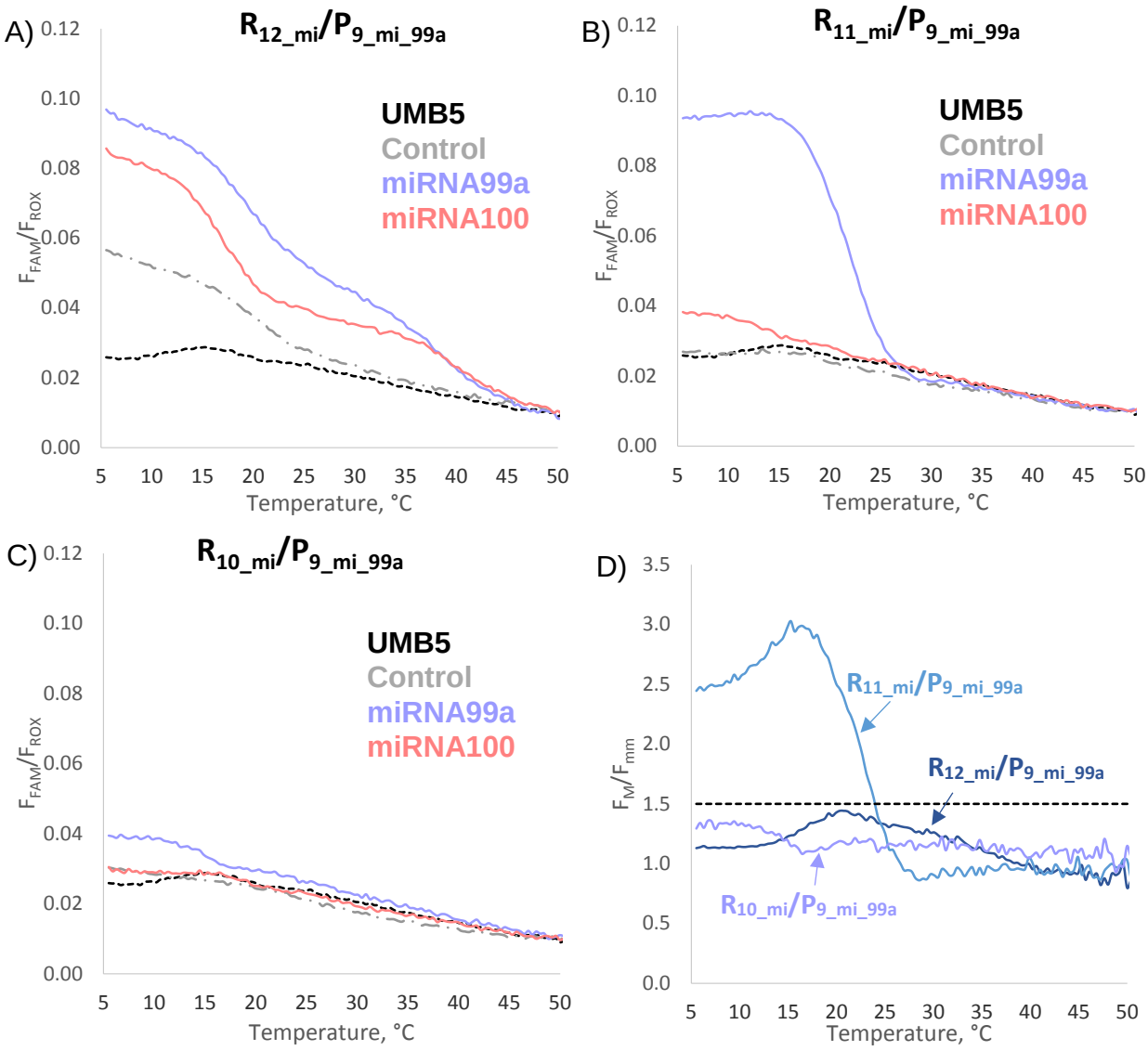

Figure 51. R_{11_mi} is the best R length for differentiating the mismatched analyte in miRNA analytes.

A-C) The melt curves for UMB5, the Control, miRNA99a, and miRNA100 are represented by the black dashed, grey dotted dashed, coral, and purple lines, respectively.

D) The differentiation range for Owl Sensor $R_{11\_mi}/P_{9\_mi\_99a}$ Owl Sensor with RNA analytes.

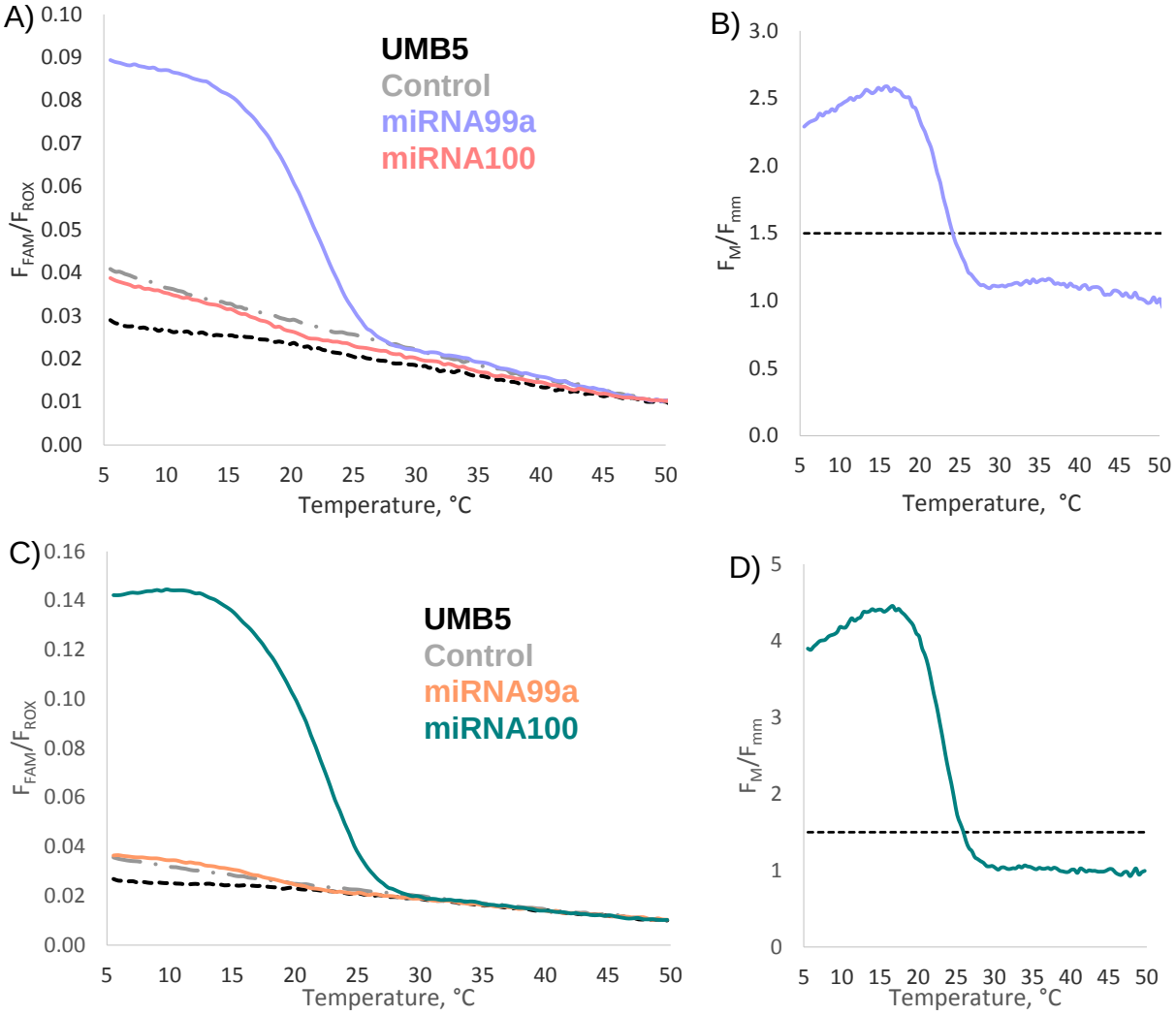

Figure 52. Optimized melt curve and differentiation of miRNA Analytes.

A) The melt curve for $R_{11\_mi}/P_{9\_mi\_99a}$ where UMB5, the Control, miRNA99a, and miRNA100 are represented by the black dashed, grey dotted dashed, purple, and salmon lines, respectively.

B) The differentiation range for Owl Sensor $R_{11\_mi}/P_{9\_mi\_99a}$ Owl Sensor with RNA analytes extends from 5-25.7°C.

C) The melt curve for $R_{11\_mi}/P_{9\_mi\_100}$ where UMB5, the Control, miRNA99a, and miRNA100 are represented by the black dashed, grey dotted dashed, orange, and teal lines, respectively.

D) The differentiation range for Owl Sensor $R_{11\_mi}/P_{9\_mi\_100}$ Owl Sensor with RNA analytes extends from 5-24.1°C.

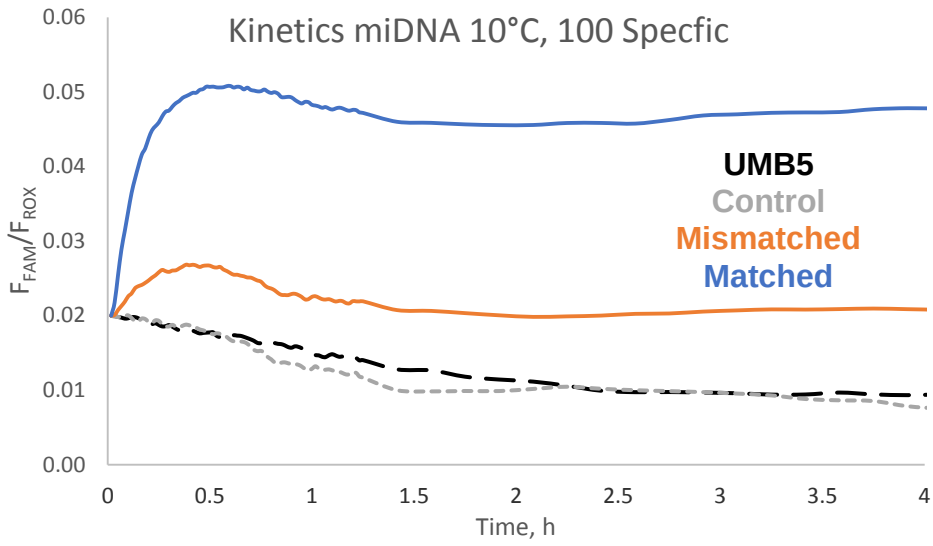

Figure 53. Kinetic analysis of miDNA Analytes.

REFERENCES

1. Alberta truck's oversized load blamed for Washington bridge collapse. *British Columbia - CBC News* [Online] May 26, 2013. http://www.cbc.ca/news/ (accessed June 8, 2016).

2. Jansen, B. (2014, July 15). NTSB: Truck strike caused I-5 bridge collapse. *USA Today* [Online] July 15, 2014. http://www.usatoday.com/ (accessed June 8, 2016)

3. Veiga MI, Ferreira PE, Jörnhagen L, MalmbergM, Kone A, Schmidt BA et al. *Novel polymorphisms in Plasmodium falciparum ABC transporter genes are associated with major ACT antimalarial drug resistance*. PLoSOne, 2011. 6: e20212.

4. Cummings MP, Segal MR. *Few amino acid positions in rpoB are associated with most of the rifampin resistance in Mycobacterium tuberculosis*. BMC Bioinformatics, 2004. 5: p.137.

5. Zhang L, Liu Y, Song F, Zheng H, Hu L, Lu H et al. *Functional SNP in the microRNA-367 binding site in the 3'UTR of the calcium channel ryanodine receptor gene 3 (RYR3) affects breast cancer risk and calcifi cation*. Proc Natl Acad Sci USA, 2011. 108: p. 13653–13658.

6. Lee SH, DeCandia TR, Ripke S, Yang J. *Estimating the proportion of variation in susceptibility to schizophrenia captured by common SNPs.* Nat Genet, 2012. 44: p. 247–250.

7. A. Piatek, S.T., A. C. Pol, A. Telenti, L.P. Miller, F. R. Kramer, D. Alland, *Molecular beacon sequence analysis for detecting drug resistance in Mycobacterium tuberculosis.* Nature Biotechnology, 1998. 16: p. 359-363.

8. Dangisso, M. H., Datiko, D. G., & Lindtjørn, B. *Low case notification rates of childhood tuberculosis in southern Ethiopia*. BMC Pediatrics, 2015. *15*: p. 1-10.

9. J. Guo, J.J., N. J. Turro, *Fluorescent hybridization probes for nucleic acid detection.* Anal Bioanal Chem, 2012. 402: p. 3115–3125.

10. Wetmur, J.G., *DNA Probes: Applications of the Principles of Nucleic Acid Hybridization.* Critical Reviews in Biochemistry and Molecular Biology, 1991. 26: p. 227-259.

11. S. Tyagi, F.K., *Molecular Beacons: Probes that Fluoresce upon Hybridization.* Nature Biotechnology, 1996. 14: p. 303-308.

12. H. J. Tanke, R.W.D., T. Raap, *FISH and immunocytochemistry: towards visualizing single target molecules in living cells.* Curr Opin Biotechnol, 2005. 16: p. 49-54.

13. Kolpashchikov, D.M., *A Binary DNA Probe for Highly Specific Nucleic Acid Recognition.* J. Am. Chem. Soc. , 2006. 128: p. 10625-10628.

14. Y. V. Gerasimova, A.H., J. Ballantyne, D. M. Kolpashchikov, *A Single Molecular Beacon Probe Is Sufficient for the Analysis of Multiple Nucleic Acid Sequences.* ChemBioChem, 2010. 11: p. 1762-1768.

15. Y. V. Gerasimova, D.M.K., *Detection of bacterial 16S rRNA using a molecular beacon-based X sensor.* Biosens. Bioelectron., 2013. 41: p. 386-390.

16. Stancescu, M. *Optimization of molecular beacon-based multicomponent probes for analysis of nucleic acids*. PhD, University of Central Florida, Orlando, FL, USA, 2015.

17. Zhang Y., Heym B., Allen B., Young D., and Cole S.T.: *The catalase-peroxidase gene and isoniazid resistance of Mycobacterium tuberculosis*. Nature, 1992. 358: p. 591-593.

18. Banerjee A., Dubnau E., Quemard A., Balasubramanian V., Um K.S., Wilson T., Collins D., de Lisle G., and Jacobs W.R. *inhA, a gene encoding a target for isoniazid and ethionamide in Mycobacterium tuberculosis*. Science 1994; 263: p. 227-230.

19. Mdluli K.R., Slayden A., Zhu Y., Ramaswamy S., Pan X., Mead D., Crane D.D., Musser J.M., and Barry C.E. *Inhibition of a Mycobacterium tuberculosis beta-ketoacyl ACP synthase by isoniazid***.** Science, 1998. 280: p. 1607-1610.

20. Sreevatsan, S., Pan, X., Zhang, Y., Deretic, V., & Musser, J. M. *Analysis of the oxyR-ahpC region in isoniazid-resistant and -susceptible Mycobacterium tuberculosis complex organisms recovered from diseased humans and animals in diverse localities.* Antimicrobial Agents and Chemotherapy, 1997. *41*: p. 600–606.

21. Murray, C. J. L., Styblo, K. Rouillon, A. *Tuberculosis in developing countries: burden, intervention, and cost.* Bull. Int. Union against Tuberculosis and Lung Disorders, 1990. 65: p. 6−24.

22. http://unafold.rna.albany.edu/, The DINAMelt Web Server.

23. H. Urakawa, S.E.F., H. Smidt, J. C. Smoot, E. H. Tribou, J. J. Kelly, P. A. Noble, D. A. Stahl, *Optimization of Single-Base-Pair Mismatch Discrimination in Oligonucleotide Microarrays.* Applied and Environmental Microbiology, 2003. 69: p. 2848–2856.

24. SantaLucia, J. Jr., Hicks, D. *The thermodynamics of DNA structural motifs*. Annu. Rev. Biophys. Biomol. Struct. 2004. 3:, p. 415-440.

25. Demidov, V. V.; Frank-Kamenetskii, M. D. *Two sides of the coin: affinity and specificity of nucleic acid interactions.* Trends Biochem Sci*.,* 2004. 29: p. 62-71.

26. Rothemund, PWK. *Folding DNA to create nanoscale shapes and patterns*. Nature, 2006. 440: p. 297-302.

27. Han, D., Pal, S., Nangreave, J. Deng, Z. Liu, Y., and Yan, H. *DNA Origami with Complex Curvatures in Three-Dimensional Space*. Science, 2011. 332: p. 342-346.

28. Zadegan, R.M.; Norton, M.L. *Structural DNA Nanotechnology: From Design to Applications*. Int. J. Mol. Sci. 2012. 13: p. 7149-7162.

29. Eichman, B. F., Vargason, J. M., Mooers, B. H. M., & Ho, P. S. *The Holliday junction in an inverted repeat DNA sequence: Sequence effects on the structure of four-way junctions.* Proc Natl Acad Sci USA, 2000. 97: p. 3971–3976.

30. Kolpashchikov DM. *An Elegant Biosensor Molecular Beacon Probe: Challenges and Recent Solutions***.** Scientifica (Cairo). 2012: 928783.

31. A.Tsourkas, M.A.B., S. D. Rose, G. Bao, *Hybridization kinetics and thermodynamics of molecular beacons.* Nucleic Acids Research, 2003. 31: p. 1319-1330.

32. Servín-González LS, Granados-López AJ, López, JA. *Families of microRNAs Expressed in Clusters Regulate Cell Signaling in Cervical Cancer*. Int J Mol Sci, 2015.16: p. 12773-90.

33. Cornett EM, O'Steen MR, Kolpashchikov DM. *Operating Cooperatively (OC) Sensor for Highly Specific Recognition of Nucleic Acids.* PLoS One, 2013. 8: e55919.